2009

DEVELOPMENT OF A MECHANICAL CAVOPULMONARY ASSIST DEVICE FOR THE FAILING FONTAN PATIENTS

Jugal Kapadia
Virginia Commonwealth University

DEVELOPMENT OF A MECHANICAL CAVOPULMONARY ASSIST DEVICE FOR THE FAILING FONTAN PATIENTS

A Thesis submitted in partial fulfillment of the requirements for the degree of Master of Science in Mechanical Engineering at Virginia Commonwealth University.

by

JUGAL YATINKUMAR KAPADIA
Bachelor of Engineering, U.V. Patel College of Engineering, India, 2007

Director: DR. AMY L. THROCKMORTON
QIMONDA ASSISTANT PROFFESOR, DEPARTMENT OF MECHANICAL ENGINEERING

Virginia Commonwealth University
Richmond, Virginia
December, 2009

Acknowledgement

I have worked with a great number of people whose contribution to this thesis deserves special mention. It is a pleasure to convey my gratitude to them all in my humble acknowledgment.

I would like to acknowledge Virginia Commonwealth University, without which this research would never have been possible. I thank my mentor Dr. Amy Throckmorton for her never ending support, advice and guidance throughout my research, as well as in my personal life. Above all and most needed, she has provided so much encouragement. Through the power of her knowledge, she has navigated me to brighter horizons of life. Her confidence in my abilities continues to motivate me each day to achieve excellence. Her intuition and zest has made her a constant oasis of ideas and passion in science, which exceptionally inspired and enriched my growth as a student and researcher. I am indebted to her more than she knows. I am appreciative to all my committee members for their guidance and constructive feedback and for dedicating their precious time from the midst of all their activities. I gratefully acknowledge Dr. Mossi for her advice and moral support towards my educational career. I am thankful to her in every possible way and hope to keep up our collaboration in the future.

Many thanks go in particular to Dr. Poorna Mane. I am much indebted to her for her valuable advice. She has always been a very supportive friend throughout my research. I wish her the best of luck in all of her future endeavors. My special thanks go to my colleagues Sonya and Steven for creating a pleasant working atmosphere in the lab. Thank you for all of your assistance and fun during the work we had. I convey special acknowledgment to Ravi, Leena and Vivek for being great friends. Thank you for all of your help and guidance. Furthermore, I would like to thank my childhood school friends Parth, Deval, Ketan, Nishad and Anuj who have always been supportive, encouraging and helped me in every possible way.

My parents deserve special mention for their unconditional support and prayers. My father, Yatinkumar Kapadia, is the person who cultivated a learning character in me, showing me the joy of intellectual pursuit ever since I was a child. My mother, Parul Kapadia, is the one who raised me with her caring and gentle love. My brother Jalay is always a supportive and a caring sibling.

Words fail me to express my appreciation to my fiancé Krishma whose dedication, love and persistent confidence in me, has enriched my life. Her patience and encouragement has upheld me, particularly in those many days in which I spent more time with my computer then with her. For that reason, I would also thank the Shroff family for warmly accepting me as a member of the family. Finally, I would like to thank everybody who was important to the successful realization of the thesis, as well as expressing apology that I could not mention everyone personally one by one.

Table of Contents

List of Tables

Page

List of Figures

Page

Abstract

DEVELOPMENT OF A MECHANICAL CAVOPULMONARY ASSIST DEVICE FOR THE FAILING FONTAN PATIENTS

By Jugal Yatinkumar Kapadia, M.S.

A Thesis submitted in partial fulfillment of the requirements for the degree of Master of Science in Mechanical Engineering at Virginia Commonwealth University.

Virginia Commonwealth University, 2009

Major Director: Dr. Amy L. Throckmorton
Qimonda Assistant Professor, Department of Mechanical Engineering

The long term objective of this research is to develop a collapsible, percutaneously inserted, axial flow blood pump to improve blood flow in the cavopulmonary circulation. Through this research, the experimental evaluation of five blood pump prototypes and hemolysis testing of one blood pump prototype were performed.

All prototypes demonstrated acceptable hydraulic performance. A comparison of the experimental results with numerical predictions demonstrated a 10-20% deviation, an

acceptable range per industry standard. Hemolysis testing of a four bladed adult blood pump showed plasma free hemoglobin level of 20.04 mg/dL and maximum NIH (normalized index of hemolysis) level was 0.017 g/100L.

This thesis project serves as a solid foundation from which to continue development of this suited intravascular axial flow blood pump. Successful completion of this research will lead to a novel percutaneously inserted axial flow pump for infants and adult patients with a failing Fontan physiology.

Chapter 1: Motivation and Significance

In the United States approximately 40,000 newborns are born with significant congenital heart anomalies (1). This constitutes approximately 1% of the 4 million babies born each year (1). Chronic and untreated cardiac defects may, over time, lead to congestive heart failure (CHF) (2). A unique subset of pediatric patients includes those born with functionally single ventricle (3). These patients represent 1% of 40,000 pediatric patients suffering from congenital heart disease (CHD) every year (1). In these patients, however, the single ventricle is responsible for maintaining the systemic and pulmonary blood circulation (3).

A normal heart physiology consists of a pulmonary and systemic blood circulation. Pulmonary circulation comprises of deoxygenated blood entering right atrium from inferior and superior vena cava. Blood from right atrium enters right ventricle from where the blood is pumped to pulmonary arteries to lungs (pulmonary circulation). Oxygenated blood from lungs enters left atrium through pulmonary veins. Ultimately blood entering left ventricle from left atrium is again pumped to the different parts of the body through aorta (systemic circulation). In contrast, for single ventricle patients, a substantial number undergo a three staged surgical palliation. The Fontan surgery is the surgical treatment paradigm for complex single-ventricle physiology. This came into

existence in 1971 when Dr. Francis Fontan reported a new approach of separating the systemic and pulmonary circulations for the patients with functionally one ventricle (4; 5; 6). As shown in **Figure 1**, initially at neonatal stage, the Norwood, a shunt is placed

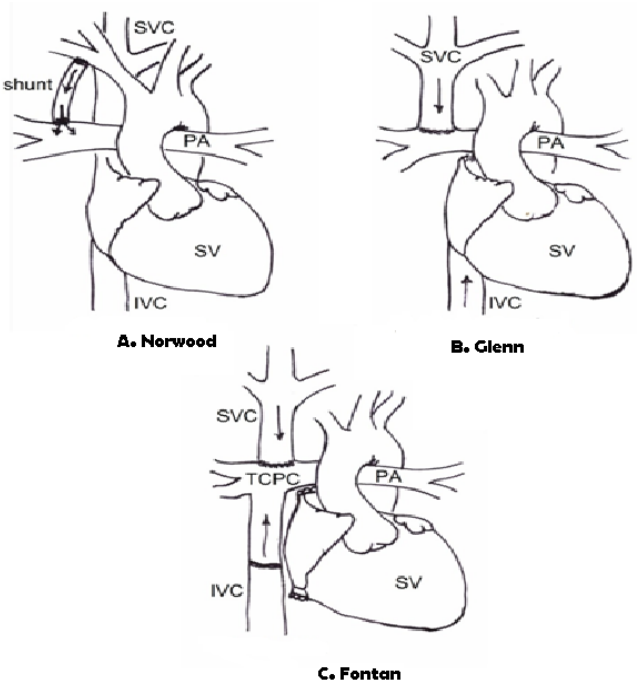

Figure 1: Three staged Fontan operation. SVC- Superior vena cava, IVC- Inferior vena cava, SV- Single ventricle, PA- Pulmonary artery, TCPC-Total Cavopulmonary connection

between aorta and pulmonary arteries with the intention of reducing blood desaturation and development of the pulmonary vasculature (4). The second staged palliation is often performed at the age of 4 to 12 months, in which the Glenn shunt is introduced and the superior vena cava is connected to the pulmonary artery.

By the age of 3 or 5, depending upon the growth of vascular structures, the Fontan circuit is completed by connecting the inferior caval vein to the pulmonary artery leading

to total cavopulmonary connection (TCPC) (4). **Figure 1** illustrates the TCPC in the Fontan configuration. The Fontan physiology was observed to reduce mortality and morbidity in the short-term postoperatively (5). Arterial hypoxemia is eliminated, volume overload to the single ventricle is reduced, and quality of life is improved (6).

The Fontan operation, however, remains an imperfect solution for patients with complex congenital heart problems (7). A study performed on 261 patients undergoing a Fontan surgery at Children's Hospital of Boston concluded that the perioperative death rate is 30%, indicating a high-risk procedure. Postoperative event-free survival rates at 1, 5, 10, 20 and 25 years were 80.1%, 77.5%, 74.8%, 72.2%, 68.3% and 53.6% respectively, indicating complications mounting over time (8). There are a number of complications associated with the Fontan operation which include early and late mortality, inefficient in exercise tolerance, residual cardiomegaly, arrhythmias, increased venous pressure and congestion and chronic low cardiac output (4). Clinicians are frequently impressed by the ability of most patients with a Fontan circulation to lead a reasonably normal life, including mild to moderate sport activities (5). A majority of patients show progressive decline of functional status post-Fontan operation. Non-cardiac complications associated with long-term effects of Fontan physiology are liver dysfunction, coagulation disorders and protein losing enteropathy [lymphatic dysfunction]. Over time, these complications lead to heart failure (4-7).

Infants, children and adults with end-stage heart failure may require mechanical circulatory support using an artificial heart pump or blood pump (9; 10). Mechanical circulatory assistance improves the recovery of ventricular function by decreasing the

work load and may serve as a bridge to cardiac transplantation (11). The most common method of mechanical circulatory support in pediatric patients is extracorporeal membrane oxygenation (ECMO). The ECMO unit operates completely outside of the body and is a complicated network of tubing and instruments, which increases the risk of clot formations or thrombosis (12; 13). Another alternative for supporting pediatric patients extracorporeally was intra-aortic balloon pumps (IABPs). IABPs are not suitable for infants because of the difficulty in synchronizing to their rapid heart rates, and the balloons themselves are not small enough to be effective in babies (14; 15; 16). Neither of these methods proves to be reliable and effective for long term bridge to transplantation (17).

Current medical therapies for CHD are only marginally successful and thus there is a long-waiting list for cardiac transplantation (18). The shortage of donor organs and complication of donor-recipient size matching for pediatric patients have motivated researchers to seek alternative solutions, such as the development of an effective mechanical circulatory support device for bridge to cardiac transplantation(19; 20). As a viable alternative, ventricular assist devices (VAD) have been employed in pediatric and adult patients successfully with heart failure (21).

VADs can be designed to augment flow from the left (systemic circulation) or right (pulmonary circulation) side of the heart (11). Commercially available VADs, however, as approved by the FDA are specifically designed for systemic congestive heart failure, thus the capacity and pressure generation far exceeds levels that are required to support the Fontan (cavopulmonary) circulation (22). No cavopulmonary assist devices

have been successfully developed to augment the blood flow in the total cavopulmonary connection in patients with a failing Fontan physiology (23).

To address this growing need for novel circulatory support strategies for failing Fontan patients, research currently focuses on development of a collapsible, percutaneously inserted and magnetically levitated axial flow blood pump to mechanically augment pressure in the cavopulmonary circulation in pediatric and adult patients(22). The axial flow pump will be percutaneously inserted into a vein distal to the heart, fed toward the single ventricle, and located in the inferior vena cava (IVC) at the entrance of the total cavopulmonary connection (TCPC). This intravascular blood pump consists of a catheter-mounted impeller, motor and protective cage filaments. **Figure 2** shows the conceptual design of the collapsible axial flow blood pump and its placement in the IVC. The design includes a magnetically levitated suspension for the rotation of the blood pump and also allows blood flow path not to be obstructed by suspension components, centering of the pump when subjected to external disturbances and low energy consumption attained by extensive use of permanent magnets (PMs). This pump is designed to operate as a bridge-to-transplant, bridge-to-recovery, bridge-to-hemodynamic stability or bridge-to-surgical reconstruction.

This thesis research represents the initial design and development phase of axial flow blood pumps for augmentation of pressure at the cavopulmonary site in failing Fontan patients.

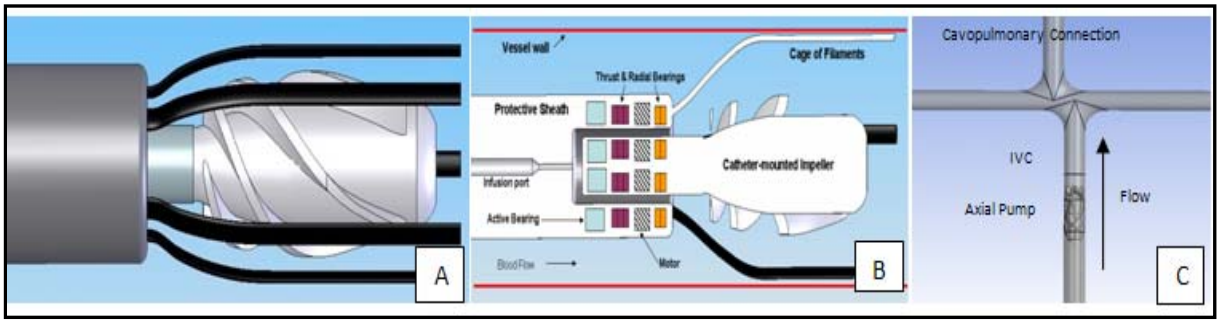

Figure 2: Intravascular Cavopulmonary Assist Device. A) Complete perspective of blood pump, B) Cross-sectional view of pump with components: protective sheath, infusion port, active bearing, thrust and radial bearings, catheter-mounted impeller, motor, cage of filaments, C) Blood pump percutaneously-placed in the inferior vena cava (IVC) to drive blood through the lungs.

Chapter 2: Project Objectives

This research project developed, planned, prepared, and executed the evaluation of blood pump designs using numerical analysis and experimental testing of prototypes.

The following specific aims have been achieved during this M.S. thesis research:

1. Developed computer aided design models of four blood pump designs for rapid prototyping based on pump design equations and an evolving design using numerical analysis.
2. Coordinated the construction of a hydraulic test loop for blood pump performance testing.
3. Carried out numerical simulations for the four bladed adult pump prototype (14 mm in diameter) using ANSYS CFX software.
4. Designed and coordinated the construction of a protective cage of filaments to shield the vessel wall from contacting the rotating impeller.
5. Experimentally completed the hydraulic testing of two axial flow blood pump prototypes without a protective cage and three axial flow blood pump prototype with the protective cage. A blood analog solution was used. The results of the four bladed

6. adult axial flow blood pump prototype without the protective cage was compared to the numerical predictions.
7. Performed hemolysis testing or blood bag experiments on the four bladed adult pump prototype (14 mm in diameter) without the protective cage in the hydraulic flow loop and analyzed the results in order to predict the blood damage caused by the proposed pump design.

This research project represents the initial steps toward developing an effective bridge-to-transplant or recovery therapeutic option for thousands of infants, children and adults suffering from heart failure in the United States and addresses a significant human health problem.

Chapter 3: Materials and Methods

3.1 Experimental Process

3.1.1 Axial Flow Blood Pump Prototypes

The geometry and characteristics of the axial pump were generated using Ansys CFX turbomachinary design software 11.0 SP 1.0, computational fluid dynamics software for designing turbomachinary (18). Using SolidWorks software, the exact geometry of the CFD model could be used to generate a 3-D model for prototype manufacturing. Pump prototypes were then created using the SolidWorks through the lofting tool (including surface lofting). **Figure 3** shows the SolidWorks drawing of the four bladed blood pump design. The prototypes included two housing regions (inlet length of pipe and outlet section) and the pump itself. The prototype sections were manufactured using a rapid prototyping technique called stereolithography (SLA) equipped with solid-state (Nd: YVO) lasers. **Figure 4** displays the blood pump prototypes that were constructed and evaluated in this research. **Table 1** represents detailed characteristics of four blood pump prototypes.

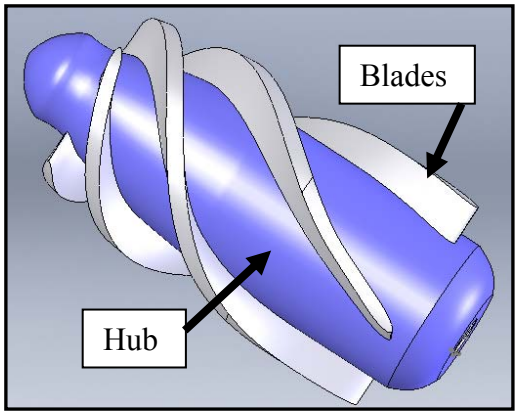

Figure 3: SolidWorks image of blood pump prototype

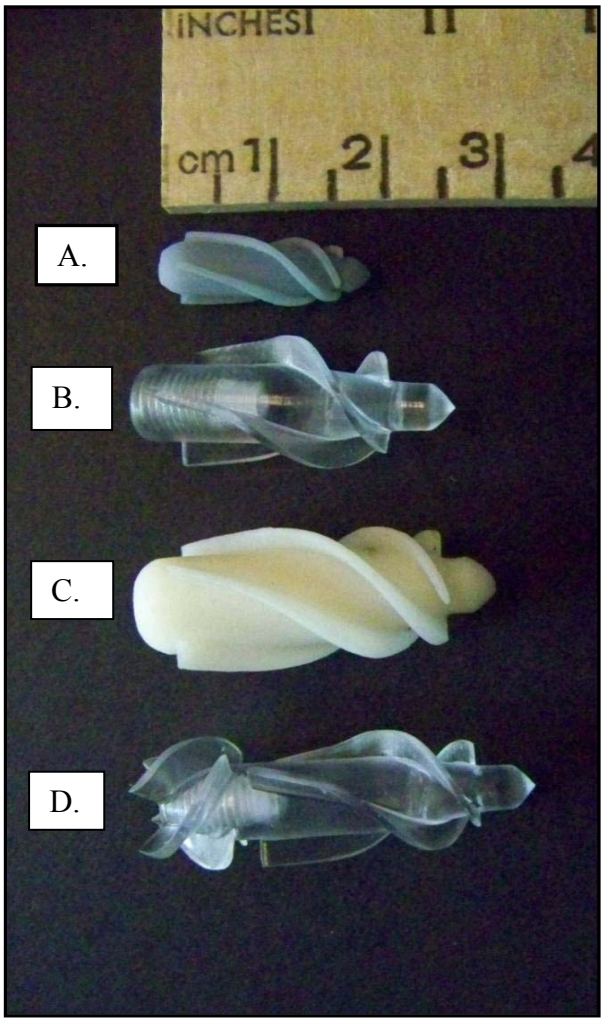

Figure 4: Blood pumps constructed and evaluated in this research. A. Infant blood pump prototype. B. Adult blood pump with 3-bladed impeller. C. Adult blood pump with 4-bladed impeller. D. Adult blood pump with 3-bladed impeller and a diffuser

Table 1: Detailed characteristics of four blood pump prototypes

Characteristics	Infant blood pump prototype (4 bladed impeller)	Adult blood pump prototype 4 Bladed Impeller	3 Bladed Impeller	3 Bladed Impeller and Diffuser
Number of blades	4	4	3	3-Imp & 4-Diff
Hub diameter (leading edge)	3.50 mm	5.60 mm	4.75 mm	4.75 mm
Hub diameter (trailing edge)	5.50 mm	10.0 mm	8.00 mm	8.00 mm
Blade height	1.00 mm	2.00 mm	3.00 mm	3.00 mm
Tip clearance	0.25 mm	2.00 mm	2.00 mm	2.00 mm
Length	18.50 mm	30.5 mm	28.6 mm	34.2 mm

The two housing regions were made of a transparent Acrylic resin material. Length of the inlet housing was determined to be approximately 5 times the inlet diameter of the pump to reasonably obtain a fully developed flow. The ends of the housing were designed such that they mounted to test loop without any leakage or dramatic change in fluid cross sectional area. Special care was taken during the design of the housing to ensure a smooth transitional fluid path. The housing also provided an acceptable clearance for the fluid between the blade tip and housing (0.25mm). **Figure 5(a)** and **Figure 5(b)** illustrate the SolidWorks model for the housing regions and the pump. **Figure 6** displays the actual prototype location in the housing.

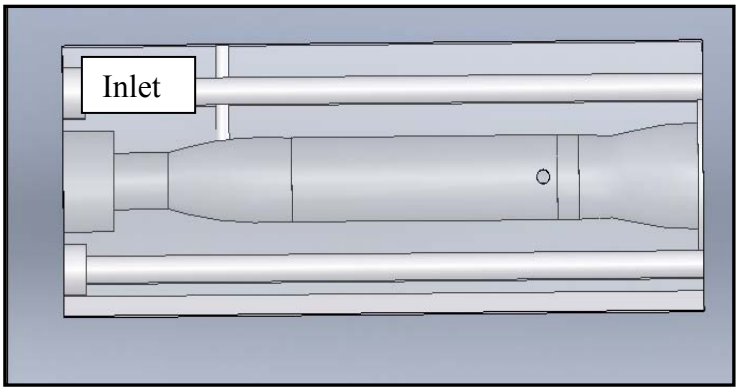

Figure 5(a): Part of housing at inlet tank

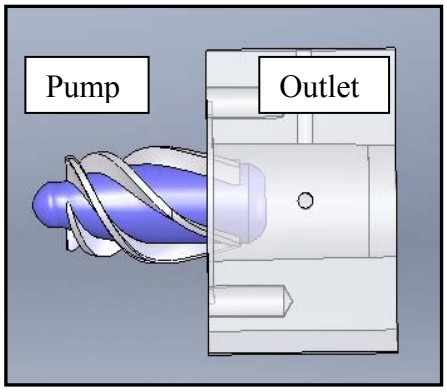

Figure 5(b): Part of housing at outlet tank

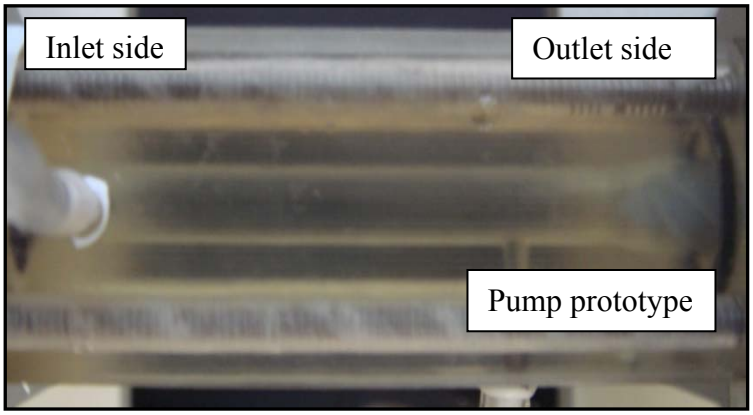

Figure 6: Actual prototype photograph of the combined housing parts and prototype position between the two

3.1.2 Hydraulic Flow Loop

The hydraulic flow loop **(Figure 7a and Figure 7b)** was designed and constructed for the hydraulic performance testing of the prototypes. The flow loop consisted of an inlet and outlet reservoir tank, differential pressure transducer, its amplifier, clamp, flow probe, flow meter, pump housing, motor, its controller, Labjack U12 and pump prototype.

Motor shaft assembly was controlled and drove rotation of the impeller at the desired speed. The shaft was coupled to the motor at rear end using a shaft coupling and aligned by mechanical bearings. We used a high speed, brushless DC motor (MicroMo Electronics Inc., Clearwater, FL, USA) with a motor controller. Pressure taps were located in the inlet and outlet reservoir tanks to capture the pressure rise across the pump using a differential pressure transducer (Validyne Engineering, Northridge, CA, USA). The pump housing was fixed between the tanks with the flanges at the inlet and outlet tank, and the prototype being tested was placed into the housing and mounted to the drive shaft. Fluid passed from the inlet tank into the outlet tank passing across the impeller. Fluid from the outlet tank continued to flow to the inlet tank through flexible Tygon tubing. A flow probe and a clamp were connected to the Tygon tubing, and the flow rate was varied by increasing and decreasing the resistance to the flow in the flexible tubing (i.e. by partially opening and closing the clamp). The flow rate through the loop was measured using the ultrasonic flow probe and the flow meter. Data collection software (Labjack Corporation, Lakewood, CO, USA) was employed for simultaneous measurement of the pressure rise and the flow rate. A sampling rate of 50 Hz was deemed acceptable given the steady flow conditions being tested. At a specific rotational speed, the pressure rise between the inlet and outlet tank was recorded with the clamp fully opened to allow a maximum flow rate. The clamp in the flow was then incrementally closed to increase the flow resistance, resulting flow reduction and increase in pressure.

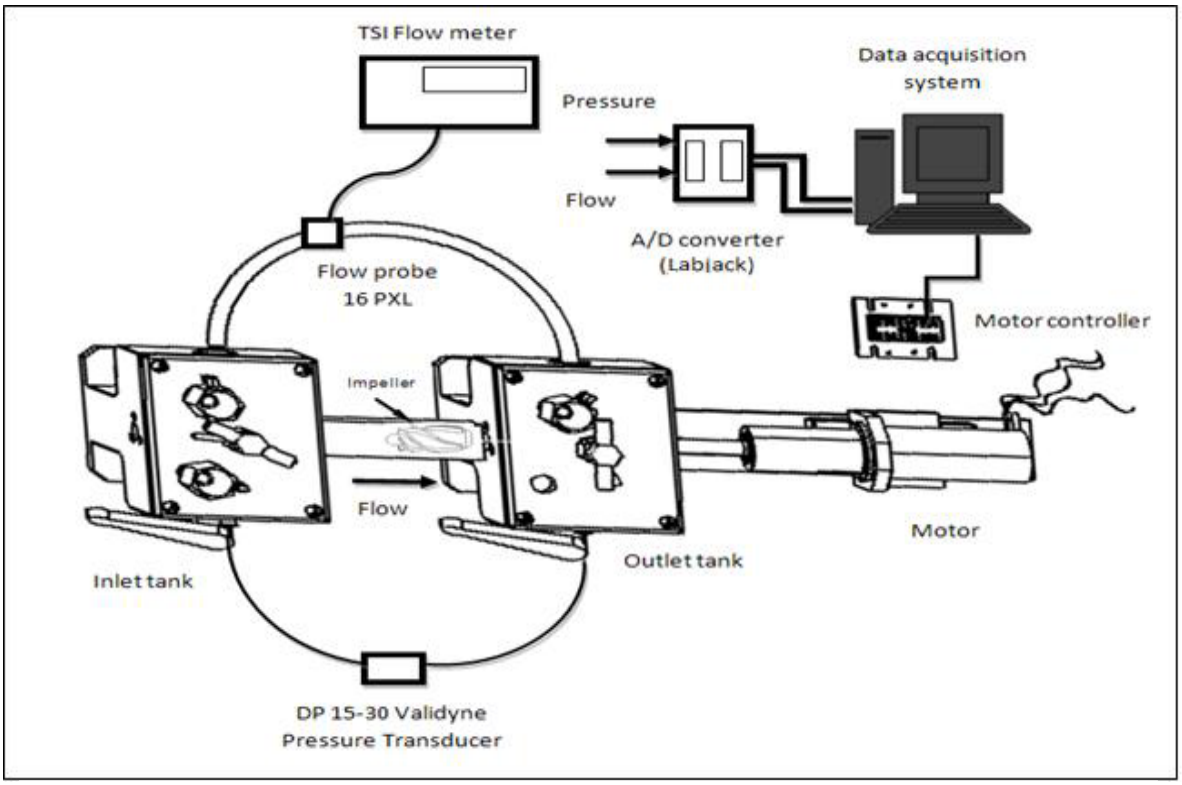

Figure 7(a): Schematic diagram of the hydraulic test loop

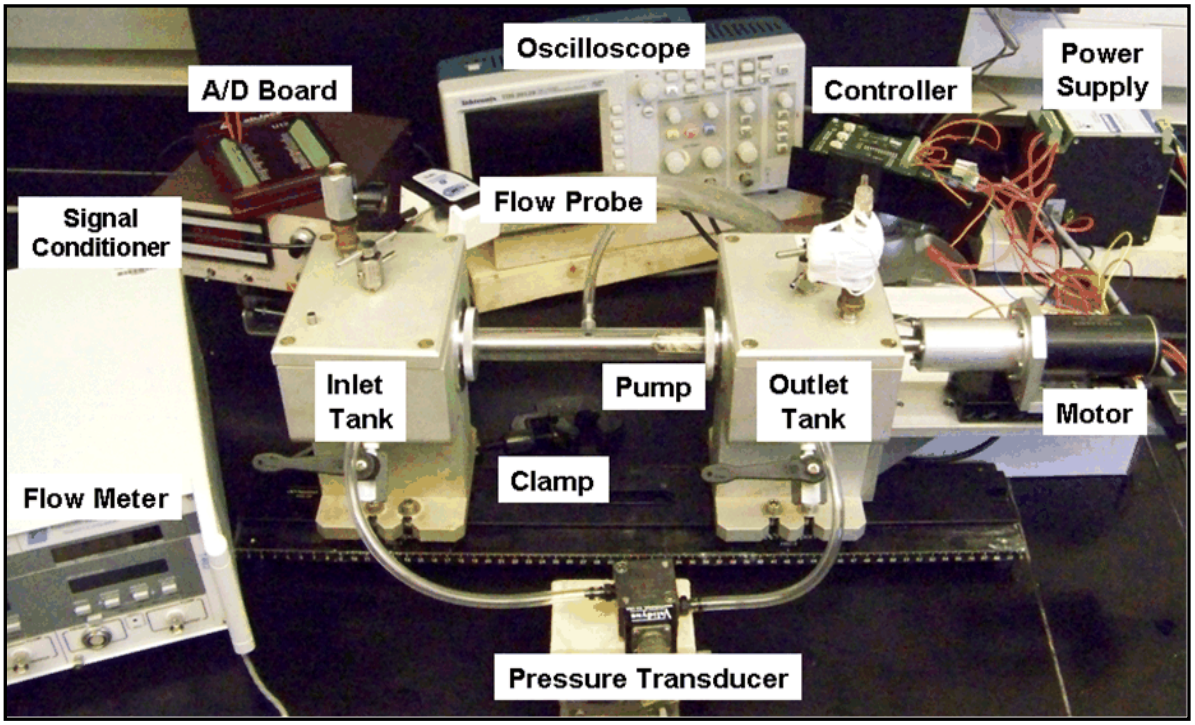

Figure 7(b): Experimental configuration of hydraulic flow loop, including two reservoir tanks, motor, motor controller, power supply, prototype, flow meter and probe, clamp

Design modifications in the hydraulic test loop were recommended by the manufacturer to reduce cost, improve production, and decrease vibration of the drive shaft. Originally 0.5" inner diameter seal (American High Performance Seals) was used for the fluid – shaft seal. The major problem associated with this fluid seal was high friction between the rotating shaft and fluid seal. Due to high friction, the shaft was not able to rotate at a speed more than 50 RPM. A new fluid seal was recommended by our industrial partner, 3 D Design & Manufacturing LLC. This fluid seal was softer and had a slightly larger clearance which decreased the friction and enabled rotation up to 8500 RPM. Lubrication of the ball bearing also improved operability. The former test rig **(Figure 8a)** consisted of two ball bearings and bearing mounts, mounts for the motor and translatory stage mount; whereas, the new test rig **(Figure 8b)** consisted of a single ball bearing, a needle bearing, and a single mount for motor and translatory stage.

Further modifications were also made in the test rig for blood bag experiments (hemolysis testing). The first blood bag experiment carried out with the test loop (latest rig design) was ineffective with high trauma levels. A major cause of this blood damage was due to shear stress generated by the rotating shaft in direct contact with the blood and cell accumulation at fluid seal site. After observing the damage caused, the rig was modified and a new shaft sleeve was added in the outlet tank to protect red blood cells from the rotating shaft. This sleeve was embedded with an infusion port to flush out all the blood particles that may accumulate. **Figure 8c** illustrates the new modified shaft sleeve for the blood bag experiments.

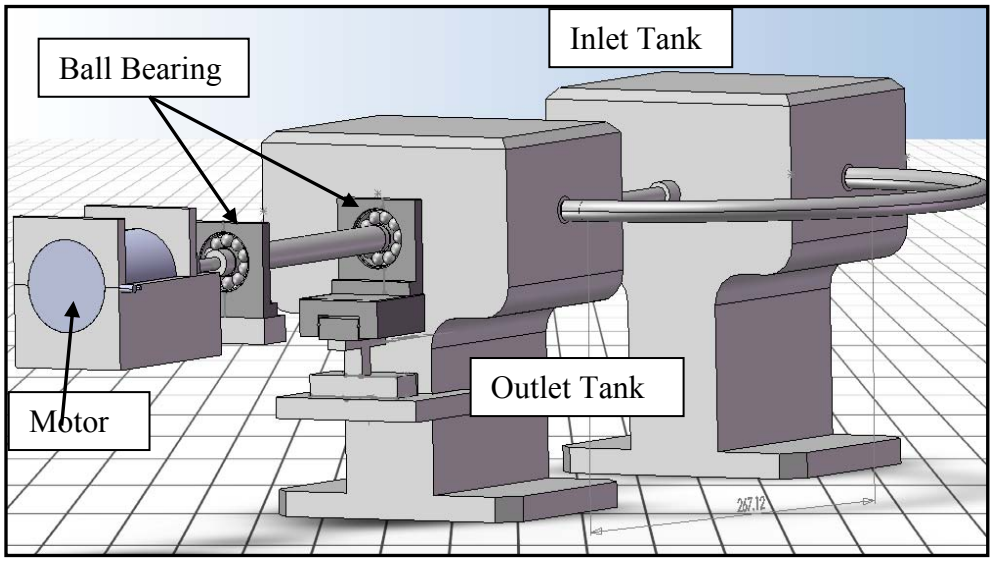

Figure 8(a): Test loop before design optimization with two ball bearings and AHP fluid seal

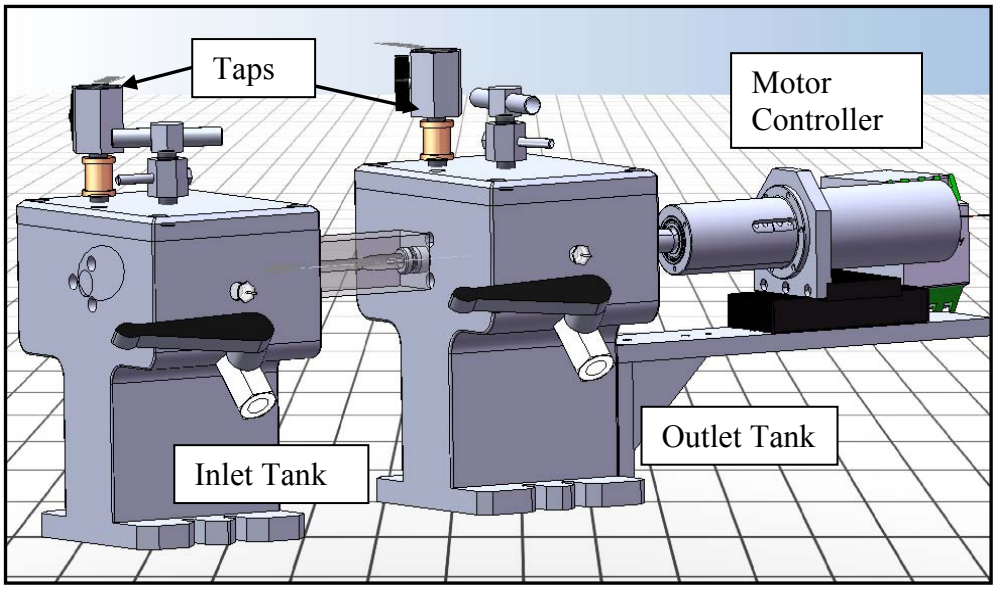

Figure 8(b): Test loop after design optimization with a single ball bearing

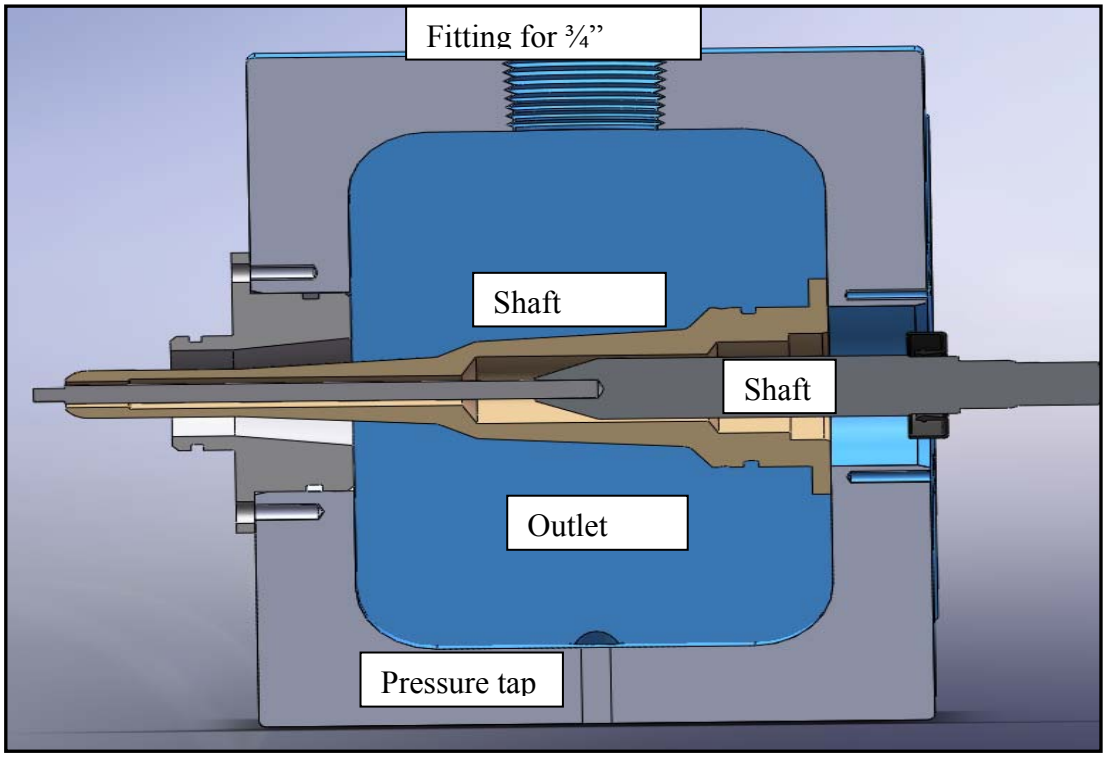

Figure 8(c): Modified design with shaft housing for blood bag

3.1.3 Blood Analog Solution

A water and glycerin solution was appropriately mixed as the blood analog fluid. Blood behaves as a Newtonian fluid for shear stresses greater than 7 Pascal, as would be expected in the fluid domain of this pump. The instruments used for preparing the water/glycerin solution or blood analog solution were a hydrometer and a Cannon–Fenske Viscometer (18). The following sections detail the procedure and technique used for each fluid property determination.

Figure 9: Hydrometer

Hydrometer

A hydrometer **(Figure 9)** measures the specific gravity of a fluid relative to water. It comprises a thin glass tube diverging into a cylindrical region at the bottom base and contains lead or another type of metallic beads in the base region. It drops a shorter distance into less dense liquids and goes deeper in a liquid with a higher density as relative to water. We added 500 ml of the water/glycerin solution into a large graduated cylinder. The hydrometer was lowered into the cylinder and allowed to buoyantly stabilize. Readings were then taken on the scale for the specific gravity.

Cannon-Fenske Viscometer

Cannon-Fenske viscometer **(Figure 10)** was employed to measure the viscosity of the solution in units of centistokes. The dynamic viscosity (μ) of fluid can then be calculated from the given formula:

$$\mu\ (cP) = \text{viscous constant } (cSt/s) * \text{density } (g/cm^3) * \text{drain time}(s) \qquad [1]$$

Drain time is the measured time that passes between line 1 and line 2 of the viscometer. The more time that the fluid takes to pass through that distance, the higher the viscosity of the fluid. The viscous constant depends on the size of the viscometer. Size 50 was selected, which has a capillary tube characteristic constant of 0.004 cst/s ± 0.0002 and viscosity range from 0.8 to 4.

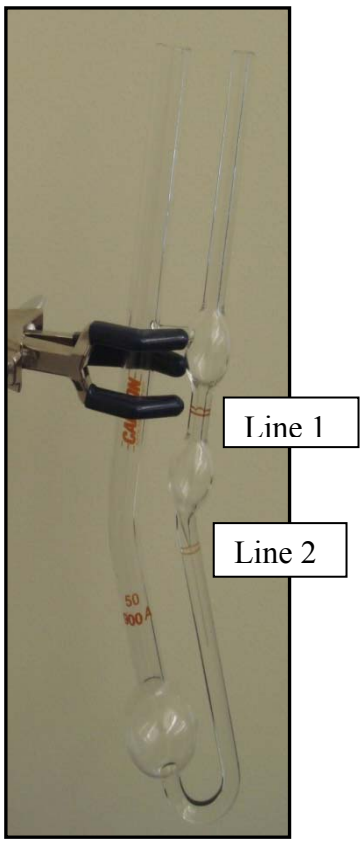

Figure 10: Canon-Fenske viscometer

The viscosity of the fluid was measured as follows:

1. Rinse the viscometer with soap and water to remove any residual water/glycerin solution.
2. Introduce the fluid sample into the viscometer by immersing the tube with smaller diameter into the fluid and applying suction using a pipette suction bulb. Adequately fill it with fluid and no air bubbles.
3. Invert the viscometer immediately and record the drain time between line 1 and line 2 using a stop watch.
4. Complete 5 to 6 times to show repeatability and to increase confidence in the measurements.

3.1.4 Pressure Transducer Calibration

A major objective of this study is to characterize the pressure generation of the axial flow prototype. In the test rig, the differential pressure transducer DP15-36 was used with CD 223 dual channel digital transducer indicator. This indicator was connected to the Labjack U12 A/D converter (data acquisition system) which was interfaced to the PC. Pressure readings in voltage were stored in data files. For the transducer calibration, two water columns with nozzles at the bottom were used, as shown in **Figure 11**. These two nozzles were connected using tubing to either side of the differential transducer. One of the water column levels was kept constant. For the other water column, the height was incrementally reduced from 60 inches to 40 inches. This resulted in a differential pressure reading as achieved due to the height difference between the water columns (h1-h2). The pressure differential as generated was indicated by CD223 dual channel digital transducer indicator. The transducer output was demodulated, amplified, and filtered to produce an input proportional to the pressure measurement, D.C. output. The output was displayed by a 7-segment gas plasma display. Individual channel ZERO and SPAN controls are provided to set the gains of the demodulator/amplifier as appropriate to the physical measurement.

Output of the digital transducer indicator was wired to Labjack U12 A/D converter which was connected to a PC through USB cable. Labjack software was installed on the PC, and the LJ stream (test) was carried out at 50 scans/minute. Data files of sampled voltage readings were generated for each individual water level and thus each pressure measurement for variable water column. Twenty different data points were

collected thereby obtaining twenty pressure difference readings. These voltage measurements for different heights were carried out five times. Average of the voltage measurements for each individual height difference was calculated.

Figure 11: Pressure transducer calibration experimental set up

3.1.5 Flow meter calibration

Two flow probes (8PXL and 16PXL) were specifically calibrated by the company Transonic Systems Incorporated. Flow meter correlations were carried out to obtain calibration curves for the flow probes. The blood pump was rotated at 6500 RPM. The flow meter sensor was set to the water/glycerin solution by operating sensor controls in Program menu Bar. Flow meter was connected to Labjack U12 from rear panel ports to interface it with the PC. Sampling rate for the Labjack was set to 50 Hz. Excel data files were generated in the same way as for pressure transducer calibration in order to derive a mathematical relationship between the physical flow rate (L/min) and measured voltage.

A clamp was used to occlude the flexible tubing with the ultrasonic flow probes. By clamping the flexible tube to varying degrees, different flow rates were achieved for both the flow probes. Thus, 20-25 different flow rates were recorded from the digital readout of the flow meter. By this procedure, 20-25 data files were obtained with respective voltage reading and the recorded physical readout; a correlation curves were generated between the flow rate and voltage to use for data analysis.

3.1.6 Motor and Controller Set Up

We purchased and used a brushless DC servomotor 4490H024BK1155 for rotating the blood pump at a controlled speed. Two controller configurations were used during the project.

Initial Configuration: Originally the motor was controlled by the motion controller MCBL 3003/06 S. It is an external motion controller for brushless DC

servomotors with linear Hall sensors, which can be operated without additional encoders. MCBL 3003/06 S is based on high performance digital signal processing processor (DSP) that enables high control quality, precise positioning and very low speeds. The motor was connected to the drive shaft through a coupling. The rotation of the motor was interfaced to motion controller, and connections were specified according to the configuration in **Table 2**. To power the motor and controller, we used a PSM 24-360S (Rhino Power Supplies-PSM series). The maximum output power is 360 W. The power supply was connected to the controller according to the configuration in **Table 3**.

Table 2: Motor-controller interfacing characteristics

Connection	Characteristic
Ph A	Motor phase A (brown)
Ph B	Motor Phase B (orange)
Hall C	Hall sensor C (grey)
Hall B	Hall sensor B (Blue)
SGND	GND signal (black)
+ 5V	VCC (red)
Hall A	Hall sensor A (green)
Ph C	Motor phase C (yellow)

Table 3: Controller-power supply interfacing

Connection	Characteristic
TXD	RS 232 TXD
RXD	RS 232 RXD
AGND	Analog GND
Fault	Error output
Anln	Analog input
+24 V	+24 V
GND	GND
3.In	3rd supply

Care was taken to accurately connect the power supply to the motor as a polarity change could destroy an internal fuse. The motion manager software was downloaded from Faulhaber group website to activate the motor controller. The controller was interfaced to PC via 9 pin null modem F-F RS232 cable. In order to drive a motor via the Motion Manager, follow this procedure:

1. Connect drive unit to a serial interface of the PC (e.g. COM1) via null modem cable and switch on.
2. Start the FAULHABER Motion Manager software.
3. Activate serial interface as communication.
4. Set desired transfer rate and node address.
5. Press “send” button.
6. The settings are transferred to the controller.

When using the motion manager, the most common commands were these subsequent terms:

1. Activate drive

“EN” Command and the “send” button

2. Operate motor

“V100” Drives motor with 100 rpm velocity

3. Change direction of rotation

“dirin” changes the direction

4. Disable drive

“di” disables the driver and motor stops rotating

After running a few experiments, there was a sudden overheating of the motor, and the internal fuse of the controller blew. Then we employed the same motor-controller set up again tried the run the pump, but the same problem occurred. We lost two controllers and motors attempting to rotate the blood pump. The manufacturer (Faulhaber Group) informed us that there was fault in the controller which led to this failure. They recommended that we consider using a new Servo Amplifier BLD 5018 which is a 2-quadrant pulse width modulator (PWM) speed controller.

New configuration: The new controller became a 2-quadrant PWM speed controller Servo amplifier BLD 5018 that does not require an external encoder. The rotational speed was controlled by hall sensors. The adjustment of the motor speed set value and the speed adaptation as well as the current limitation can be set by internal trimmers. The same 24 Volt power supply was used for this new configuration. In this controller, the speed may be set by an external potentiometer or an external voltage.

The servo amplifier consists of two connectors X1 and X2. Connector X1 is a 5 pin power and motor supply connector. Connector X2 is a 9 pin signal command connector. It also has 3 internal potentiometers to control speed range (maximum and minimum speed), current through the motor and the actual rotational speed. **Table 4** shows configuration for connectors X1 and X2, motor and power supply.

In order to drive a motor via the Servo amplifier BLD 5018, this procedure was followed:

1. Connect “Rev” to GND 8 or low level to turn the shaft in clockwise direction.
2. Connect “Dis” initially to low level or GND 8 to turn off the motor. “Dis” not connected or high level motor starts running.
3. Connect Motor to L1, L2 and L3.
4. Connect Hall sensors H1, H2 and H3 as well as Hall sensor to supply to “UH4” and GND to “GND 5” from hall sensors.
5. Set the speed limit potentiometer to set maximum and minimum speed.
6. Connect the supply voltage.
7. Adjust the speed of rotation and current with speed potentiometer and Imax potentiometer (preferably keep Imax to left position to have pass current of 6 A).

Table 4: Configuration for connectors, motor and supply

Pin number	Connector X2	Motor
1	H1 (hall sensor)	Hall sensor A (green)
2	H2 (hall sensor)	Hall sensor B (blue)
3	H3 (hall sensor)	Hall sensor C (grey)
4	UH (supply voltage for hall sensor +5 V)	Red
5	GND (ground for hall sensor)	Black
6	Dis (Control input disable)	
7	Rev (control direction of the rotation)	
8	GND (ground for control and set value input)	
9	Spd (set value input for speed)	
	Connector X1	
1	Ub (Supply voltage)	Supply +ve
2	L1 (Motor winding 1)	Brown
3	L2 (Motor winding 2)	Orange
4	L3 (Motor winding 3)	Yellow
5	GND (ground for supply voltage)	Supply – ve or gnd

For stopping the motor, it is not advisable to make the set value to 0, but to support this through a disable toggle switch. Inductors were used in series between the 3-phase brushless DC-servomotors and motor windings of Connector X1 to prevent overheating of the motor while running. Inductors used were having 220 μH with high current tolerances. The rotational speed was determined by measuring the frequency of the pulses (signal) between the one of the hall sensor terminal and GND 5. Frequency of the signal was measured using a digital oscilloscope and connecting a probe to these two terminals. The relation between the RPM and frequency of the signal is as follows:

1 pulse = 1 revolution

25 Hertz signal = 25 revolutions per second

Hence, 25 X 60 revolutions per minute = 1500 RPM

3.1.7 Hemolysis testing for the adult blood pump prototype

After instrument calibration and fixing the motor controller, we performed a blood bag experiment to assess the level of blood trauma. The hemolysis evaluation was carried out using fresh bovine whole blood in order to test the blood compatibility of the pump. The blood bag studies were performed in the flow loop that was used for estimating hydraulic performance of the blood pump. A constant flow rate of approximately 3.7 LPM was maintained for a pump rotational speed of 3000 RPM for 6 hours. To investigate the degree of hemolysis for this device, blood samples were tested every hour for plasma free hemoglobin.

Several modifications were made to the hydraulic loop that was used for testing the flow performance of the blood pump prototype before performing blood bag experiments. A shaft sleeve was added to the outlet tank in order to protect red blood cell from directly contacting the rotating shaft as shown in **Figure 8c**. The inlet and the outlet port for the pressure measurements were used as access ports to sample or introduce blood. A thermocouple was inserted into the inlet tank through the opening on the lid in order to measure the blood temperature in the flow loop. The rig was partially submerged into a warm water bath throughout the experiment to maintain temperature of the blood around 37^{o}C. The filling valve on the lid of the outlet tank was used for introducing the blood through IV set. The internal aluminum surfaces of the inlet and the outlet tank were anodized. This electrochemical processing thickened the naturally occurring oxides of aluminum tank. The flow loop was filled with phosphate buffered saline (PBS) solution for three hours to wet the internal surface which was going to be exposed to blood.

Fresh bovine blood was collected from a healthy donor. A large bore, 14 gauge needle was used for the venipuncture. Blood was then collected in a standard 500mL blood bags containing citrate phosphate dextrose adenine (CDPA) anticoagulant and stored at 4^{o}C during the transport. Transportation time was less than two hours and on arriving blood bags were gently placed into a water bath maintained at 37^{o}C. The PBS solution was drained from the test loop.

Blood was then introduced into the loop after filtering it through a 150 micron filter. After the blood temperature was equilibrated to 37^{o}C, a blood sample was collected for the baseline measurement (initial condition, time=0). The pump was rotated

increasing the speed gradually in order to reduce the sudden shear that could damage the blood cells exposed to impeller blades and to follow clinical startup procedures. Within 15 minutes the pump reached rotated at 3000 RPM, and flow rate was maintained at 3.7 LPM. Then, the blood sample was collected at an interval of every hour. Approximately 4-7 ml of blood was collected as a sample from the inlet tank and the same amount of blood was re-introduced from the outlet tank in order to maintain the constant volume of blood within the circuit. The total amount of blood added to the system was less than 1% of the total circulating volume and therefore should have had a negligible effect on the results. After taking the sample of blood, the sleeve (for the shaft) was flushed with saline solution to wash any of the accumulated blood particles in the shaft sleeve clearance. An infusion port was present at rear end of the sleeve for introducing the flushing saline solution.

From each sample, 2 ml of blood was used to measure the sample hematocrit. (Hematokrit 210 from Andreas Hettich GmbH & Co). Two measurements of hematocrit were completed for each sample by rotating the samples at 4000 RPM for 7 minutes. The measurements were averaged. Additionally two separate 2 ml samples were transferred to tubes containing ethylenediamine tetra acetic acid (EDTA). These samples were also centrifuged for 8 minutes at 4000 RPM. Using a transfer pipette, the plasma layer was introduced into a 1.5mL polystyrene disposable cuvette for spectrophotometric analysis. The optical density or absorbance was determined for 4 wavelengths: 576.5 nm, 596nm, 593nm and 560 nm. The spectrophotometer was calibrated using a blank cuvette prior to each analysis of the sample for all 4 wavelengths. The plasma free hemoglobin was

calculated based on the weighted difference in absorbance measurements using **equation 2** (24):

$$\Delta pfHb(mg/dl) = A_1 - A_2 - 176(A_2 - A_3)\left(\frac{\lambda_1 - \lambda_2}{\lambda_3 - \lambda_4}\right) \qquad [2]$$

Taking the plasma free hemoglobin value obtained from the above equation, the normalized index of hemolysis (N.I.H) was calculated as described in **equation 3** (24):

$$N.I.H(mg/dl) = V * \frac{\Delta pfHb}{\Delta t * Q} * \frac{(100 - Hct)}{100} \qquad [3]$$

where $\Delta pfHb$ corresponds to plasma free hemoglobin (mg/dl) over the time interval, Hct represents hemotocrit (%), Δt is the sampling time in minutes, Hb corresponds to total hemoglobin concentration, Q represents the flow rate in liters per minute, and V is the circulating volume of the hydraulic loop in liters. This index represents the degree of hemolysis for blood pump rotated in a hydraulic test loop for 6 hours. A statistical analysis was performed to interpret the results, and this will be discussed under the statistical analysis section later in this thesis.

3.1.8 Protective cage design for adult blood pump prototype

In addition to blood bag experiments, the research involved the development of a protective cage of filaments. Anatomically, the filaments of the cage would act as a stent to prevent the vessel wall from collapsing during rotation of the pump and to ensure no blade-vessel wall contact. This cage will also help in stabilizing the position of the blood

pump in the IVC. Hydraulic testing of the blood pump with cage was carried out in the same test loop (**Figure 7(b)**). After several designs, we devised the optimal design with the help of our research team and manufacturers. The cross sectional area of the housing was widened to 18 mm throughout (with no tapering at the ends and still being a valid diameter in patients). Along with this new design, new flanges for the inlet and outlet tank were built with the same inner diameter. The cage filaments and catheter for these filaments were designed using SolidWorks. **Figure 12** shows of the protective cage with filaments and supporting catheter. Five elliptically designed filaments were arranged radially around the impeller, and the length of these filaments was sufficient enough to surround the entire impeller. The catheter and protective cage with filaments were placed into the cylindrical housing and were supported using a ringed collar at the inlet tank of the flow loop. The filaments were designed to minimize flow disturbances and pressure loss across the assembly. The protective cage was made of 316-stainless steel. **Figure 13** illustrates the SolidWorks model for the protective cage assembly with the catheter support and a collar embedded into the housing. In order to achieve fully developed flow from the inlet tank to the blood pump housing was designed to be 200 mm in length. **Figure 14** illustrates the adult blood pump (4-bladed) mounted onto the drive shaft and placed into the radially arranged filaments.

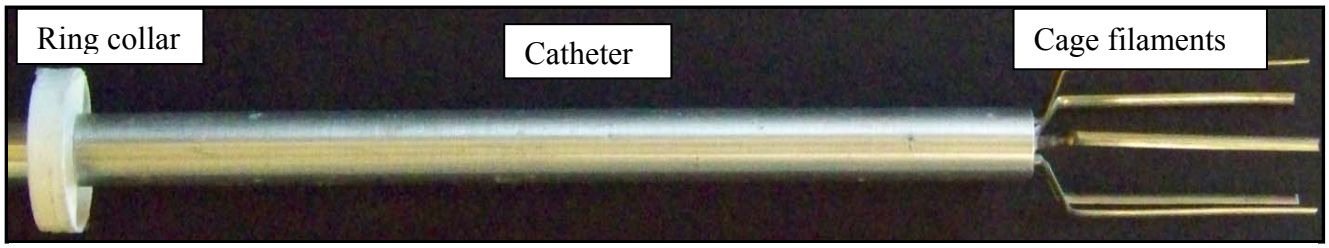

Figure 12: Protective cage with radially arranged filaments and supporting catheter

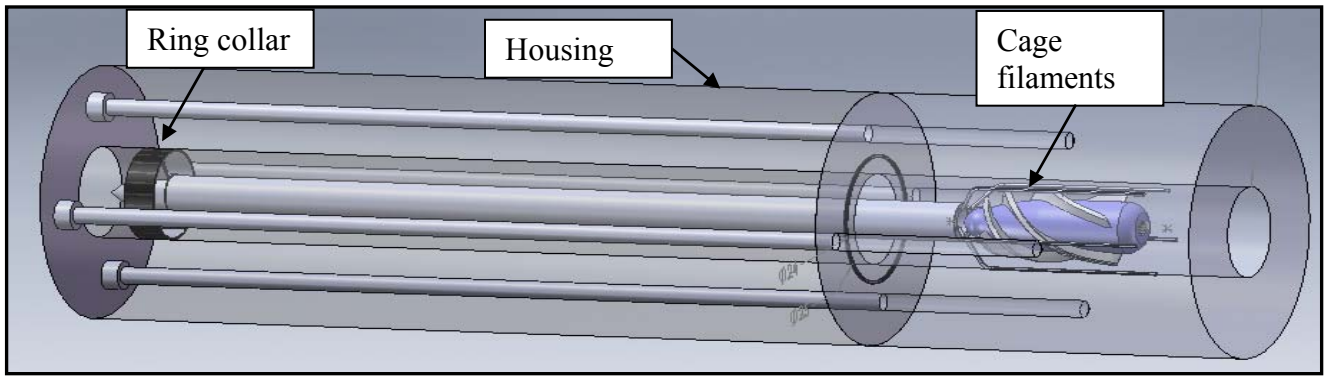

Figure 13: SolidWorks drawing of cage design for the adult blood pump prototype

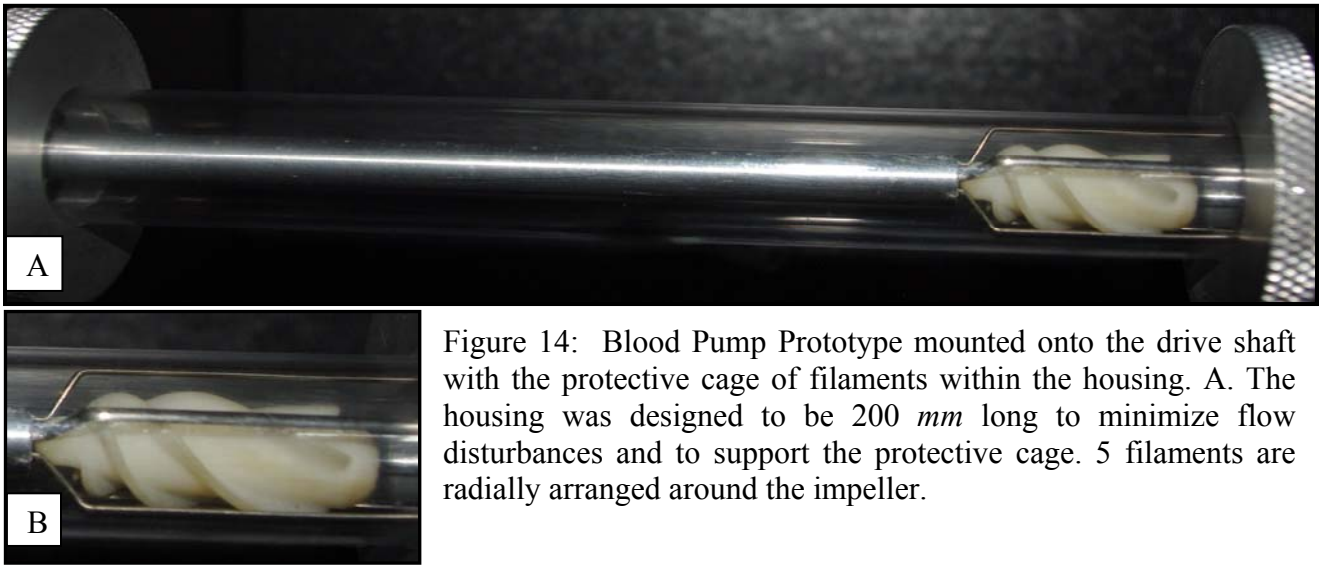

Figure 14: Blood Pump Prototype mounted onto the drive shaft with the protective cage of filaments within the housing. A. The housing was designed to be 200 *mm* long to minimize flow disturbances and to support the protective cage. 5 filaments are radially arranged around the impeller.

After completing the experimental studies (hydraulic and hemolysis testing) for the blood pump prototypes, the next step was to complete the numerical analysis (i.e. computational fluid dynamics analysis) using CFD software. A comparison between the numerical analysis and the experimental results is critically important for the design validation.

3.2 Computational Fluid Dynamics

With the advent of modern, high-speed, computer systems, numerical simulations, provide valuable physical insight during the preliminary design stage of pump development. Computational fluid dynamics (CFD) involves the replacement of governing partial differential equations (Navier-Stokes equations) of fluid flow with algebraic expressions to obtain a numerical description of the flow field (18). Since exact solutions are available for few physical flow circumstances, integration of these governing equations in practice is mainly done via numerical methods. ANSYS CFD software has been used to design centrifugal and axial flow blood pumps (25). Thus, the ANSYS turbomachinery software suite was used for computational modeling in this study.

Bladegen, a turbomachinery design software was employed to create the blade geometries for the blood pump. Software users can modify existing blade designs or create completely new designs. ANSYS CFX-Mesh and Turbogrid were used to generate mesh for the CFD analysis (18). A grid density and a convergence study were performed to ensure grid quality. In this study grid was incrementally modified until the

performance results deviated less than 3%. After successful mesh generation, boundary conditions for the computational model were then set to carry out numerical simulations. The no-slip boundary condition was assigned to stationary walls so as to consider zero fluid velocity along these walls.

The k-ε turbulence model was used for the numerical simulations of the blood pump design (22). The k-ε turbulence model solves the equations for ε, the turbulence kinetic energy, and the dissipation rate of k. The dissipation rate of k is also defined as the amount of k per mass and time converted to internal fluid energy by viscous motion. Inflow rate and rotational speed was specified for each simulation. Viscosity of fluid was set to 3.5 cP which is similar to the viscosity of blood. A constant fluid density of 1,100 kg/m³ was applied for the simulations. The performance curves obtained from the simulations were compared with the experimentally measured hydraulic performance of the adult blood pump without the protective cage.

3.3 Statistical Analysis

3.3.1 Statistical analysis for the instrument calibration

All of the statistical calculations were carried out in an Excel spreadsheet. A level of significance or α value of 0.05 was assumed according to industry standard.

REGRESSION AND NORMALITY TESTING

A regression analysis was performed using a linear model on the calibration data for the pressure transducer and ultrasonic flow meter. In this method characteristic constants (β_0, β_1) were obtained that reflect the trends of the data mathematically. These

characteristic constants were assigned confidence intervals based on a 95% level. A normality check was performed using residual errors from the regression model, according to:

$$d_i = e_i / \sqrt{MSE}$$

Where d_i represents the standardized residuals at the i-th value, e_i corresponds to the residual error at the i-th value, and the MSE is the mean squared error. Approximately 95% of the values of d must fall in the interval of -2 to +2 to indicate normality. These terms were obtained from the analysis of variance identity:

$$\sum_{i=1}^{n} (y_i - \bar{y})^2 = \sum_{i=1}^{n} (\hat{y} - \bar{y})^2 + \sum (y_i - \hat{y})^2 \qquad [4]$$

SS Total **SS Regression** **SS Residual or Error**

Where SS signifies the squared sum, y_i reflects the measured value, $\bar{y}$ indicates the mean of the data and $\hat{y}$ represents the predicted y value obtained from the regression line. It was expected from the statistical analysis that mean of residuals or errors between the predicted and measured values should be approximately zero to indicate randomness.

The F-test for the regression analysis supported the significance of the coefficients and polynomial models based on data normality and a preset α value of 0.05. A Student T-test was also performed to ensure that the coefficients of the polynomial have values other than zero (null hypothesis each coefficient tested equals zero). The following table lists the statistical tests performed and their conditions (null and alternative hypothesis):

Statistical test	H_0 (null hypothesis)	H_a (Alternative hypothesis)
Regression F-test	$B_0 = \beta_1 = \beta_2 = \ldots = 0$	$B_0 \neq \beta_1 \neq \beta_2 \neq \ldots \neq 0$
Student T-test	$\beta_i = 0$, for i = 0, 1, 2 ..	$\beta_i \neq 0$, for i = 1, 2, 3 …

The regression analysis was performed for the flow and pressure calibration data to determine maximum and minimum values within a 95% confidence interval. These values were used to generate the error bars or range of deviation for each pressure and flow measurement.

3.2.2 Statistical comparison between experimental data and numerical simulations for adult blood pump prototype

To qualitatively compare the variation between experimental performance and computational results of the adult blood pump design, experimental data and CFD results were plotted on the same scatter plot. A nondimensional analysis was then performed to quantitatively compare the CFD predictions to experimental data for 4 bladed blood pump and compare the variation between the hydraulic performance of three blood pump prototypes with protective cage of filaments (18). The nondimensional analysis procedure involved collapsing the experimental and computational data for the blood pump at four different rotational speeds into pressure coefficients and flow coefficients:

$$\Psi = C_\Psi (\Delta P/\rho N^2 R^2) \qquad [5]$$

$$\Phi = C_\Phi (Q/NR^3) \qquad [6]$$

where Ψ represents the pressure coefficient, Φ is the flow coefficient, ρ denotes the density of the fluid in kilograms per cubic meter, R signifies radius of the impeller in millimeters, N indicates rotational speed (RPM), Q denotes the flow rate in L/min, ΔP is the pressure of the pump in mmHg, C_Ψ is a pressure factor equal to 1.2157 x 10^{10}, and C_Φ symbolizes a flow factor equal to 1.5195 x 10^5 (18). The coefficients for each data point were calculated and graphed to create a scatter plot. A regression analysis was then performed using a polynomial regression model for both sets of results. The statistical regression model generated characteristic constants (β_0, β_1, β_2) as described in the following equation, where the subscript 'type' indicates the pump prototype:

$$\psi_{TYPE} = \beta_3\left(\phi_{TYPE}{}^3\right) + \beta_2\left(\phi_{TYPE}{}^2\right) + \beta_1\left(\phi_{TYPE}\right) + \beta_0 \qquad [7]$$

The F-test for the regression analysis supported the significance of the coefficients and polynomial models based on data normality and a preset α value of 0.05. This procedure was carried for experimental and computational results and two separate mathematical equations were obtained. The equations were used to compare the hydraulic performance with the numerical results obtained through CFD simulations.

3.2.3 Statistical analysis for the hemolysis testing of the adult blood pump (4-bladed) prototype

The hemolysis test was run six times in order to increase power to the experiment thereby reducing the probability of Type II error in the experiment. Statistical power is a means of defining reliability of experimental results and concluding that the results are less likely to be due to chance only (26). Additionally, the regression model was run for

the experimental data to obtain R^2 and R^2 adjusted value to estimate the degree of correlation in the data. The Ryan Joiner normality estimation was performed on the plasma free hemoglobin level data obtained from the experiment to prove normal distribution of the data (a p-value greater than 0.1). A box plot was generated from the experimental results to show the graphical representation of the variability in plasma free hemoglobin level at each individual hour. Details of the variability in the experimental data is shown including mean, maximum, minimum, and maximum and minimum 95% confidence interval value of plasma free hemoglobin level at each hour starting from 0 to 6^{th} hour of the experiment.

A 1-way ANOVA (analysis of variance) was performed to evaluate the impact of time on the plasma free hemoglobin level of the experiment. For pairwise comparison between the means of the plasma free hemoglobin value at each time (i.e. 0, 1, 2 … 6 hour), the Tukey's test was performed. This analysis was performed using the statistical software; Minitab 15 and JMP 7.0.

Chapter 4: Results

4.1 Fluid property measurements

The density and viscosity of the test fluid were measured to ensure that a true blood analog was created and that values reasonably matched those used in the computational modeling. **Table 5** lists those fluid properties.

Table 5: Viscosity measurements and specific gravity of water/glycerin

Experiment	Drain time (sec)	Density (g/cm³)	Viscosity
1	792.324±1	1.098±0.0002	3.4798 ± 0.174
2	784.456±1	1.098±0.0002	3.4453 ± 0.172
3	802.342±1	1.098±0.0002	3.5238 ± 0.176
4	797.564±1	1.098±0.0002	3.5029 ± 0.175
5	801.798±1	1.098±0.0002	3.5214 ± 0.176
Average	795.697±1	1.098±0.0002	3.4946 ± 0.175

4.2 Pressure Transducer Calibration

Figure 15 presents the calibration results for the pressure transducer. A pressure range from 0 to 30 mmHg was achieved by varying the height difference from 0 inch to 16 inch. Twenty different data points were taken. The results show the expected linear trend between the measured pressure and the output voltage. Each data point on the graph

represents an average voltage for 5 measurements for each specific height difference and thus pressure examined. Excellence in repeatability is apparent by the closeness and overlap of data points and correlation coefficient (R^2) value of 0.99. The characteristic equation, Pressure (mmHg) = 41.21 (measured voltage) – 0.994, was used to obtain pressure from any voltage reading during the pump performance testing.

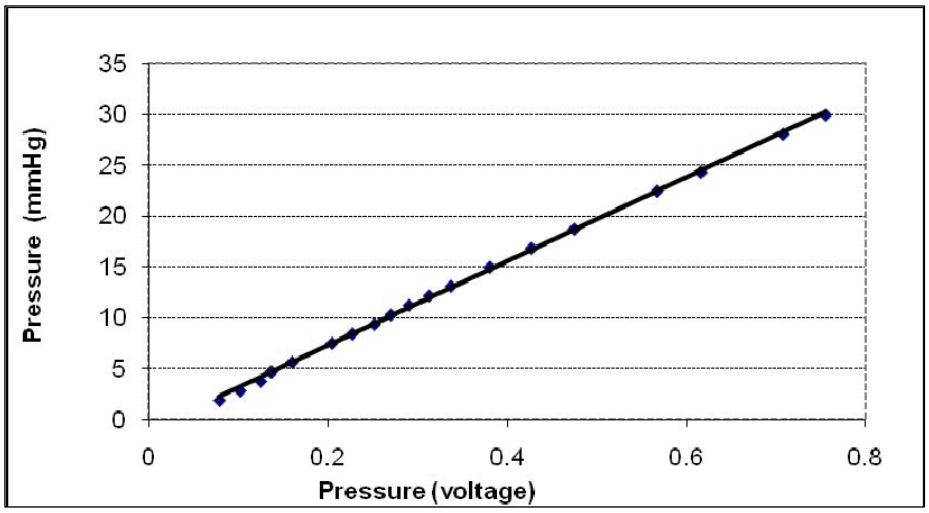

Figure 15: Pressure transducer calibration (relation between physical pressures and respective voltage)

4.3 Ultrasonic Flow Meter Calibration

Flow meter correlations were completed using the water/glycerin solution and by rotating the pump at 6500 RPM. The ½" and 1" flexible tubes were clamped to provide resistance and subsequently adjust the flow rate. Twenty six different flow rates were measured at 6500 RPM with a range of 55 to 525 ml/min were generated for 8PXL (smaller) flow probe and twenty different flow rates were measured with a range of 1.5 to 5.1 L/min for 16PXL (larger) flow probe. **Figure 16** and **Figure 17** demonstrate the

calibration results for flow probes. The regression trend line equation, Flow rate = 482.58 (measured voltage) – 6.4132, was obtained from the data for 8PXL flow probe, and Flow rate= 493.69 (measured voltage) – 6.1018 was obtained from the data for 16PXL; both trendlines have excellent correlation coefficient values of 0.99.

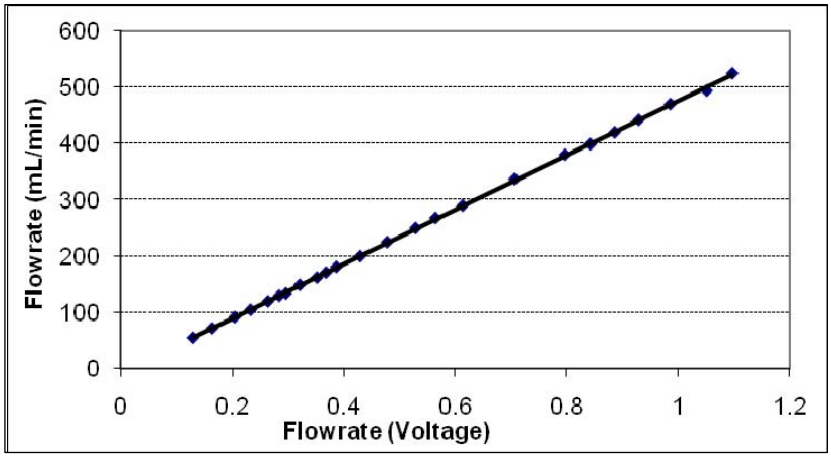

Figure 16: Flow meter calibration (relation between flow rate and voltage) for 8PXL flow probe

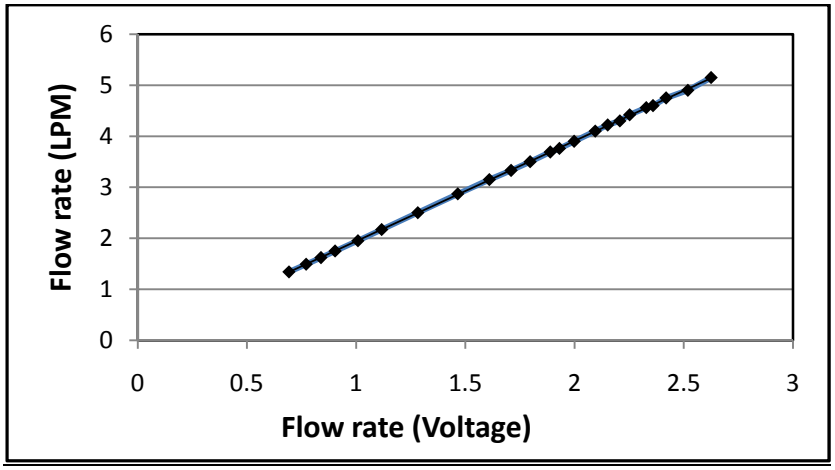

Figure 17: Flow meter calibration (relation between flow rate and voltage) for 16PXL flow probe

4.4 Prototype hydraulic testing

Building upon the instrument calibration, we then evaluated the hydraulic performance of the blood pump prototypes. The experimental test rig was arranged as shown in **Figure 6**. Initially the infant blood pump was hydraulically tested. Pump prototype was examined at three different rotational speeds of 5500 RPM, 6500 RPM and 7500 RPM. For each specific rotational speed 13 to 15 different flow rates were generated by clamping the Tygon tubing to different extents. Corresponding changes in the pressure between inlet and outlet of pump were achieved and measured. Pressure transducer and flow meter were connected to data acquisition system. Data was collected by the data acquisition system running at sampling rate of 50 Hz. Excel data files were generated for the following by interfacing labjack with the PC. Using the calibration equations, the performance curves for the pediatric blood pump prototype over the three different rotational speeds were determined. **Figure 18** illustrates hydraulic performance curves for the pediatric prototype (pressure rise and flow rate). The infant blood pump prototype was able to generate a pressure rise of 4-17 mmHg with a flow rate of 50-450 ml/min at three different rotational speeds of 5500, 6500 and 7500 RPM.

Secondly, the adult blood pump prototype (4-bladed) was hydraulically tested. For this experiment, the housing used was larger in size, and the Tygon tube was also larger in diameter as the flow rates are higher for adult prototype. In this experiment 20 to 30 different flow rates were generated for each rotational speed and respective pressure rise were measured. Using the calibration equations, the performance curves for the adult

blood pump prototype over the five different rotational speeds were determined. **Figure 19** illustrates performance curves for the adult pump prototype (pressure rise and flow rate). The adult blood pump prototype was able to generate a pressure rise of 2-30 mmHg with a flow rate of 0.2-11 Liters/min over four different rotational speeds.

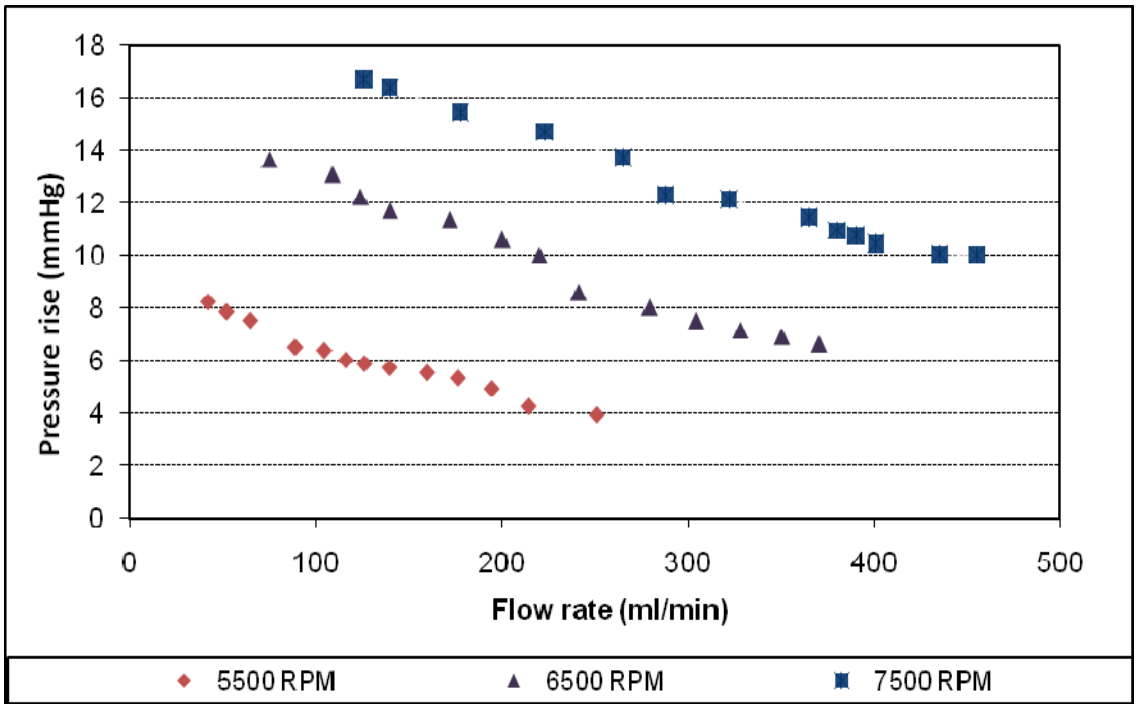

Figure 18: Hydraulic performance of axial flow infant blood pump prototype

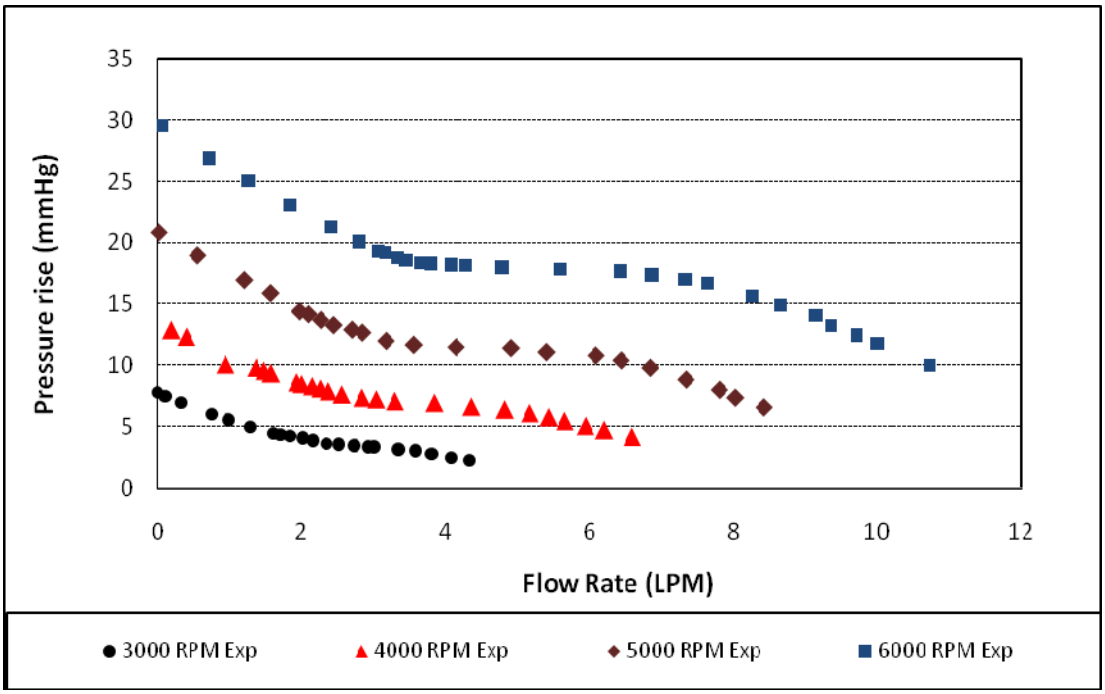

Figure 19: Hydraulic performance of axial flow adult blood pump prototype

4.5 Adult blood pump prototype (4-bladed) hydraulic testing with the cage filaments

The adult blood pump prototype with a protective cage of filaments was rotated at speeds of 4000 to 7000 RPM. The fluid properties of the blood analog fluid were measured and found to be similar to that of blood: 3.451 ± 0.173 cP and a specific gravity of 1.098 ± 0.002. **Figure 20** illustrates the pressure-flow characteristic performance

curves for the adult blood pump prototype with the protective cage of filaments over the examined rotational speeds. The hydraulic performance of the prototype met expectations with an increasing pressure rise for lower flow rates and an increasing pressure generation at higher rotational speeds. The 4-bladed impeller prototype was able to generate a pressure rise of 4 to 28 *mmHg* for flow rates of 0.5 to 13 L/ min at rotational speeds of 4000 to 7000 RPM.

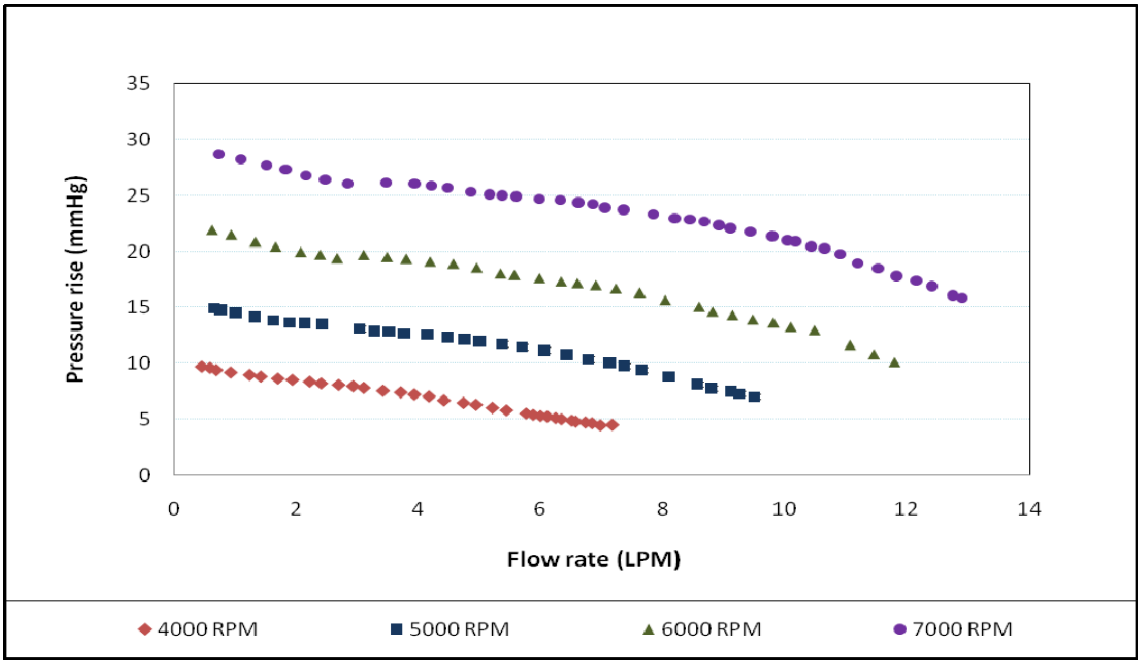

Figure 20: Hydraulic performance of adult blood pump prototype with protective cage of filaments

4.6 Hydraulic testing of 3- bladed blood pump and 3 bladed impeller with a diffuser blood pump with protective cage of filaments

For the hydraulic testing of the blood pumps with 3 impeller blades and 3 impeller blades with the diffuser blades, the same test rig was used. Again the blood pumps were rotated at 4000 to 7000 RPM. The fluid used was having the properties similar to the blood analog solution used for the hydraulic testing of a 4 bladed adult blood pump. **Figure 21** and **Figure 22** shows the pressure flow performance curves for the blood pumps with 3 impeller blades and 3 impeller blades with the diffuser blades respectively. The blood pump having 3 impeller blades only produced pressure rises of 4 to 22 mmHg for flow rates of 0.5 to 10 L/min at rotational speeds of 4000 to 7000 RPM. The blood

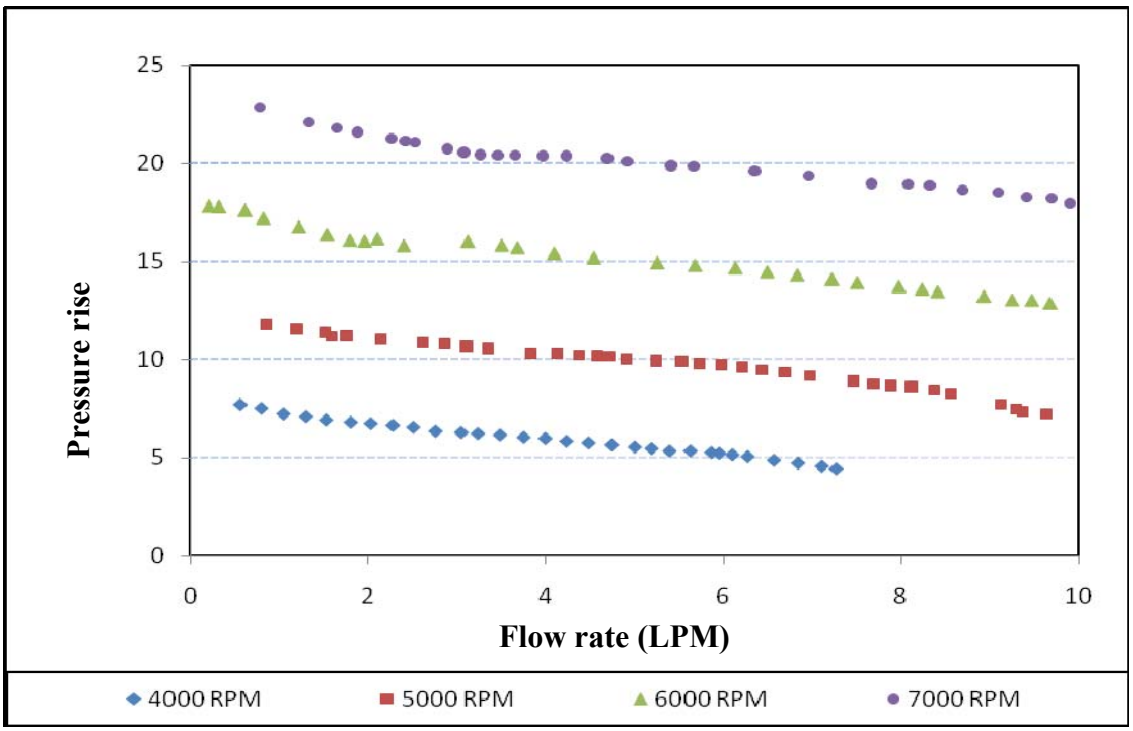

Figure 21: Hydraulic performance of blood with 3 impeller blades and without a diffuser

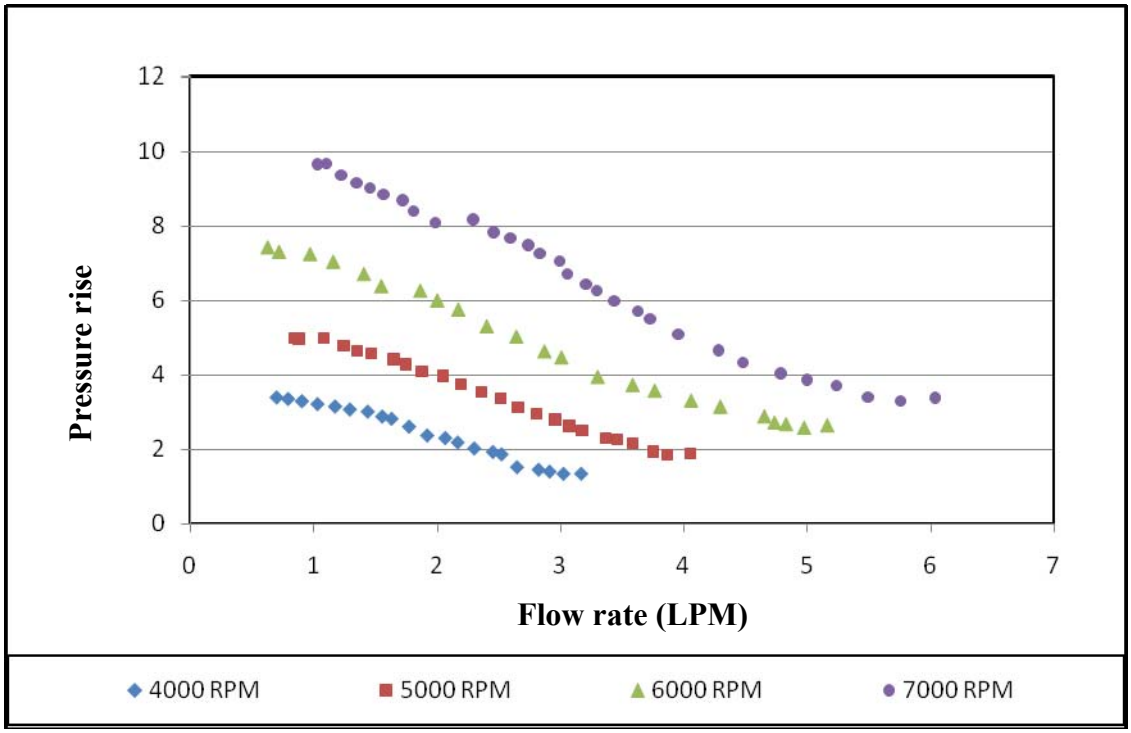

Figure 22: Hydraulic performance of blood pump with 3-bladed impeller and diffuser blades

pump with a diffuser, however, was able to generate a pressure rise of 1 to 10 mmHg with the flow rates of 0.6 to 6 L/min at rotational speeds of 4000 to 7000 RPM.

4.7 Hemolysis results for adult blood pump (4-bladed) prototype

Blood bag experiments were carried out to predict the blood damage that would be caused by the blood pump design. Specifically, the adult blood pump with the 4-bladed impeller was tested. Plasma free hemoglobin level was calculated for each hour during the six hour experiment using **Equation 2**. Using the value of plasma free hemoglobin level N.I.H (normalized index of hemolysis) was calculated using **Equation 3**. **Table 6** shows plasma free hemoglobin level calculated at each hour relative to initial

value (i.e. at time t= 0 hour plasma free hemoglobin level= 0) for six experiments. **Table 7** illustrates maximum N.I.H level for each experiment. These values were calculated from the hematocrit value and spectrophotometric analysis readings. **Figure 23** demonstrates the graphical representation of the plasma free hemoglobin vs. time (hour) for six experiments. Maximum plasma free hemoglobin level was calculated to be 20.04 mg/dl at the end of one of the six hour experiment. Maximum NIH level was found to be 0.017 g/100L.

Table 6: Plasma free hemoglobin level at different time for six experiments

Time	1st time	2nd time	3rd time	4th time	5th time	6th time
Hour	Plasma free hemoglobin level (mg/dL)					
0	0	0	0	0	0	0
1	2.8	1.25	2.96	3.67	2.68	1.17
2	4.86	5.1	7.5	6.42	7.11	3.71
3	7.36	8.81	8.46	7.65	10.33	6.68
4	12.46	10.12	10.83	11.35	14.3	9.84
5	16.76	12.86	13.56	14.11	16.27	13.71
6	19.52	16.54	17.2	15.32	20.04	17.91

Table 7: Maximum NIH level for each experiment

Normalized Index of Hemolysis (g/100 L)					
1st time	**2nd time**	**3rd time**	**4th time**	**5th time**	**6th time**
0.015	0.011	0.013	0.011	0.016	0.017

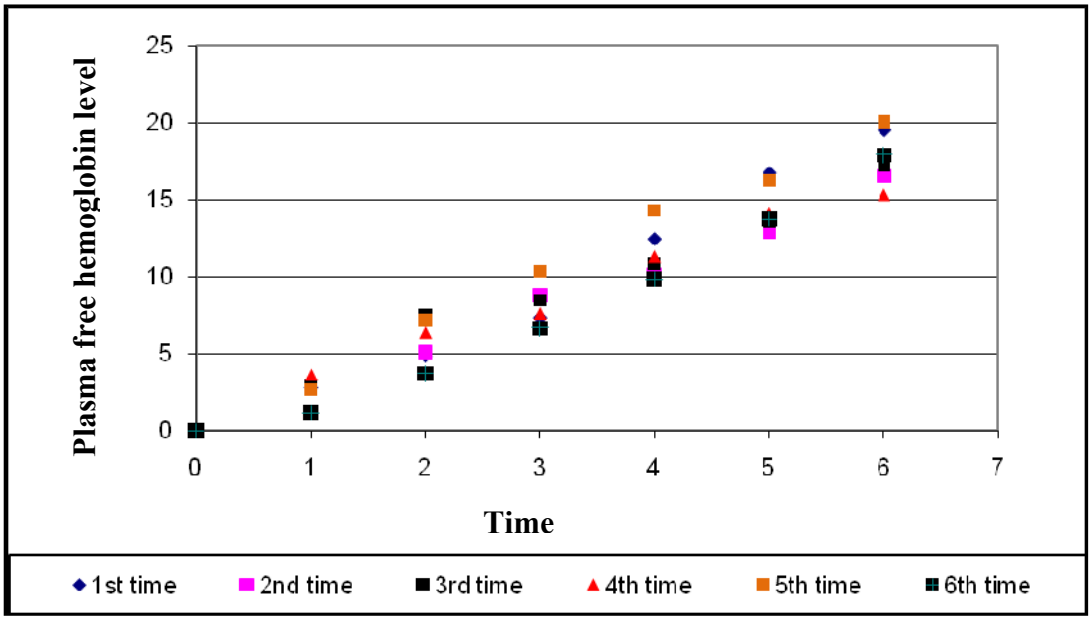

Figure 23: Graphical representation of plasma free hemoglobin level vs. time (hour) for six experiments

4.8 Computational fluid dynamics predictions

Computational fluid dynamics analysis was performed on the adult pump prototype design having a 4-bladed impeller. The pressure rise across the adult axial flow blood pump was determined for flow rates of 0.5-10 L/min over rotational speeds of 2000 to 6000 RPM with the k-ε turbulence model. **Figure 24** illustrates the pressure-flow performance curves for this computational model. Each data point corresponds to a steady state simulation for a specific flow rate and rotational speed; we completed 64 steady state simulations. The static pressure rise across the pump for a given rotational speed decreased with increasing flow rate as expected due to flow losses. A pressure range of 3-29 mmHg was achieved for the pump design over these operating conditions.

The pressure performance curves show the ability of the blood pump to deliver adequate flow range with desired pressure rises necessary to augment blood flow at cavopulmonary site of adult patients with failing Fontan physiology.

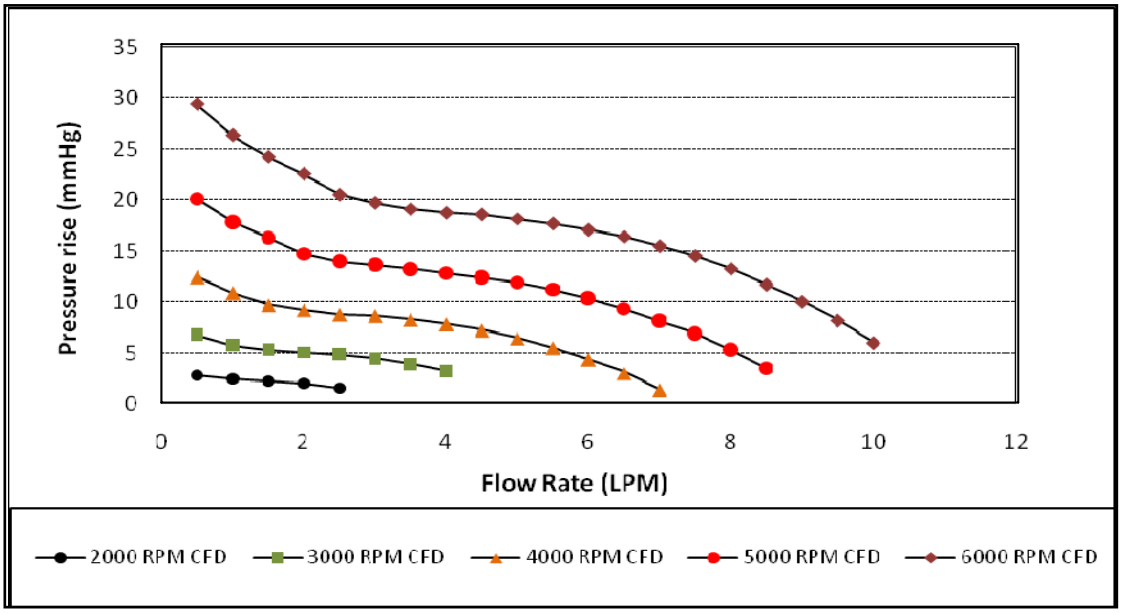

Figure 24: CFD predictions for hydraulic performance of adult blood pump design

4.9 Statistical Analysis and Results

4.9.1 Pressure Transducer

A linear regression analysis was performed, which produced a mathematical relationship between the physical pressure and the voltage measured during the calibration of the pressure transducer. The linear fit line for the pressure calibration curve with confidence intervals was determined:

Pressure mmHg = 44.216 ± 0.9454 (measured voltage) – 0.994 ± 0.3617 [8]

To support the conclusion of normality, **Figure 25** demonstrates that the standard and residuals fall well within +2 and -2. **Table 8** shows student T-test performed on the linear fit line for pressure transducer calibration data showing the significance for use each coefficient indicated by the p-value for each coefficient and student F-test for the regression analysis supporting the significance of the coefficients and the polynomial expression. The mean of the residuals was approximately zero, showing randomness in the data.

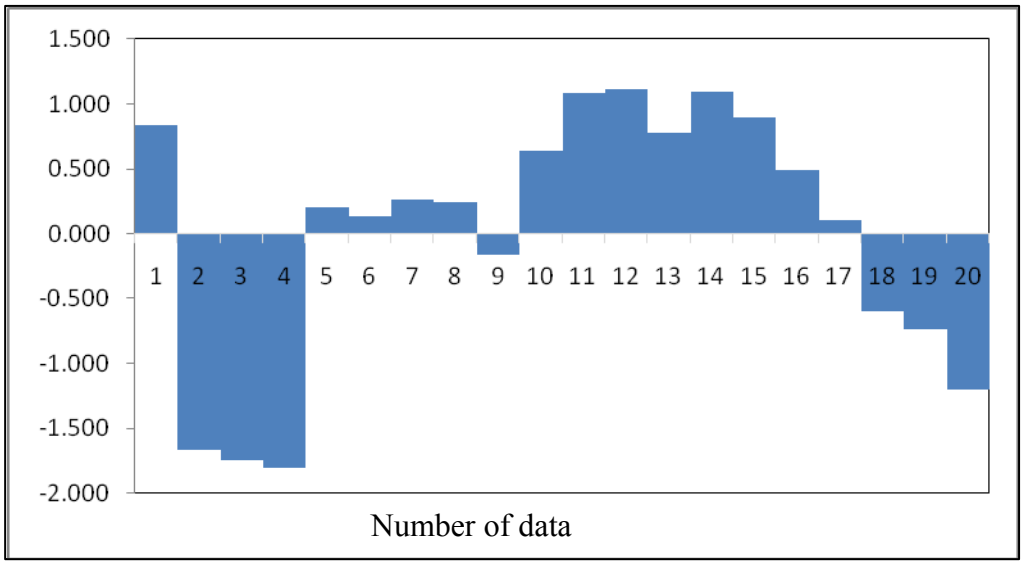

Figure 25: Standard Residual Plot for the Pressure Transducer Calibration

Table 8: Statistical parameters for the pressure transducer calibration

	Value	Confidence Interval	P value	R^2 adj	Mean Residuals	f (0.05, 1, 18)	f□
Slope (β_1)	41.216	± 0.9454	< 0.001	0.99933	-1.6×10^{-15}	4.414	28564.9335
Slope (β_0)	-0.994	± 0.3617	< 0.001				

4.9.2 Ultrasonic Flow Meter

A similar analysis was completed for the flow meter calibration. The linear fit lines for the flow calibration curves were calculated to be:

Flow (ml/min) = 482.5 ± 4.967 (measured voltage) – 6.413 ± 3.054 [9] and

Flow (ml/min) = 493.69 ± 1.489 (measured voltage) – 6.1018 ± 0.930 [10]

Likewise, the standardized residuals also fall within +2 and -2 as shown in **Figure 26** and **Figure 27**. **Table 9** and **Table 10** show student T-test performed on the linear fit line for pressure transducer calibration data showing the significance for use each coefficient indicated by the p-value for each coefficient and student F-test for the regression analysis supporting the significance of the coefficients and the polynomial expression. Again the mean of the residuals for both the flow probes calibration data was near to zero thus demonstrating randomness of the data.

Table 9: Statistical parameters for the flow meter calibration for 8PXL flow probe

	Value	Confidence Interval	P value	R^2 adj	Mean Residuals	f (0.05, 1, 18)	f□
Slope (β_1)	1.9655	± 0.009	< 0.001	0.9999	$3.73x10^{-16}$	4.301	212648.3
Slope (β_0)	-0.0237	± 0.016	< 0.001				

Table 10: Statistical parameters for the flow meter calibration for 16PXL flow probe

	Value	Confidence Interval	P value	R^2 adj	Mean Residuals	f (0.05, 1, 18)	f□
Slope (β_1)	493.69	± 1.498	< 0.001	0.99982	$5.33x10^{-14}$	4.279	108569.163
Slope (β_0)	-6.1018	± 0.9303	< 0.001				

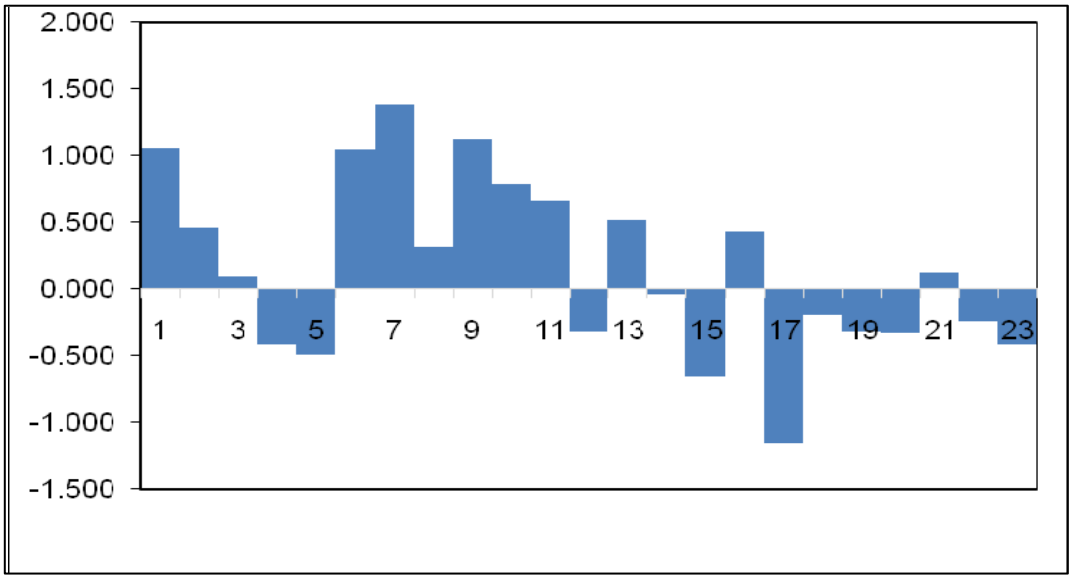

Figure 26: Standard Residual Plot for the Flow Meter Calibration Data for 8PXL flow probe

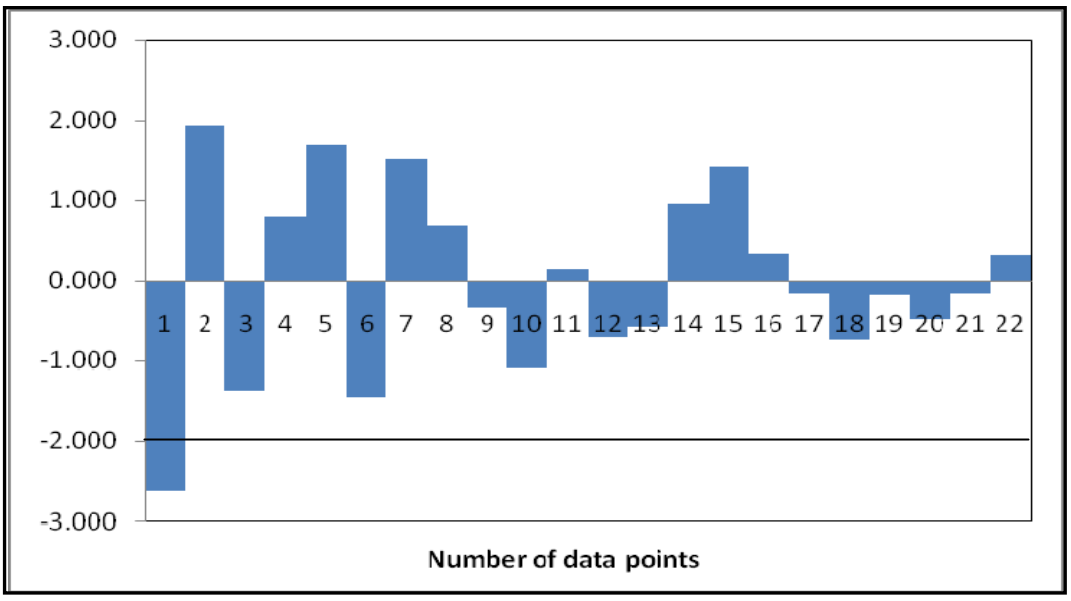

Figure 27: Standard Residual plot for the Flow Meter Calibration Data for 16PXL flow probe

4.9.3 Infant blood pump prototype hydraulic testing and comparison with computational analysis

Using the confidence intervals calculated from the statistical analysis of pressure transducer and flow meter calibration curve, error approximation for the pressure-flow experimental data points was calculated for infant blood pump prototype at different flow rates and three different rotational speeds. The confidence intervals for both pressure and flow calibration were to evaluate the minimum and maximum experimental error existing in the experimental data. **Figure 28** shows the pressure-flow performance results for the pediatric blood pump prototype along with the error bars and comparison with computational predictions. Less than 20% deviation was qualitatively observed between the experimental and CFD predictions.

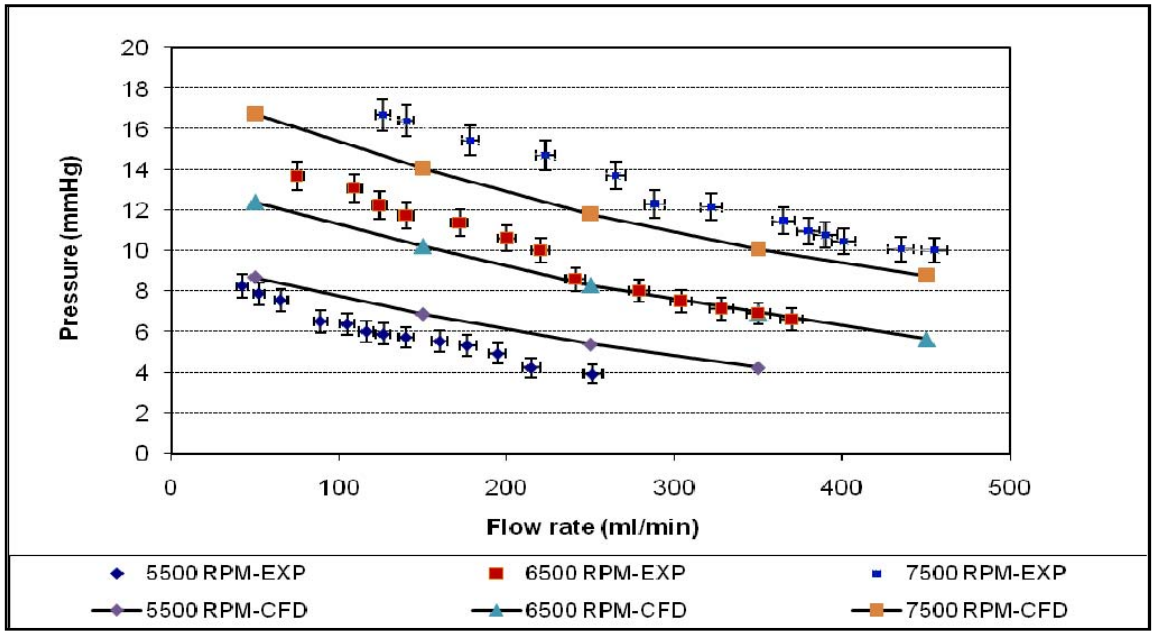

Figure 28: Pressure-flow performance curves for numerical predictions and experimental results of the infant blood pump design

4.9.4 Statistical analysis for adult blood pump prototype and comparison with computational predictions

Using the 95% confidence interval for the upper and lower limit from the statistical analysis performed on the calibration data of the pressure transducer and flow meter, an error approximation was determined for the experimental data of the adult blood pump rotated at five different rotational speeds. These error approximations were plotted as error bars on the discrete data points indicating maximum and minimum error existing in the experimental data. **Figure 29** shows the comparison between experimental and CFD predictions for adult blood pump prototype. Less than 10-20% deviation was qualitatively observed between the experimental and CFD predictions.

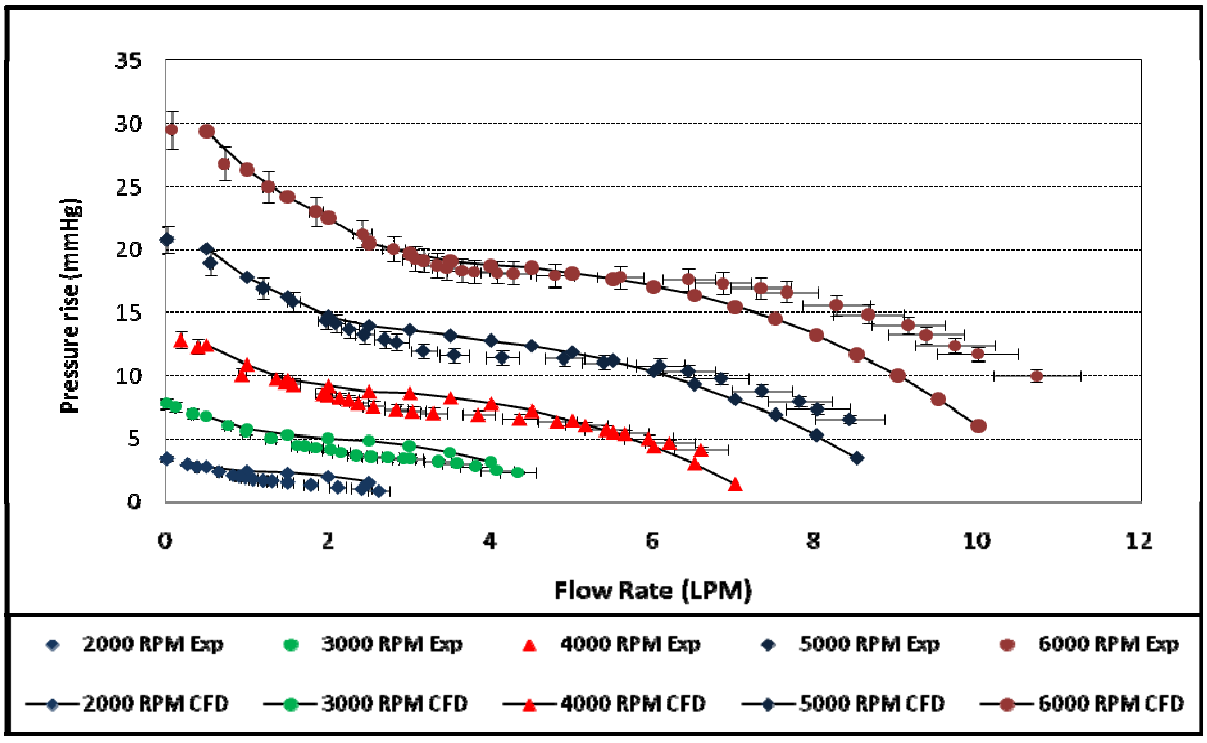

Figure 29: Pressure-flow performance curves for numerical predictions and experimental results of the adult blood pump design

NON DIMENSIONAL ANALYSIS

The nondimensional analysis was carried out to quantitatively compare the experimental hydraulic performance of adult blood pump prototype to numerical predictions. The pressure and flow coefficients for experimental data and CFD data sets were calculated. **Figure 30** shows the pressure coefficient as function of the flow coefficient for experimental and CFD data for adult blood pump prototype. The third order polynomial trendlines were determined to be, as follows:

$$\Psi_{EXPERIMENTAL} = -0.63752\,(\Phi)^3 + 0.921886\,(\Phi)^2 - 0.5025\,(\Phi) + 0.180977 \quad [11]$$

$$\Psi_{CFD} = -1.0421(\Phi)^3 + 1.10335\,(\Phi)^2 - 0.48014\,(\Phi) + 0.183749 \quad [12]$$

Table 11 lists the results of the regression analysis. Experimental and CFD data sets were found to be normal according the Ryan-Joiner normality test. The F-test was completed and indicated a strong significance ($p<0.0001$) in the correlation of the polynomial regression expressions to capture the trends of the experimental and CFD data. The correlation coefficients (R^2) and adjust R^2 values were above 0.915 for experimental data of the polynomial fit line and above 0.985 for CFD predictions. In addition, a Student T-test was performed on each of the regression coefficients. This T-test indicated the significance for each of the coefficients in the regression models.

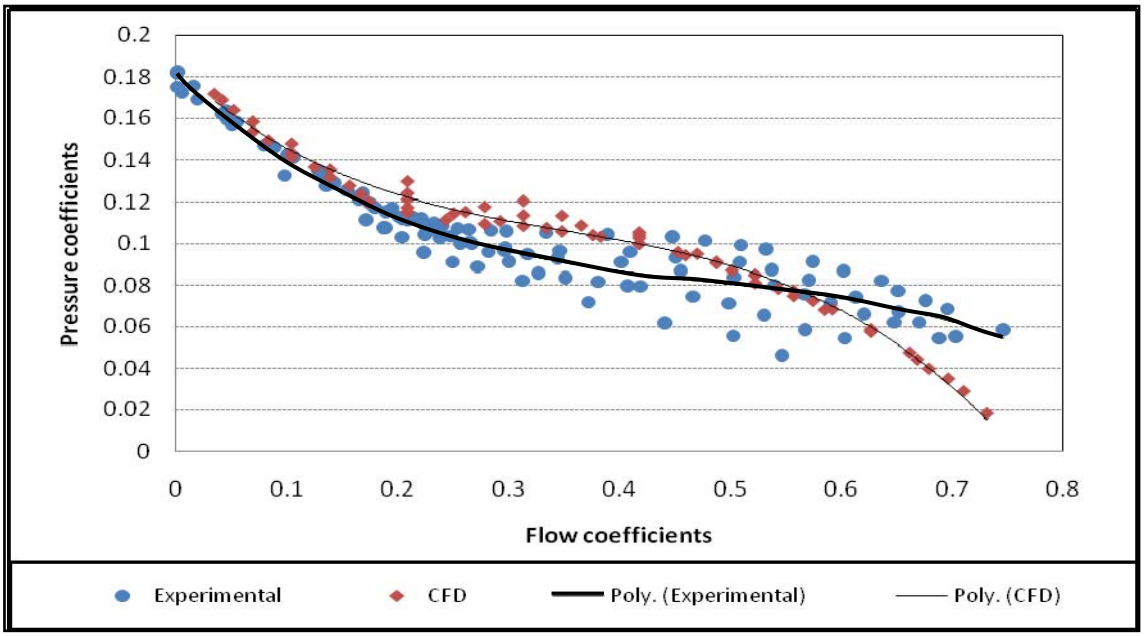

Figure 30: Graphical Representation of Pressure coefficient as a function of flow coefficient for experimental and CFD results for adult blood pump prototype

Table 11: Polynomial Regression Analysis of the Nondimensional Coefficient Data

Type	β_3	**p-val.**	β_2	**p-val.**	β_1	**p-val.**	β_0	**p-val.**	**F-test**	R^2	R^2_{adj}
Experimental Data	-0.6375	<0.0001	0.9219	<0.0001	-0.5025	<0.0001	0.18098	<0.0001	<0.0001	0.918	0.916
CFD Data	-1.0421	<0.0001	0.1033	<0.0001	-0.4801	<0.0001	0.1837	<0.0001	<0.0001	0.990	0.989

Using the regression models, we quantified the deviation among the experimental and CFD data sets for the hydraulic performance of the prototypes. The maximum and mean difference between the two sets of data was calculated to be 16.6 % and 10.1 % respectively.

4.9.5 Statistical results of hemolysis testing of blood pump (4-bladed) prototype

A statistical analysis was conducted on the blood bag experimental results to confirm the reliability of the data and estimate the correlation in the data. RJ normality test was run with the experimental data to prove normality. **Figure 31** shows a normal probability plot for plasma free hemoglobin data. This plot was generated in statistical software Minitab 15. The results of RJ normality evaluation supported the assumption of normal distribution of data based on the p-value greater than 0.1. A regression model was executed for the experimental data with a linear model fit to the data. The regression model was run in JMP 7.0. **Figure 32** illustrates graphical representation of a linear fit to the experimental data. Regression model provided R^2 and R^2 adjusted value of 0.96 and 0.95 respectively proving a strong correlation of the data.

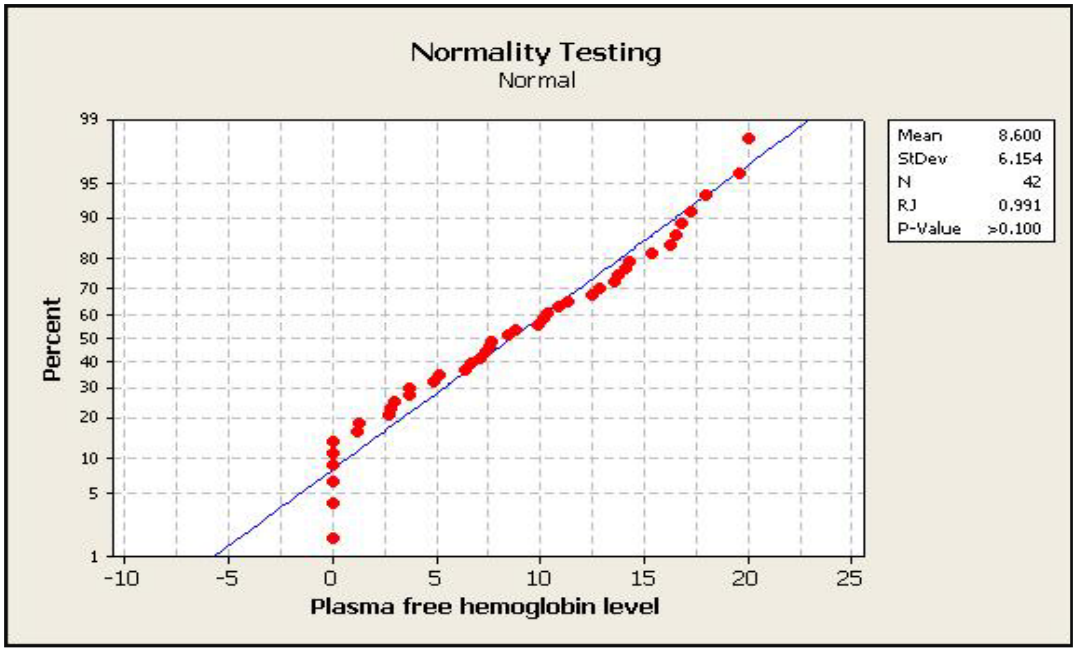

Figure 31: RJ Normality evaluation for the blood bag experiment results of adult blood pump prototype

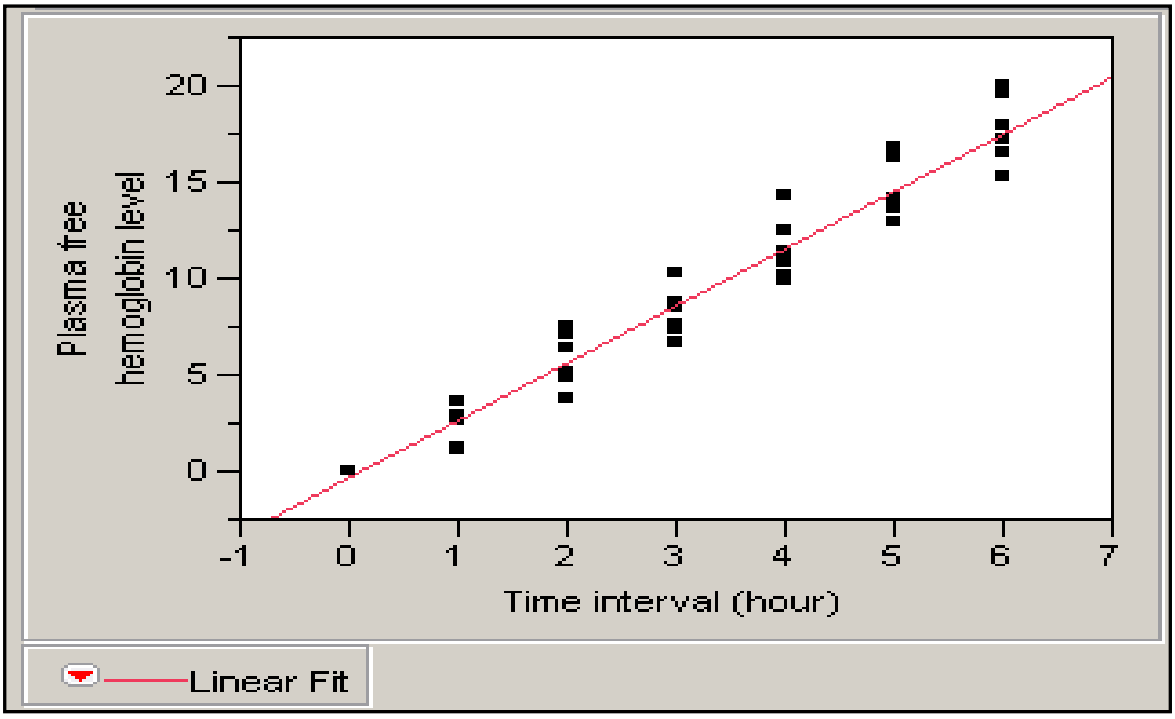

Figure 32: Linear model fit to the blood bag experimental data

Figure 33 demonstrates the box plot generated in JMP 7.0 from the experimental results to show the graphical representation of the variability of the plasma free hemoglobin level at each individual hour. Details of the variability in the experimental data is shown in the variability table containing mean, maximum, minimum, and maximum and minimum 95% confidence interval value of plasma free hemoglobin (pfHb) level at each hour starting from 0^{th} to 6^{th} hour of the experiment.

A 1-way ANOVA was performed as the output (plasma free hemoglobin level) is dependent on a single factor "time". **Table 12** shows results of 1-way ANOVA performed on hemolysis results of the blood bag experiment. It can be observed that the mean are significantly different for each time.

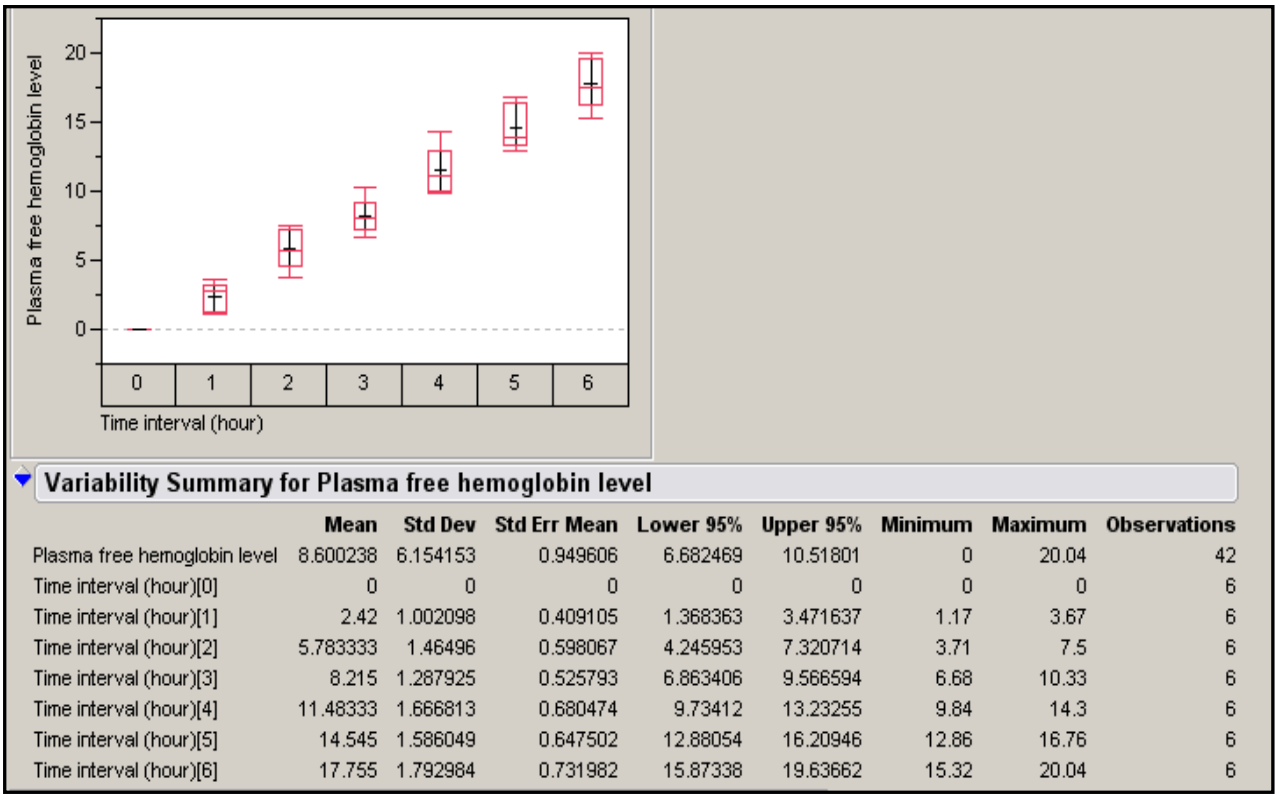

Variability Summary for Plasma free hemoglobin level

	Mean	Std Dev	Std Err Mean	Lower 95%	Upper 95%	Minimum	Maximum	Observations
Plasma free hemoglobin level	8.600238	6.154153	0.949606	6.682469	10.51801	0	20.04	42
Time interval (hour)[0]	0	0	0	0	0	0	0	6
Time interval (hour)[1]	2.42	1.002098	0.409105	1.368363	3.471637	1.17	3.67	6
Time interval (hour)[2]	5.783333	1.46496	0.598067	4.245953	7.320714	3.71	7.5	6
Time interval (hour)[3]	8.215	1.287925	0.525793	6.863406	9.566594	6.68	10.33	6
Time interval (hour)[4]	11.48333	1.666813	0.680474	9.73412	13.23255	9.84	14.3	6
Time interval (hour)[5]	14.545	1.586049	0.647502	12.88054	16.20946	12.86	16.76	6
Time interval (hour)[6]	17.755	1.792984	0.731982	15.87338	19.63662	15.32	20.04	6

Figure 33: Box plot for the six hour blood bag experiment with six repetitions

Table 12: One-way ANOVA: Plasma free hemoglobin level versus Time interval (hour)

Source	DF	SS	MS	F	P		
Time interval (hour)	6	1486.23	247.70	130.20	0.000		
Error	35	66.59	1.90				
Total	41	1552.82					
S = 1.379 R-Sq = 95.71% R-Sq(adj) = 94.98%							
		Individual 95% CIs For Mean Based on					
		Pooled StDev					
Level N Mean StDev	--+---------+---------+---------+-------						
0 6 0.000 0.000	(-*-)						
1 6 2.420 1.002	(-*-)						
2 6 5.783 1.465	(-*-)						
3 6 8.215 1.288	(-*-)						
4 6 11.483 1.667	(-*-)						
5 6 14.545 1.586	(-*-)						
6 6 17.755 1.793	(-*)						
	--+---------+---------+---------+-------						
	0.0 6.0 12.0 18.0						
Pooled StDev = 1.379							

Tukey's analysis was performed after 1-way ANOVA to carry out pairwise comparison between pfHb data average at each hour to the averages at subsequent hour. From the analysis it was concluded that there was not a significant difference between 2nd and 3rd hour levels of plasma free hemoglobin.

4.9.6 Statistical results for three blood pump prototypes with protective cage of filaments

The hydraulic testing of three blood pump prototypes with the protective cage of filaments was the last set of experiments in this thesis project. The pressure transducer and flow meter were again calibrated for this experiment, and a statistical analysis was performed. On obtaining values for upper and lower limit of 95% confidence interval, maximum and minimum pressure and flow measurement errors that is possible during the experiment was calculated. **Figure 34, Figure 35** and **Figure 36** shows pressure-flow performance curve of experimental results with error bars for adult blood pump prototype (4-bladed), blood pump with 3 impeller blades and a blood pump with impeller and a diffuser along with protective cage of filaments respectively.

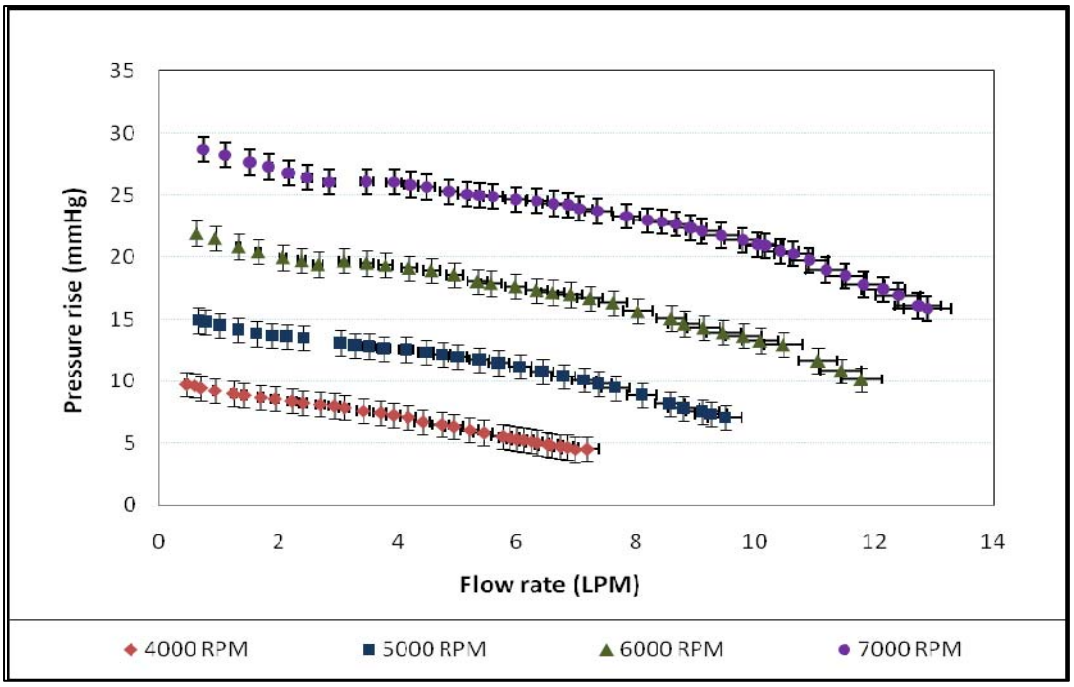

Figure 34: Pressure-flow performance curve of experimental results for adult blood pump prototype (4-bladed) with protective cage of filaments

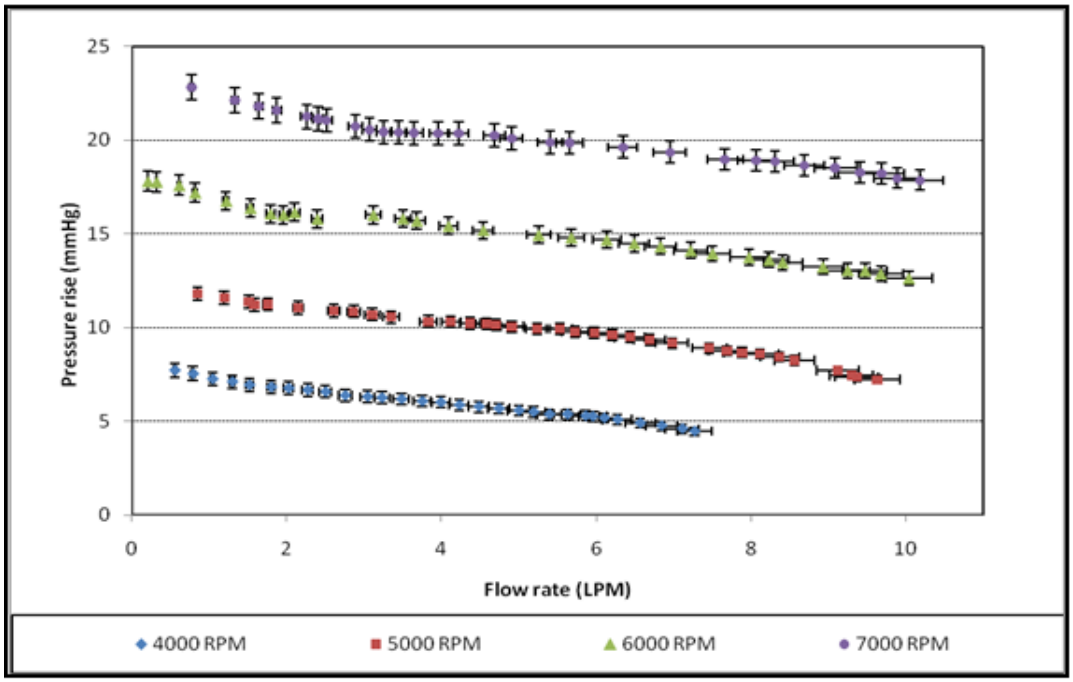

Figure 35: Pressure-flow performance curve of experimental results for adult blood pump prototype (3-bladed impeller) with protective cage of filaments

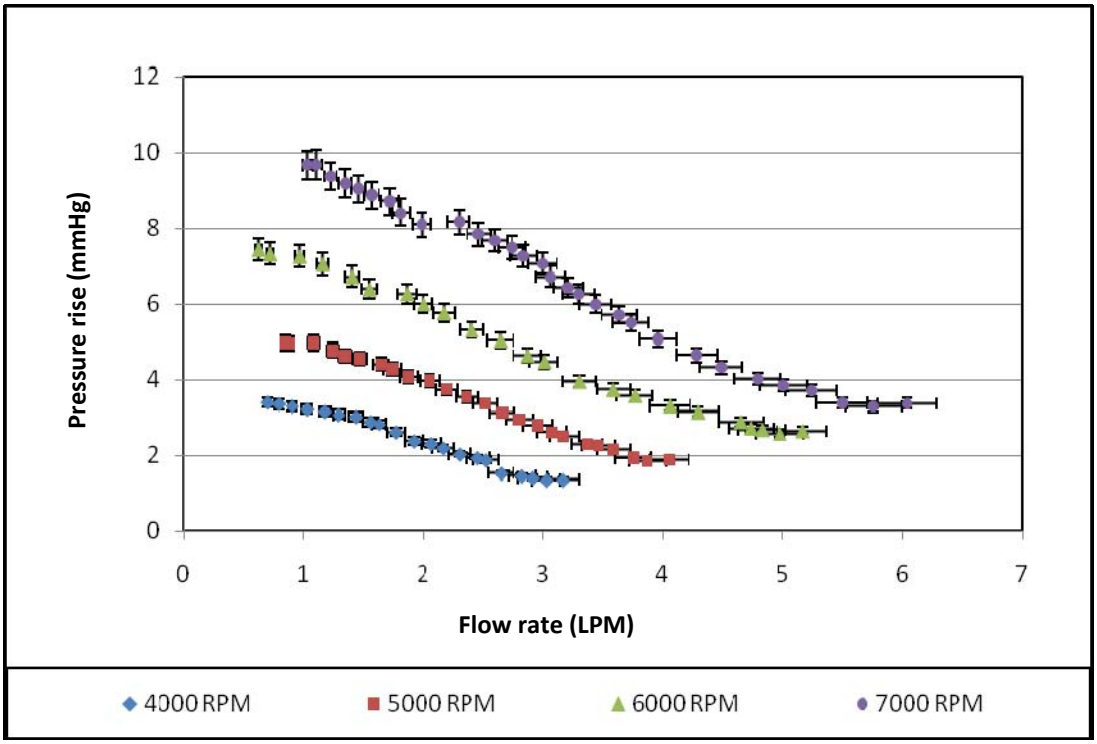

Figure 36: Pressure-flow performance curve of experimental results for blood pump with 3 impeller blades and a diffuser along with a protective cage of filaments

NON DIMENSIONAL ANALYSIS

The nondimensional analysis was carried out to compare the three prototypes quantitatively to one another. The pressure and flow coefficients for each prototype and all data sets were calculated. **Figure 37** shows the pressure coefficient as function of the flow coefficient for all of the blood pump prototypes. The third order polynomial trendlines were determined to be, as follows:

$$\Psi_{\text{4-Bladed Impeller}} = -0.0960\,(\Phi)^3 + 0.1310\,(\Phi)^2 - 0.0912\,(\Phi) + 0.1120 \quad [13]$$

$$\Psi_{\text{3-Bladed Impeller}} = -0.0423\,(\Phi)^3 + 0.0799\,(\Phi)^2 - 0.0787\,(\Phi) + 0.1402 \quad [14]$$

$$\Psi_{\text{3-Bl. Imp \& Diffuser}} = 0.5285\,(\Phi)^3 - 0.4105\,(\Phi)^2 - 0.0036\,(\Phi) + 0.0586 \quad [15]$$

Table 13 lists the results of the regression analysis. All experimental data sets were found to be normal according the Ryan-Joiner normality test. The F-test was completed and indicated a strong significance ($p<0.0001$) in the correlation of the polynomial regression expressions to capture the trends of the experimental data. The correlation coefficients (R^2) and adjust R^2 values were above 0.92 for all of the polynomial fit lines. In addition, a Student T-test was performed on each of the regression coefficients. This T-test indicated the significance for each of the coefficients in the regression models.

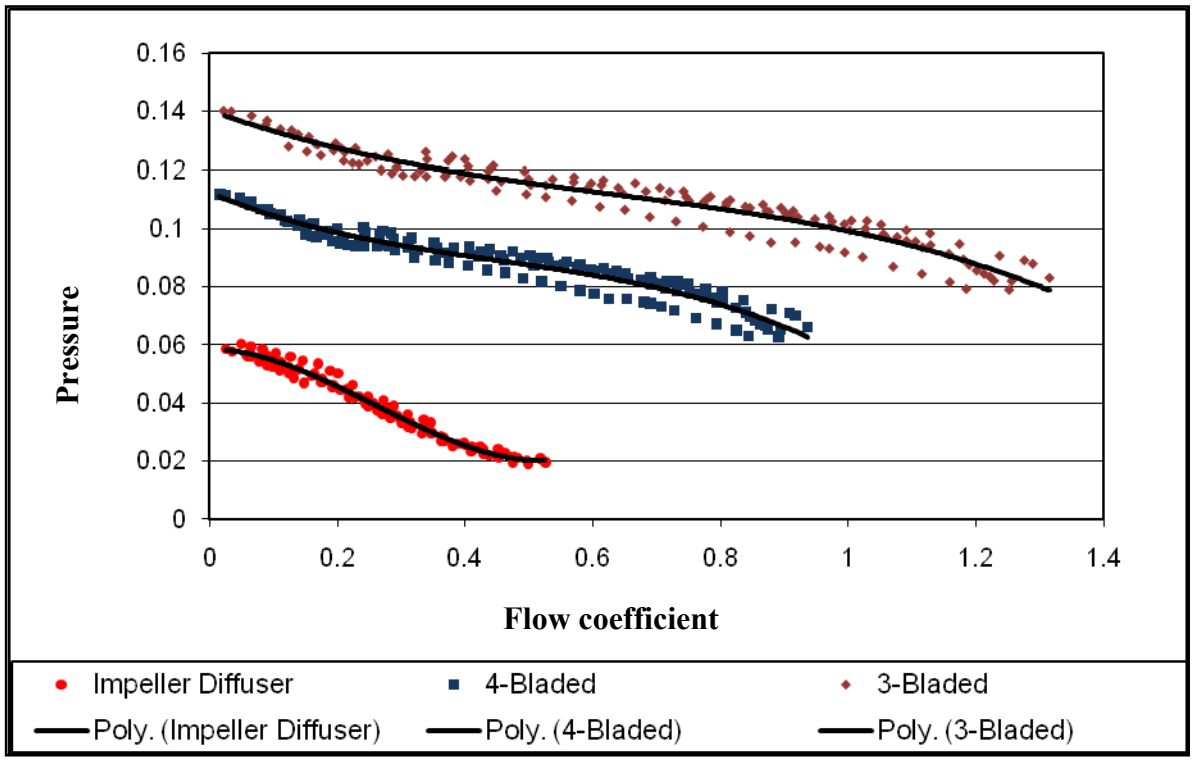

Figure 37: Graphical Representation of Pressure coefficient as a function of flow coefficient for all three blood pump prototypes

Using the regression models, we quantified the deviation among the three experimental data sets for the hydraulic performance of the prototypes. **Table 14** shows the average and maximum deviation in the data sets. The following comparisons were performed: 1) 3-bladed impeller to 3-bladed impeller having a 4-bladed diffuser, 2) 4-bladed impeller to the 3-bladed impeller having a 4-bladed diffuser, 3) 3-bladed impeller to 3-bladed impeller having a 4-bladed diffuser. This deviation analysis revealed that the 4-bladed impeller outperformed the 3-bladed impeller by an average difference of 26%

and a maximum difference of 43%. The 4-bladed impeller outperformed the 3-bladed impeller with 4-bladed diffuser by an average deviation of 215%. The 3-bladed impeller also outperformed the 3-bladed impeller with 4-bladed diffuser by an average deviation of the 148% (27).

Table 13: Polynomial regression analysis of the Nondimensional coefficient data

Type	β_3	p-val.	β_2	p-val.	β_1	p-val.	β_0	p-val.	F-test	R^2	R^2_{adj}
3-Bladed Impeller	-0.0423	<0.0001	0.0799	<0.0001	-0.0787	<0.0001	0.1402	<0.0001	<0.0001	0.93	0.93
4-Bladed Impeller	-0.0960	<0.0001	0.1310	<0.0001	-0.0912	<0.0001	0.1120	<0.0001	<0.0001	0.93	0.93
3-Bld. Imp w/ Diff	0.5285	<0.0001	-0.4105	<0.0001	-0.0036	0.023	0.0586	<0.0001	<0.0001	0.98	0.98

Table 14: Maximum and average percent deviation for data set comparisons for three different possible combinations

Compared	**3-Bladed Impeller**	**4-Bladed Impeller**	**3-Bladed Impeller**
to:	**3-Bld. Imp & 4-Bld. Diff.**	**3-Bld. Imp & 4-Bld. Diff.**	**4-Bladed Impeller**
Maximum	330%	470%	43%
Mean	148%	215%	26%

Chapter 5: Discussion

Treatment of congenital heart diseases has been a challenging problem for clinicians (1). Each year there are thousands of infants born with congenital heart defects. These cardiac malformations constitute a wide range of anomalies including right and left sections of the heart(3). Out of this large group of patients with complex congenital abnormalities, there exist a considerable number of patients with functionally single ventricle(3). For patients with such cardiac malformations, the single ventricle is responsible for maintaining both the systemic and pulmonary blood circulations which are connected in parallel. Single ventricular physiology leads to arterial desaturation and a chronic volume overload to the single ventricle leading to a congestive heart failure (4; 5).

Patients with failing single ventricle or Fontan physiology are left with an option of heart transplantation. An inadequate supply of hearts and donor/recipient size variance leave clinicians with an option of employing mechanical circulatory support systems (9).

Ventricular assist devices (VADs) have been extensively used for left and right ventricular assist support (9). There are more than few options available to the clinicians for treating biventricular heart failure. These long term mechanical circulatory supports have been successfully employed in adult and pediatric patients with heart failure (1).

VADs are specifically design to augment the blood flow in systemic or pulmonary circulations. Thus, the commercially available VADs for left and right ventricular support have flow and pressure generation that are significantly different (higher) from flow requirements to support the Fontan (cavopulmonary) circulations(28). Currently, there are no mechanical circulatory supports specifically designed for augmenting blood flow at cavopulmonary site of failing Fontan patients that are available commercially(17). Provoked by this noble need of a long term cavopulmonary assist device for failing Fontan patients, research has been ongoing at different universities and institutions for the development of a device that could be employed as a bridge-to-transplant or bridge to recovery for these Fontan patients.

Rodefeld and coworkers at the Indiana University School of Medicine initiated providing a mechanical circulatory support in an animal model by inserting 2 Hemopumps in the SVC and IVC. Improvement in the hemodynamic condition of a pump-supported Fontan circulation compared to the passive Fontan physiology proved the feasibility of treating failing Fontan patients with a mechanical circulatory support (24). The study also explored the effect of pulsatile flow on hemodynamic condition at pulmonary site. No significant benefit was observed for pulsatile flow over a non-pulsatile flow condition at the cavopulmonary site during *in vivo* experiment (24; 29). This research group is also working on development of a percutaneously implantable expandable propeller blood pump for augmentation of blood flow at cavopulmonary site (23). The concept is based on the blood pump design of Reitan *et al.* developed for a mechanical circulatory support at the left ventricular site (30). Reimer *et al.* at Stanford

University have carried out *in vivo* testing with sheep model to evaluate hemodynamic and physiological response on applying Thoratec HeartMate II axial flow blood pump at the cavopulmonary site (31). This study showed a significant improvement in cardiac output, IVC and arterial pressure returning to baseline (similar to biventricular circulation). Nevertheless, the study states the concern about thrombosis particularly for pump rotating at higher flow rates (31; 32). A team at University of Colorado is also developing an axial flow blood pump for augmenting blood flow at the inferior vena cava of TCPC (total cavopulmonary connection) site(33). The hydraulic testing of this blood pump demonstrated promising results. The study, however, does not provide detailed information about the motor-drive configuration for the blood pump and the obstruction of flow during rotational failure (33).

Contributing to the ongoing research in the field of cavopulmonary assist device, this thesis project focuses on the initial design and development phase of a percutaneously inserted, collapsible and magnetically levitated axial flow blood pump. The axial flow blood pump will be placed in the IVC slightly below the TCPC. The rotation of this blood pump will help in augmenting the blood flow at the cavopulmonary site and thereby improve the hemodynamic condition. The axial flow blood pump will help in reducing venous hypertension and force the blood flow through pulmonary arteries by overcoming the vascular resistance. Blood pump rotational speed and position will be controlled by motor-magnetic suspension system. This blood pump could be employed as a bridge-to-transplant or bridge-to-recovery for the patients with failing Fontan physiology. Bladegen, a turbomachinery software was used to create the blade

design for these blood pumps. After creating the design of the blood pumps a 3-D model of these blood pumps were created in SolidWorks for rapid prototyping. This project represents the hydraulic and hemolysis testing of four blood pump designs with one of them designed for infants. These blood pumps differed from each other on the basis of hub diameter, number of blades, impeller and diffuser parts. Computational analysis was also carried out for the adult blood pump prototype with 4 impeller blades. The optimal design was also evaluated out of the three adult blood pumps with the protective cage depending upon the hydraulic performance.

5.1 Infant axial flow blood pump prototype

Hydraulic test was performed for the infant axial flow blood pump using the experimental set up constructed as shown in the **Figure 8(b)**. Water-glycerin solution with a viscosity and specific gravity similar to that of blood was used as the fluid medium for the experiment. The blood pump was rotated at 5500, 6500 and 7500 RPM and pressure rise and flow rate were measured using a pressure transducer and flow meter. The blood pump was able to generate a pressure rise of 4-17 mmHg with a flow rate of 50-450 ml/min. Comparison of the experimental results with computational predictions showed a deviation of less than 20% as shown in **Figure 28**. These deviations could have occurred due to following reasons:

1. The pump was centered using visual techniques within the housing and may not have been exactly centered, thereby reducing performance of the pump.

2. Manufacturing tolerances for the housing and the pump were not included in the CFD model, thus the CFD represents a theoretical geometry, not exactly that of the prototype.

3. Turbulent flow conditions should dominate flow regions in the axial flow pump with Reynolds (Re) numbers greater than 3000. Nevertheless, the fluid conditions may reside in the transitional regime making CFD modeling using commercial codes a challenge (18).

4. Thorough care was taken to remove all of the air bubbles while the flow loop was filled for conducting experiment. However, minute air bubbles might have settled at different sites of the loop, thus creating a small variation in the measurement of flow rate and pressure difference.

5.2 Adult axial flow blood pump (4-bladed) prototype

Hydraulic, computational analysis and hemolysis test were conducted for the adult blood pump design. The blood pump was rotated at 3000, 4000, 5000 and 6000 RPM and respective pressure rise and flow rate were measured. It was observed that the blood pump was able to generate a pressure rise of 2-30 mmHg with a flow rate of 0.2-11 Liters/min at four different rotational speeds. This range of flow rate and pressure rise is enough to augment blood flow in adult patients with failing Fontan physiology. The comparison between the experimental results and computational analysis showed a deviation of less than 15% as shown in **Figure 29**. This deviation could have occurred due to manufacturing tolerances for the housing and the pump, air bubbles that could

have settled at different sites of the experimental rig and k-ε turbulence model selected for computational studies might not capture the exact flow characteristics.

The hemolysis test (blood bag experiment) was conducted six times and the maximum plasma free hemoglobin level that was observed was 20.04 mg/dL at the end of one of the six experiments. This value of plasma free hemoglobin could be considered reasonable compared to the clinically available VADs for left and right ventricular support (31; 24). The maximum NIH (normalized index of hemolysis) level was calculated to be 0.017 g/100L for one of the experiment. This value of NIH level is smaller enough compared to commercially available VADs. **Table 15** shows NIH values for selected VADs. One-way ANOVA carried out on plasma free hemoglobin level data for all six experiments showed that the treatment mean values were significantly different except between 2nd and 3rd hour. Significance for these data means could be obtained with additional hemolysis studies (n>6).

Table 15: Normalized Index of Hemolysis values for selected VADs (34-37)

Pump	Type	N.I.H (g/100L)
Valvo Pump	Axial	0.03
MicroMed-DeBakey	Axial	0.0028
Berlin Incor I	Axial	0.006
HeartMate II	Axial	0.005

5.3 Hydraulic testing of blood pumps with protective cage

The hydraulic testing of three blood pump prototypes with a protective cage of filaments was performed. Protective cage and a supporting catheter were designed in

order to stabilize the position of the blood pump at cavopulmonary site and protecting the caval vein from the rotating part of the blood pump. The following three pump prototypes were tested: 1) pump having four impeller blades only, 2) pump having three impeller blades only, and 3) pump having three impeller blades and four diffuser blades. The blood pumps were rotated at four different rotational speeds from 4000 to 7000 RPM. Adult blood pump (4-bladed impeller) was able to generate a pressure rise of 4 to 28 mmHg for flow rates of 0.5 to 13 L/ min at rotational speeds of 4000 to 7000 RPM. Blood pump with three impeller blades only was able to generate a pressure rises of 4 to 22 mmHg for flow rates of 0.5 to 10 L/min at rotational speeds of 4000 to 7000 RPM. Unlike the 3 bladed blood pump without a diffuser, blood pump with a diffuser was able to generate a pressure rise of 1 to 10 mmHg with flow rates of 0.6 to 6 L/min at a rotational speed of 4000 to 7000 RPM.

Despite the lower pressure generation from the blood pump with a diffuser, the performance falls within the design range that would support a failing Fontan physiology. The blood pump prototype without the diffuser blades generated strong flow vortices and irregular flow patterns. These vortices would contribute to activation of platelets and possible shearing of red blood cells (27). The quantitative comparison revealed that the 4-bladed impeller outperformed the 3-bladed impeller by an average of 26%. The 4-bladed impeller outperformed the 3-bladed impeller with 4-bladed diffuser by an average deviation of 215%. The 3-bladed impeller also outperformed the 3-bladed impeller with 4-bladed diffuser by an average deviation of the 148%.

5.4 Study Limitations and Future Work

This research project focuses on the initial phase in development of the cavopulmonary assist device. There are several limitations in this study and opportunities for further research and development. The hydraulic performance of the blood pump prototypes with a protective filament cage was carried out; however, the computational analysis is necessary for further validation of the design. Numerical analysis is also important to predict flow vorticity, internal fluid dynamics, and shear stress at different sites of the design. These results could be compared to the experimental results with expectation of minimum deviation. Transient flow simulations should be performed to provide physical insight into the fluid-blade interaction and fluid-filaments interaction. These predictions would help in further optimization of the cage filament design and help in evolving with the exact geometry of the blood pump. Numerical analysis also plays an important role in blood damage predictions (hemolysis and thrombosis). The next step after the CFD analysis would be conducting the blood bag experiments to measure the hemolysis levels produced by the rotating blades of blood pump and cage filaments. Parallel to this ongoing work, particle image velocimetry measurements are to be conducted for further visualization the flow behavior at the cavopulmonary site. These measurements will help to obtain information about any irregular flows. The results will further help in validating the CFD analysis and assist in developing the optimal blood pump design for the cavopulmonary site in the failing Fontan patients.

From the current studies it is observed that the 4-bladed blood pump (with and without a protective cage of filaments) was able to generate enough pressure rises at comparatively lower rotational speeds. The comparison of experimental results with the numerical predictions showed less than 10-20% deviation, thereby validating the blood pump design. Moreover, the hemolysis results also showed lower pfHb and NIH levels compared to commercially available VADs. Hence, as of now this blood pump design could be considered an optimal design.

Chapter 6: Conclusion

This ongoing research will develop a mechanical circulatory support for augmenting blood flow at the cavopulmonary site in failing Fontan physiology and thereby, provide a bridge-to-transplant or recovery for these patients. In particular, this thesis project represents the initial design and development phase of an axial flow blood pump as a mechanical device for assisting blood flow in the total cavopulmonary connection in Fontan patients. This study includes the hydraulic performance of an infant and adult blood pump prototype along with CFD analysis for the adult blood pump (4-bladed). The hydraulic performance results showed that the blood pumps generate an adequate pressure rise to overcome the vascular resistance in pulmonary arteries and thereby improving the hemodynamic condition in the Fontan physiology. Hemolysis experiments were also conducted with the adult blood pump prototype (4-bladed), and results were acceptable indicating a reduced risk of blood damage during operational conditions. Along with the two previous blood pumps, two other adult blood pumps were designed with a protective cage of filaments. Filament cage was designed with an intention of stabilizing the position of the blood pump at targeted site and protecting the caval veins from rotating parts of the blood pump. The hydraulic performance of these two new blood pumps and the previous adult blood pump with the protective cage of

filaments showed satisfactory results. The next step for this research is the integration of the pump design and the motor-magnetic suspension design.

The success of this research will provide clinicians with a new option for treating infants, adolescents and adult patients with failing Fontan physiology and thereby address a significant human health problem.

Bibliography

Bibliography

1. *Mechanical support of the functionally single ventricle.* **Ravishankar, C and Gaynor, J W.** 2006, Cardiol Young, Vol. 16, pp. 55-60.

2. *Intravascular Mechanical Cavopulmonary Assistance for Patients with Failing Fontan Physiology.* **Sonya, S, et al.** In press, Artif Organs.

3. *Univentricular heart.* **Khairy, P, Poirier, N C and Mercier, L A.** 2007, Circulation, Vol. 115, pp. 800-812.

4. *The Fontan Circulation.* **Gewillig, M.** 2005, Heart, Vol. 91, pp. 839-846.

5. *Outcome after a "perfect" Fontan operation.* **Fontan, F, et al.** 1990, Circulation, Vol. 81, pp. 1520-1536.

6. *Definitive palliation with cavopulmonary or aortopulmonary shunts for adult with single ventricle physiology.* **Gatzoulis, M A, et al.** 2000, Heart, Vol. 83, pp. 51-57.

7. *The Fontan procedure: lessons from the past.* **Bull, K.** 3, 1998, Heart, Vol. 79, pp. 213-214.

8. *Long-Term Survival, Modes of Death, and Predictors of Mortality in Patients With Fontan Surgery.* **Khairy, P, et al.** 2008, Circulation, Vol. 117, pp. 85-92.

9. *Mechanical circulatory support in children with cardiac disease.* **Duncan, B, et al.** 1999, J Thorac Cardiovasc Surg, Vol. 117, pp. 529-542.

10. *Mechanical Circulatory Support for the Pediatric Patient.* **Carberry, K E, et al.** 2, 2007, Crit Care Nurs Q, Vol. 30, pp. 121-142

11. *Use of a ventricular assist device as a bridge to transplantation in a patient with single ventricle physiology and total cavopulmonary anastomosis.* **Russo, P, et al.** 4, 2008, Pediatric Anesthesia, Vol. 18, pp. 320-324.

12. *Utility of extracorporeal membrane oxygenations for early graft failure following heart transplantation in infancy.* **Mitchell, M, et al.** 2000, J Heart Lung Transplant, Vol. 19, pp. 834-839.

13. *Outcome of pediatric patients treated with extracorporeal life support after cardiac surgery.* **Kolovos, N S, et al.** 2003, Ann Thorac Surg, Vol. 76, pp. 1435-1441.

14. *Augmentation of pulmonary blood flow by a right artial balloon pump after the Fontan operation.* **Jacobs, M, et al.** 1987, Circulation, Vol. 76, pp. S72-S76.

15. *Commentary of circulatory support in infants and children.* **Pennington, G D.** 1994, Semin Thorac Cardiovasc, Vol. 6, pp. 161-162.

16. *Circulatory support in infants and children.* **Pennington, G D and Swartz, M T.** 1993, Ann Thorac Surg, Vol. 35, pp. 233-237.

17. *Pediatric Circulatory Support: Current Strategies and Future Directions. Biventricular and Univentricular Mechanical Assistance.* **Throckmorton, A L and Chopski, S G.** 5, 2008, ASAIO J, Vol. 54, pp. 491-497.

18. **Throckmorton, A L.** *Axial Flow VAD for Infants and Children.* s.l. : Univ of Virginia, 2006.

19. *Heart Transplantation in Children after Mechanical Circulatory Support: Comparison of Heart Transplantation with Ventricular Assist Devices and Elective Heart Transplantation.* **Coskun, O, et al.** 2005, ASAIO J, pp. 495-497.

20. *Centrifugal pump left heart assist in pediatric cardiac operations.* **Karl, T, et al.** 1991, J Thorac Cardiovasc Surg, Vol. 102, pp. 624-630.

21. *Ventricular Assist Devices as a Bridge to Cardiac Transplant.* **Holman, W L, et al.** 6, 1997, Ann. Surg., Vol. 225, pp. 695-706.

22. *Mechanical axial flow blood pump to support cavopulmonary circulation.* **Throckmorton, A L, Kapadia, J Y and Madduri, D.** 11, 2008, Int J Artif Organs, Vol. 31, pp. 970-982.

23. *Performance of a 3-Bladed Propeller Pump to Provide Cavopulmonary Assist in the Failing Fontan Circulation.* **Throckmorton, A L, et al.** 2008, Ann Thorac Surg, Vol. 86, pp. 1343-1347.

24. *Cavopulmonary assist: circulatory support for the univentricular Fontan Circulation.* **Rodefeld, M D, et al.** 2006, Ann Thorac Surg, Vol. 81, pp. 264-271.

25. *Numerical Design and Experimental Hydraulic Testing of an Axial Flow Ventricular Assist Device for Infants and Children.* **Throckmorton, A L, et al.** 6, 2007, ASAIO J, Vol. 53, pp. 754-761.

26. **Montgomery, Douglas C.** *Design and Analysis of Experiments.* 7th Edittion. s.l. : John Wiley & Sons, Inc., 2008.

27. *Hydraulic Testing of Intravascular Axial Flow Blood Pump Designs with a Protective Cage of Filaments for Mechanical Cavopulmonary Assist.* **Kapadia, J Y, et al.** In press, ASAIO J.

28. *Axial Flow Blood Pumps.* **Song, X, et al.** 2003, ASAIO J, Vol. 49, pp. 355-364.

29. *Twenty-four hour cardiopulmonary stability in a model of assisted newborn Fontan circulation.* **Myers, C, et al.** 2006, Ann Thorac Surg, Vol. 81, pp. 264-71.

30. *Left ventricular heart failure model for testing cardiac assist devices.* **Reitan, O, Steen, S and Ohlin, H.** 2003, ASAIO J, Vol. 48, pp. 71-75.

31. *Axial Flow VAD support of Total Cavopulmonary Connection Circulation.* **Reimer, R K, et al.** 2, 2004, ASAIO J, Vol. 50, p. 130.

32. *Mechanical support of total cavopulmonary connection with an axial flow pump.* **Riemer, R K, et al.** 2, 2005, J Thorac Cardiovasc Surg, Vol. 130, pp. 351-354.

33. *Initial experience with the development and numerical and in vitro studies of a novel low-pressure artificial right ventricle for pediatric Fontan patients.* **Wang, R, et al.** 2006, ASAIO J, Vol. 52, pp. 682-692.

34. *Development of the Valvo Pump: An Axial Flow Pump Implanted at the Heart Valve Position.* **Mitamura, Y, et al.** 2, 1999, Artifical Organs, Vol. 130, pp. 566-571.

35. *Design and performance testing of an axial-flow ventricular assist device developed at the Fu Wai Hosptial at Beijing.* **Zhang, Y, et al.** 11, 2008, Journal of Artificial Organs, Vol. 31, pp. 983-987.

36. *In vitro performance of a centrifugal, a mixed flow, and an axial flow blood pump.* **Araki, K, et al.** 11, 1998, Artificial Organs, Vol. 31, pp. 366-370.

37. *A miniature implantable axial flow ventricular assist device.* **DeBakey, ME.** 2, 1999, The Annals of Thoracic Surgery, Vol. 68, pp. 637-640.

Appendix

Spread sheet for Pressure-flow relation for adult blood pump prototype (4-bladed)

4000 RPM													
Pressure(v)		Flow rate(V)		Press error(-)	Minimum Press	Pressure (mmHg)	Maxim Press	Press error(+)	Flow error(-)	Flow min	Flow rate(LPM)	Flow max	Flow error(+)
0.11		3.36		0.06	4.07	4.13	4.19	0.06	0.05	6.54	6.59	6.63	0.05
0.12		3.17		0.06	4.64	4.71	4.77	0.06	0.04	6.16	6.20	6.25	0.04
0.13		3.04		0.06	4.96	5.03	5.09	0.06	0.04	5.90	5.94	5.99	0.04
0.14		2.89		0.06	5.37	5.43	5.49	0.06	0.04	5.61	5.65	5.69	0.04
0.15		2.77		0.06	5.69	5.75	5.81	0.06	0.04	5.39	5.43	5.47	0.04
0.16		2.64		0.06	6.01	6.07	6.14	0.06	0.04	5.13	5.17	5.21	0.04
0.16		2.46		0.06	6.31	6.38	6.44	0.06	0.04	4.78	4.82	4.86	0.04
0.17		2.23		0.07	6.54	6.61	6.67	0.07	0.04	4.32	4.35	4.39	0.04
0.18		1.97		0.07	6.85	6.92	6.99	0.07	0.03	3.81	3.85	3.88	0.03
0.18		1.69		0.07	6.99	7.05	7.12	0.07	0.03	3.26	3.29	3.32	0.03
0.18		1.56		0.07	7.13	7.20	7.26	0.07	0.03	3.00	3.03	3.06	0.03
0.19		1.46		0.07	7.27	7.33	7.40	0.07	0.03	2.81	2.84	2.87	0.03
0.19		1.31		0.07	7.52	7.58	7.65	0.07	0.03	2.53	2.55	2.58	0.03
0.20		1.22		0.07	7.79	7.86	7.93	0.07	0.03	2.34	2.37	2.40	0.03
0.21		1.16		0.07	8.02	8.09	8.15	0.07	0.03	2.23	2.25	2.28	0.03
0.21		1.10		0.07	8.21	8.28	8.34	0.07	0.03	2.12	2.14	2.17	0.03
0.22		1.03		0.07	8.38	8.45	8.52	0.07	0.03	1.97	2.00	2.02	0.03
0.22		0.99		0.07	8.52	8.58	8.65	0.07	0.02	1.90	1.93	1.95	0.02
0.24		0.81		0.07	9.26	9.33	9.40	0.07	0.02	1.55	1.57	1.59	0.02
0.24		0.76		0.07	9.47	9.54	9.60	0.07	0.02	1.45	1.47	1.49	0.02
0.25		0.71		0.07	9.72	9.79	9.86	0.07	0.02	1.34	1.36	1.38	0.02
0.26		0.49		0.07	9.99	10.06	10.13	0.07	0.02	0.92	0.94	0.96	0.02
0.31		0.21		0.07	12.24	12.32	12.39	0.07	0.02	0.38	0.40	0.41	0.02

0.33		0.11		0.07	12.79	12.86	12.93	0.07	0.02	0.17	0.19	0.20	0.02
5000 RPM		Rotation	83.33 Hz										
0.17		4.29		0.07	6.49	6.55	6.62	0.07	0.05	8.36	8.42	8.47	0.05
0.19		4.09		0.07	7.28	7.35	7.41	0.07	0.05	7.97	8.02	8.07	0.05
0.20		3.98		0.07	7.92	7.98	8.05	0.07	0.05	7.75	7.80	7.85	0.05
0.22		3.74		0.07	8.76	8.82	8.89	0.07	0.05	7.28	7.33	7.38	0.05
0.25		3.49		0.07	9.71	9.78	9.85	0.07	0.05	6.79	6.84	6.88	0.05
0.26		3.28		0.07	10.31	10.38	10.45	0.07	0.05	6.39	6.43	6.48	0.05
0.27		3.11		0.07	10.71	10.78	10.85	0.07	0.04	6.04	6.08	6.13	0.04
0.28		2.76		0.07	10.99	11.06	11.13	0.07	0.04	5.35	5.39	5.43	0.04
0.29		2.51		0.07	11.31	11.38	11.46	0.07	0.04	4.86	4.90	4.94	0.04
0.29		2.12		0.07	11.39	11.46	11.53	0.07	0.03	4.11	4.14	4.18	0.03
0.30		1.82		0.07	11.58	11.65	11.72	0.07	0.03	3.52	3.55	3.58	0.03
0.30		1.62		0.07	11.89	11.97	12.04	0.07	0.03	3.14	3.17	3.20	0.03
0.32		1.46		0.07	12.57	12.65	12.72	0.07	0.03	2.81	2.84	2.87	0.03
0.33		1.38		0.07	12.81	12.88	12.96	0.07	0.03	2.67	2.70	2.72	0.03
0.34		1.25		0.07	13.18	13.26	13.33	0.07	0.03	2.42	2.44	2.47	0.03
0.35		1.16		0.07	13.61	13.68	13.76	0.07	0.03	2.23	2.26	2.29	0.03
0.36		1.08		0.08	14.08	14.15	14.23	0.08	0.03	2.07	2.09	2.12	0.03
0.37		1.02		0.08	14.31	14.39	14.46	0.08	0.02	1.95	1.97	2.00	0.02
0.40		0.81		0.08	15.78	15.86	15.94	0.08	0.02	1.54	1.57	1.59	0.02
0.43		0.62		0.08	16.85	16.93	17.01	0.08	0.02	1.18	1.20	1.22	0.02
0.48		0.29		0.08	18.86	18.94	19.03	0.08	0.02	0.53	0.55	0.57	0.02
0.53		0.02		0.08	20.72	20.81	20.89	0.08	0.02	0.00	0.02	0.03	0.02
6000 RPM		Rotation	100 Hz										
0.25		5.46		0.07	9.93	10.00	10.07	0.07	0.06	10.65	10.72	10.78	0.06
0.30		5.10		0.07	11.66	11.73	11.80	0.07	0.06	9.93	9.99	10.05	0.06
0.32		4.95		0.07	12.34	12.41	12.49	0.07	0.06	9.65	9.71	9.77	0.06
0.34		4.77		0.07	13.16	13.24	13.31	0.07	0.06	9.29	9.35	9.41	0.06
0.36		4.66		0.08	13.95	14.03	14.10	0.08	0.06	9.08	9.13	9.19	0.06
0.38		4.41		0.08	14.79	14.86	14.94	0.08	0.06	8.59	8.64	8.70	0.06

0.40		4.21		0.08	15.53	15.61	15.69	0.08	0.05	8.20	8.25	8.31	0.05
0.42		3.90		0.08	16.56	16.64	16.72	0.08	0.05	7.59	7.64	7.69	0.05
0.43		3.74		0.08	16.90	16.98	17.05	0.08	0.05	7.27	7.32	7.37	0.05
0.44		3.50		0.08	17.27	17.35	17.43	0.08	0.05	6.81	6.86	6.90	0.05
0.45		3.28		0.08	17.58	17.66	17.74	0.08	0.05	6.38	6.43	6.47	0.05
0.45		2.86		0.08	17.75	17.83	17.91	0.08	0.04	5.55	5.59	5.63	0.04
0.46		2.45		0.08	17.88	17.96	18.04	0.08	0.04	4.75	4.79	4.83	0.04
0.46		2.19		0.08	18.05	18.13	18.21	0.08	0.04	4.24	4.28	4.31	0.04
0.46		2.09		0.08	18.11	18.19	18.27	0.08	0.03	4.04	4.08	4.11	0.03
0.46		1.94		0.08	18.19	18.27	18.35	0.08	0.03	3.76	3.79	3.82	0.03
0.47		1.87		0.08	18.27	18.35	18.43	0.08	0.03	3.61	3.64	3.68	0.03
0.47		1.77		0.08	18.48	18.56	18.64	0.08	0.03	3.42	3.45	3.48	0.03
0.48		1.71		0.08	18.68	18.76	18.84	0.08	0.03	3.31	3.34	3.37	0.03
0.49		1.63		0.08	19.08	19.16	19.24	0.08	0.03	3.14	3.17	3.20	0.03
0.49		1.57		0.08	19.20	19.28	19.36	0.08	0.03	3.04	3.07	3.10	0.03
0.51		1.43		0.08	19.97	20.06	20.14	0.08	0.03	2.77	2.80	2.82	0.03
0.54		1.24		0.09	21.16	21.24	21.33	0.09	0.03	2.39	2.42	2.44	0.03
0.59		0.95		0.09	22.97	23.06	23.15	0.09	0.02	1.82	1.84	1.87	0.02
0.63		0.65		0.09	24.92	25.01	25.10	0.09	0.02	1.24	1.26	1.28	0.02
0.68		0.38		0.09	26.75	26.84	26.93	0.09	0.02	0.70	0.72	0.74	0.02
0.75		0.05		0.10	29.41	29.50	29.60	0.10	0.02	0.06	0.07	0.09	0.02
3000 RPM		Rotation	50 Hz										
0.06		2.21		0.06	2.26	2.32	2.38	0.06	0.04	4.29	4.33	4.36	0.04
0.06		2.08		0.06	2.44	2.50	2.56	0.06	0.03	4.04	4.07	4.11	0.03
0.07		1.95		0.06	2.74	2.80	2.86	0.06	0.03	3.78	3.81	3.84	0.03
0.08		1.83		0.06	2.99	3.05	3.11	0.06	0.03	3.55	3.58	3.61	0.03
0.08		1.72		0.06	3.13	3.19	3.25	0.06	0.03	3.32	3.35	3.38	0.03
0.09		1.54		0.06	3.34	3.40	3.46	0.06	0.03	2.98	3.01	3.04	0.03
0.09		1.50		0.06	3.35	3.41	3.47	0.06	0.03	2.89	2.92	2.95	0.03
0.09		1.40		0.06	3.43	3.49	3.55	0.06	0.03	2.70	2.73	2.76	0.03
0.09		1.30		0.06	3.51	3.57	3.63	0.06	0.03	2.50	2.52	2.55	0.03
0.09		1.20		0.06	3.60	3.66	3.72	0.06	0.03	2.32	2.34	2.37	0.03
0.10		1.11		0.06	3.84	3.90	3.96	0.06	0.03	2.13	2.15	2.18	0.03

0.11		1.04		0.06	4.04	4.10	4.16	0.06	0.03	2.00	2.02	2.05	0.03
0.11		0.95		0.06	4.21	4.27	4.33	0.06	0.02	1.82	1.84	1.87	0.02
0.11		0.88		0.06	4.32	4.39	4.45	0.06	0.02	1.68	1.71	1.73	0.02
0.11		0.83		0.06	4.40	4.46	4.52	0.06	0.02	1.59	1.61	1.64	0.02
0.13		0.67		0.06	4.95	5.01	5.07	0.06	0.02	1.27	1.29	1.31	0.02
0.14		0.51		0.06	5.52	5.58	5.64	0.06	0.02	0.96	0.98	1.00	0.02
0.15		0.40		0.06	5.98	6.05	6.11	0.06	0.02	0.74	0.76	0.78	0.02
0.18		0.18		0.07	6.91	6.98	7.05	0.07	0.02	0.31	0.33	0.34	0.02
0.19		0.07		0.07	7.44	7.51	7.58	0.07	0.02	0.10	0.11	0.13	0.02
0.20		0.01		0.07	7.70	7.77	7.84	0.07	0.02	-0.01	0.01	0.02	0.02
2000 RPM		Rotation	33.33 Hz										
0.02		1.34		0.06	0.82	0.88	0.94	0.06	0.03	2.59	2.62	2.64	0.03
0.03		1.24		0.06	0.99	1.05	1.11	0.06	0.03	2.38	2.40	2.43	0.03
0.03		1.09		0.06	1.12	1.17	1.23	0.06	0.03	2.08	2.11	2.14	0.03
0.04		0.92		0.06	1.31	1.37	1.42	0.06	0.02	1.76	1.78	1.80	0.02
0.04		0.77		0.06	1.50	1.56	1.62	0.06	0.02	1.47	1.49	1.52	0.02
0.04		0.67		0.06	1.63	1.68	1.74	0.06	0.02	1.28	1.30	1.32	0.02
0.05		0.62		0.06	1.67	1.73	1.79	0.06	0.02	1.17	1.19	1.21	0.02
0.05		0.56		0.06	1.76	1.81	1.87	0.06	0.02	1.05	1.07	1.09	0.02
0.05		0.51		0.06	1.90	1.96	2.02	0.06	0.02	0.95	0.97	0.99	0.02
0.05		0.47		0.06	1.98	2.04	2.10	0.06	0.02	0.88	0.90	0.92	0.02
0.05		0.47		0.06	1.99	2.05	2.10	0.06	0.02	0.87	0.89	0.91	0.02
0.06		0.43		0.06	2.06	2.12	2.18	0.06	0.02	0.80	0.82	0.84	0.02
0.06		0.34		0.06	2.36	2.42	2.48	0.06	0.02	0.63	0.65	0.67	0.02
0.07		0.20		0.06	2.74	2.80	2.86	0.06	0.02	0.36	0.38	0.40	0.02
0.08		0.14		0.06	2.95	3.01	3.07	0.06	0.02	0.24	0.26	0.28	0.02
0.09		0.02		0.06	3.41	3.47	3.53	0.06	0.02	-0.01	0.01	0.02	0.02

Spreadsheet for computational data of adult blood pump prototype

6000 RPM		5000 RPM		4000 RPM		3000 RPM		2000 RPM	
0.5	29.38212	0.5	20.06155	0.5	12.45966	0.5	6.774	0.5	2.814681
1	26.32853	1	17.77903	1	10.91121	1	5.794491	1	2.466411
1.5	24.20176	1.5	16.25084	1.5	9.701268	1.5	5.307363	1.5	2.290025
2	22.52646	2	14.68963	2	9.214892	2	5.034902	2	2.003303
2.5	20.52316	2.5	13.94055	2.5	8.764543	2.5	4.85101	2.5	1.540944
3	19.71253	3	13.60579	3	8.637694	3	4.452451		
3.5	19.08504	3.5	13.17196	3.5	8.266156	3.5	3.901524		
4	18.72626	4	12.7749	4	7.808301	4	3.203483		
4.5	18.56189	4.5	12.36508	4.5	7.225099				
5	18.11454	5	11.85319	5	6.458005				
5.5	17.66494	5.5	11.19943	5.5	5.518277				
6	17.06372	6	10.34602	6	4.375141				
6.5	16.39646	6.5	9.308714	6.5	3.041357				
7	15.489	7	8.108534	7	1.404338				
7.5	14.52225	7.5	6.891841						
8	13.23876	8	5.27734						
8.5	11.70832	8.5	3.460182						
9	10.04954								
9.5	8.178338								
10	6.015912								

Spreadsheet for hydraulic performance of adult pump with 3 bladed impeller and protective cage

Pressure(v)	Flow rate(V)	Press error(-)	Minimum Press	Pressure (mmHg)	Maxim Press	Press error(+)	Flow error(-)	Flow min	Flow rate(LPM)	Flow max	Flow error(+)
0.09	2.93	0.22	4.25	4.47	4.68	0.22	0.10	7.17	7.27	7.37	0.10
0.10	2.87	0.22	4.38	4.60	4.82	0.22	0.09	7.02	7.11	7.21	0.09
0.10	2.76	0.22	4.54	4.76	4.98	0.22	0.09	6.75	6.84	6.94	0.09
0.10	2.65	0.22	4.68	4.90	5.12	0.22	0.09	6.48	6.57	6.66	0.09
0.11	2.53	0.22	4.87	5.09	5.31	0.22	0.09	6.19	6.28	6.36	0.09
0.11	2.46	0.22	4.96	5.18	5.40	0.22	0.08	6.02	6.10	6.19	0.08
0.11	2.40	0.22	5.03	5.25	5.48	0.22	0.08	5.87	5.95	6.04	0.08
0.11	2.37	0.22	5.07	5.29	5.51	0.22	0.08	5.78	5.86	5.94	0.08

0.11		2.27		0.22	5.15	5.37	5.60	0.22	0.08	5.55	5.63	5.71	0.08
0.11		2.18		0.22	5.15	5.37	5.59	0.22	0.08	5.32	5.39	5.47	0.08
0.12		2.10		0.22	5.28	5.50	5.72	0.22	0.07	5.12	5.19	5.26	0.07
0.12		2.02		0.22	5.35	5.57	5.80	0.22	0.07	4.93	5.00	5.07	0.07
0.12		1.92		0.22	5.46	5.68	5.90	0.22	0.07	4.67	4.74	4.81	0.07
0.12		1.81		0.22	5.56	5.78	6.01	0.22	0.07	4.42	4.48	4.55	0.07
0.12		1.71		0.22	5.65	5.87	6.09	0.22	0.06	4.17	4.23	4.29	0.06
0.13		1.62		0.22	5.79	6.01	6.23	0.22	0.06	3.93	3.99	4.05	0.06
0.13		1.52		0.22	5.84	6.07	6.29	0.22	0.06	3.69	3.75	3.81	0.06
0.13		1.41		0.23	5.96	6.19	6.41	0.23	0.06	3.43	3.48	3.54	0.06
0.13		1.31		0.23	6.03	6.26	6.48	0.23	0.05	3.18	3.23	3.28	0.05
0.13		1.24		0.23	6.09	6.31	6.54	0.23	0.05	2.99	3.05	3.10	0.05
0.13		1.12		0.23	6.15	6.38	6.61	0.23	0.05	2.71	2.76	2.81	0.05
0.14		1.02		0.23	6.35	6.57	6.80	0.23	0.05	2.46	2.50	2.55	0.05
0.14		0.93		0.23	6.45	6.67	6.90	0.23	0.04	2.23	2.27	2.32	0.04
0.14		0.83		0.23	6.54	6.77	6.99	0.23	0.04	1.99	2.03	2.07	0.04
0.14		0.74		0.23	6.60	6.83	7.06	0.23	0.04	1.76	1.80	1.84	0.04
0.14		0.63		0.23	6.72	6.94	7.17	0.23	0.04	1.48	1.52	1.55	0.04
0.15		0.54		0.23	6.89	7.12	7.35	0.23	0.03	1.27	1.30	1.33	0.03
0.15		0.44		0.23	7.03	7.26	7.49	0.23	0.03	1.01	1.04	1.07	0.03
0.16		0.33		0.23	7.31	7.54	7.77	0.23	0.03	0.76	0.79	0.82	0.03
0.16		0.24		0.23	7.49	7.73	7.96	0.23	0.03	0.53	0.56	0.58	0.03
5000 RPM		Rotation	83.33 Hz										
0.15		3.88		0.23	6.99	7.22	7.45	0.23	0.12	9.51	9.63	9.75	0.12
0.15		3.77		0.23	7.13	7.36	7.59	0.23	0.12	9.25	9.37	9.49	0.12
0.15		3.75		0.23	7.21	7.44	7.67	0.23	0.12	9.18	9.30	9.42	0.12
0.16		3.67		0.23	7.48	7.72	7.95	0.23	0.12	9.01	9.12	9.24	0.12
0.17		3.45		0.23	8.01	8.25	8.48	0.23	0.11	8.45	8.56	8.67	0.11
0.17		3.37		0.24	8.21	8.44	8.68	0.24	0.11	8.26	8.37	8.48	0.11
0.18		3.27		0.24	8.35	8.59	8.83	0.24	0.10	8.01	8.11	8.22	0.10
0.18		3.18		0.24	8.43	8.66	8.90	0.24	0.10	7.78	7.88	7.99	0.10
0.18		3.10		0.24	8.53	8.76	9.00	0.24	0.10	7.59	7.69	7.79	0.10
0.18		3.01		0.24	8.67	8.91	9.15	0.24	0.10	7.36	7.46	7.56	0.10
0.19		2.82		0.24	8.93	9.17	9.41	0.24	0.09	6.89	6.98	7.07	0.09
0.19		2.70		0.24	9.11	9.35	9.59	0.24	0.09	6.60	6.69	6.78	0.09
0.19		2.60		0.24	9.25	9.49	9.73	0.24	0.09	6.35	6.44	6.52	0.09

0.20		2.51		0.24	9.37	9.61	9.85	0.24	0.08	6.12	6.21	6.29	0.08
0.20		2.41		0.24	9.48	9.72	9.96	0.24	0.08	5.89	5.97	6.06	0.08
0.20		2.31		0.24	9.54	9.78	10.02	0.24	0.08	5.65	5.72	5.80	0.08
0.20		2.23		0.24	9.69	9.93	10.17	0.24	0.08	5.45	5.53	5.61	0.08
0.20		2.12		0.24	9.70	9.95	10.19	0.24	0.07	5.17	5.24	5.32	0.07
0.21		1.99		0.24	9.82	10.06	10.30	0.24	0.07	4.84	4.91	4.98	0.07
0.21		1.91		0.24	9.90	10.14	10.38	0.24	0.07	4.64	4.71	4.78	0.07
0.21		1.86		0.24	9.95	10.19	10.44	0.24	0.07	4.52	4.58	4.65	0.07
0.21		1.77		0.24	9.99	10.23	10.47	0.24	0.07	4.31	4.37	4.44	0.07
0.21		1.67		0.24	10.07	10.32	10.56	0.24	0.06	4.06	4.12	4.19	0.06
0.21		1.55		0.24	10.08	10.32	10.57	0.24	0.06	3.77	3.83	3.89	0.06
0.22		1.36		0.25	10.32	10.56	10.81	0.25	0.05	3.30	3.35	3.41	0.05
0.22		1.26		0.25	10.44	10.69	10.93	0.25	0.05	3.06	3.11	3.16	0.05
0.22		1.17		0.25	10.61	10.85	11.10	0.25	0.05	2.82	2.87	2.92	0.05
0.22		1.07		0.25	10.66	10.90	11.15	0.25	0.05	2.57	2.62	2.66	0.05
0.23		0.88		0.25	10.80	11.05	11.30	0.25	0.04	2.10	2.15	2.19	0.04
0.23		0.72		0.25	10.99	11.24	11.49	0.25	0.04	1.72	1.76	1.79	0.04
0.23		0.65		0.25	10.98	11.23	11.48	0.25	0.04	1.55	1.59	1.62	0.04
0.23		0.63		0.25	11.13	11.38	11.63	0.25	0.04	1.48	1.52	1.55	0.04
0.24		0.50		0.25	11.33	11.58	11.83	0.25	0.03	1.16	1.20	1.23	0.03
0.24		0.36		0.25	11.56	11.81	12.06	0.25	0.03	0.83	0.85	0.88	0.03
6000 RPM		Rotation	100 Hz										
0.22		4.87		0.24	10.29	10.54	10.78	0.24	0.15	11.96	12.10	12.25	0.15
0.23		4.77		0.25	10.91	11.16	11.40	0.25	0.14	11.72	11.86	12.01	0.14
0.23		4.72		0.25	11.06	11.31	11.56	0.25	0.14	11.60	11.74	11.88	0.14
0.23		4.58		0.25	11.26	11.51	11.75	0.25	0.14	11.25	11.39	11.53	0.14
0.24		4.35		0.25	11.77	12.02	12.27	0.25	0.13	10.68	10.81	10.94	0.13
0.25		4.18		0.25	12.24	12.49	12.74	0.25	0.13	10.25	10.38	10.51	0.13
0.26		4.04		0.25	12.38	12.63	12.88	0.25	0.13	9.92	10.04	10.17	0.13
0.26		3.90		0.26	12.62	12.88	13.13	0.26	0.12	9.56	9.68	9.80	0.12
0.26		3.82		0.26	12.78	13.04	13.29	0.26	0.12	9.36	9.48	9.59	0.12
0.27		3.73		0.26	12.79	13.05	13.31	0.26	0.12	9.13	9.25	9.37	0.12
0.27		3.60		0.26	12.98	13.24	13.50	0.26	0.11	8.82	8.93	9.04	0.11
0.27		3.39		0.26	13.22	13.48	13.73	0.26	0.11	8.30	8.41	8.52	0.11

0.28		3.32		0.26	13.35	13.61	13.87	0.26	0.11	8.13	8.23	8.34	0.11
0.28		3.21		0.26	13.49	13.75	14.01	0.26	0.10	7.87	7.98	8.08	0.10
0.28		3.03		0.26	13.69	13.95	14.21	0.26	0.10	7.41	7.50	7.60	0.10
0.29		2.91		0.26	13.85	14.11	14.37	0.26	0.10	7.13	7.22	7.32	0.10
0.29		2.76		0.26	14.07	14.33	14.59	0.26	0.09	6.74	6.83	6.92	0.09
0.29		2.62		0.26	14.22	14.49	14.75	0.26	0.09	6.40	6.49	6.58	0.09
0.30		2.48		0.26	14.42	14.69	14.95	0.26	0.08	6.05	6.14	6.22	0.08
0.30		2.29		0.26	14.55	14.81	15.08	0.26	0.08	5.60	5.68	5.76	0.08
0.30		2.12		0.26	14.68	14.95	15.21	0.26	0.07	5.18	5.26	5.33	0.07
0.31		1.84		0.27	14.93	15.19	15.46	0.27	0.07	4.47	4.54	4.61	0.07
0.31		1.66		0.27	15.16	15.43	15.69	0.27	0.06	4.03	4.09	4.15	0.06
0.32		1.49		0.27	15.43	15.70	15.97	0.27	0.06	3.62	3.68	3.74	0.06
0.32		1.42		0.27	15.55	15.82	16.09	0.27	0.06	3.44	3.50	3.56	0.06
0.32		1.27		0.27	15.75	16.02	16.29	0.27	0.05	3.07	3.12	3.17	0.05
0.32		0.98		0.27	15.53	15.80	16.07	0.27	0.04	2.35	2.40	2.44	0.04
0.33		0.86		0.27	15.88	16.15	16.42	0.27	0.04	2.06	2.10	2.14	0.04
0.32		0.80		0.27	15.76	16.03	16.30	0.27	0.04	1.92	1.96	2.00	0.04
0.33		0.74		0.27	15.81	16.08	16.35	0.27	0.04	1.75	1.79	1.83	0.04
0.33		0.63		0.27	16.10	16.37	16.64	0.27	0.04	1.50	1.53	1.57	0.04
0.34		0.51		0.27	16.48	16.75	17.02	0.27	0.03	1.19	1.22	1.25	0.03
0.35		0.34		0.28	16.93	17.20	17.48	0.28	0.03	0.79	0.82	0.84	0.03
0.36		0.26		0.28	17.32	17.60	17.87	0.28	0.03	0.58	0.61	0.64	0.03
0.36		0.15		0.28	17.51	17.79	18.06	0.28	0.02	0.30	0.32	0.34	0.02
0.36		0.10		0.28	17.53	17.81	18.09	0.28	0.02	0.18	0.21	0.23	0.02
7000 RPM		Rotation	116 Hz										
0.28		5.41		0.26	13.37	13.63	13.89	0.26	0.16	13.28	13.44	13.60	0.16
0.29		5.30		0.26	13.91	14.18	14.44	0.26	0.16	13.03	13.19	13.35	0.16
0.30		5.19		0.26	14.52	14.79	15.05	0.26	0.16	12.74	12.90	13.05	0.16
0.31		5.10		0.27	15.18	15.45	15.71	0.27	0.15	12.52	12.67	12.83	0.15
0.32		5.00		0.27	15.51	15.78	16.05	0.27	0.15	12.28	12.43	12.58	0.15
0.33		4.88		0.27	16.03	16.30	16.57	0.27	0.15	11.98	12.12	12.27	0.15
0.33		4.78		0.27	16.23	16.50	16.77	0.27	0.14	11.73	11.87	12.01	0.14
0.34		4.65		0.27	16.51	16.78	17.06	0.27	0.14	11.42	11.56	11.70	0.14
0.34		4.56		0.27	16.68	16.95	17.23	0.27	0.14	11.19	11.33	11.4	0.14

												7	
0.35		4.44		0.28	17.00	17.28	17.55	0.28	0.14	10.89	11.03	11.16	0.14
0.35		4.30		0.28	17.28	17.56	17.83	0.28	0.13	10.54	10.67	10.80	0.13
0.36		4.21		0.28	17.43	17.71	17.99	0.28	0.13	10.34	10.47	10.60	0.13
0.36		4.10		0.28	17.58	17.86	18.14	0.28	0.13	10.05	10.18	10.31	0.13
0.36		3.98		0.28	17.69	17.97	18.25	0.28	0.12	9.77	9.89	10.01	0.12
0.37		3.90		0.28	17.95	18.22	18.50	0.28	0.12	9.56	9.69	9.81	0.12
0.37		3.79		0.28	18.00	18.28	18.56	0.28	0.12	9.29	9.41	9.53	0.12
0.37		3.66		0.28	18.24	18.52	18.80	0.28	0.11	8.97	9.09	9.20	0.11
0.38		3.50		0.28	18.37	18.65	18.93	0.28	0.11	8.57	8.69	8.80	0.11
0.38		3.35		0.28	18.60	18.88	19.16	0.28	0.11	8.20	8.31	8.42	0.11
0.38		3.25		0.28	18.65	18.93	19.21	0.28	0.10	7.96	8.07	8.17	0.10
0.38		3.09		0.28	18.69	18.98	19.26	0.28	0.10	7.56	7.66	7.76	0.10
0.39		2.81		0.28	19.07	19.36	19.64	0.28	0.09	6.86	6.95	7.05	0.09
0.40		2.56		0.29	19.34	19.63	19.91	0.29	0.09	6.26	6.35	6.43	0.09
0.40		2.29		0.29	19.57	19.86	20.14	0.29	0.08	5.58	5.66	5.74	0.08
0.40		2.18		0.29	19.60	19.88	20.17	0.29	0.08	5.33	5.40	5.48	0.08
0.40		1.98		0.29	19.80	20.08	20.37	0.29	0.07	4.84	4.91	4.98	0.07
0.41		1.90		0.29	19.96	20.25	20.54	0.29	0.07	4.62	4.69	4.76	0.07
0.41		1.71		0.29	20.08	20.37	20.66	0.29	0.06	4.16	4.22	4.29	0.06
0.41		1.60		0.29	20.09	20.38	20.67	0.29	0.06	3.90	3.96	4.02	0.06
0.41		1.48		0.29	20.09	20.38	20.67	0.29	0.06	3.59	3.65	3.71	0.06
0.41		1.40		0.29	20.11	20.40	20.69	0.29	0.06	3.40	3.45	3.51	0.06
0.41		1.32		0.29	20.15	20.44	20.73	0.29	0.05	3.20	3.25	3.31	0.05
0.41		1.25		0.29	20.27	20.56	20.85	0.29	0.05	3.02	3.07	3.12	0.05
0.42		1.18		0.29	20.45	20.74	21.03	0.29	0.05	2.84	2.89	2.94	0.05
0.42		1.03		0.29	20.77	21.07	21.36	0.29	0.05	2.47	2.52	2.56	0.05
0.43		0.98		0.29	20.85	21.14	21.43	0.29	0.04	2.36	2.41	2.45	0.04
0.43		0.92		0.29	20.97	21.27	21.56	0.29	0.04	2.22	2.26	2.30	0.04
0.44		0.77		0.29	21.30	21.60	21.89	0.29	0.04	1.84	1.87	1.91	0.04
0.44		0.68		0.30	21.52	21.82	22.11	0.30	0.04	1.60	1.64	1.68	0.04
0.45		0.55		0.30	21.82	22.12	22.42	0.30	0.03	1.30	1.33	1.37	0.03
0.46		0.33		0.30	22.53	22.83	23.13	0.30	0.03	0.75	0.77	0.80	0.03

Spreadsheet for hydraulic performance of adult pump with impeller and diffuser and protective cage

Pressure(v)	Flow rate(V)	Press error(-)	Minimum Press	Pressure(mmHg)	Maxim Press	Press error(+)	Flow error(-)	Flow min	Flow rate(LPM)	Flow max	Flow error(+)
0.03	1.29	0.20	1.15	1.36	1.56	0.20	0.05	3.12	3.17	3.22	0.05
0.03	1.23	0.20	1.15	1.35	1.56	0.20	0.05	2.98	3.03	3.08	0.05
0.03	1.19	0.20	1.21	1.41	1.62	0.20	0.05	2.86	2.91	2.96	0.05
0.03	1.15	0.20	1.26	1.46	1.67	0.20	0.05	2.78	2.82	2.87	0.05
0.04	1.08	0.20	1.33	1.53	1.73	0.20	0.05	2.60	2.65	2.70	0.05
0.04	1.03	0.21	1.67	1.88	2.08	0.21	0.05	2.48	2.52	2.57	0.05
0.04	1.00	0.21	1.73	1.94	2.15	0.21	0.05	2.41	2.45	2.50	0.05
0.05	0.94	0.21	1.83	2.03	2.24	0.21	0.04	2.26	2.30	2.35	0.04
0.05	0.89	0.21	1.99	2.20	2.40	0.21	0.04	2.13	2.17	2.21	0.04
0.05	0.85	0.21	2.10	2.31	2.52	0.21	0.04	2.03	2.07	2.11	0.04
0.05	0.79	0.21	2.17	2.38	2.59	0.21	0.04	1.88	1.92	1.96	0.04
0.06	0.73	0.21	2.41	2.62	2.82	0.21	0.04	1.74	1.77	1.81	0.04
0.06	0.67	0.21	2.62	2.83	3.04	0.21	0.04	1.60	1.63	1.67	0.04
0.06	0.64	0.21	2.68	2.89	3.10	0.21	0.04	1.52	1.56	1.59	0.04
0.07	0.59	0.21	2.81	3.02	3.23	0.21	0.03	1.40	1.44	1.47	0.03
0.07	0.54	0.21	2.87	3.08	3.29	0.21	0.03	1.26	1.29	1.33	0.03
0.07	0.49	0.21	2.95	3.16	3.37	0.21	0.03	1.14	1.17	1.21	0.03
0.07	0.43	0.21	3.01	3.22	3.43	0.21	0.03	1.00	1.03	1.06	0.03
0.07	0.38	0.21	3.09	3.30	3.51	0.21	0.03	0.88	0.90	0.93	0.03
0.07	0.34	0.21	3.15	3.36	3.57	0.21	0.03	0.76	0.79	0.82	0.03
0.07	0.30	0.21	3.19	3.40	3.61	0.21	0.03	0.67	0.70	0.73	0.03
5000 RPM	Rotation	83.33 Hz									
0.04	1.64	0.21	1.68	1.89	2.09	0.21	0.06	3.99	4.05	4.11	0.06
0.04	1.57	0.21	1.65	1.86	2.06	0.21	0.06	3.81	3.87	3.93	0.06
0.04	1.52	0.21	1.73	1.94	2.14	0.21	0.06	3.70	3.76	3.81	0.06
0.05	1.46	0.21	1.94	2.15	2.36	0.21	0.06	3.53	3.59	3.64	0.06
0.05	1.41	0.21	2.05	2.26	2.46	0.21	0.06	3.41	3.46	3.52	0.06
0.05	1.37	0.21	2.09	2.30	2.50	0.21	0.05	3.32	3.37	3.42	0.05
0.06	1.29	0.21	2.29	2.50	2.71	0.21	0.05	3.12	3.18	3.23	0.05
0.06	1.25	0.21	2.41	2.62	2.83	0.21	0.05	3.02	3.07	3.12	0.05
0.06	1.20	0.21	2.59	2.80	3.01	0.21	0.05	2.91	2.96	3.01	0.05
0.06	1.14	0.21	2.74	2.95	3.16	0.21	0.05	2.76	2.80	2.85	0.05

0.07		1.08		0.21	2.92	3.13	3.34	0.21	0.05	2.61	2.66	2.71	0.05
0.07		1.03		0.21	3.15	3.36	3.58	0.21	0.05	2.47	2.52	2.56	0.05
0.08		0.97		0.21	3.32	3.54	3.75	0.21	0.04	2.32	2.36	2.41	0.04
0.08		0.90		0.21	3.52	3.73	3.95	0.21	0.04	2.15	2.19	2.24	0.04
0.08		0.84		0.22	3.75	3.97	4.18	0.22	0.04	2.01	2.05	2.09	0.04
0.09		0.77		0.22	3.86	4.08	4.29	0.22	0.04	1.84	1.88	1.92	0.04
0.09		0.72		0.22	4.06	4.28	4.49	0.22	0.04	1.71	1.75	1.78	0.04
0.09		0.68		0.22	4.19	4.41	4.62	0.22	0.04	1.61	1.65	1.69	0.04
0.10		0.61		0.22	4.34	4.56	4.78	0.22	0.03	1.44	1.47	1.51	0.03
0.10		0.56		0.22	4.41	4.63	4.85	0.22	0.03	1.32	1.35	1.38	0.03
0.10		0.52		0.22	4.55	4.77	4.99	0.22	0.03	1.21	1.24	1.28	0.03
0.10		0.45		0.22	4.75	4.97	5.19	0.22	0.03	1.05	1.08	1.11	0.03
0.10		0.37		0.22	4.74	4.96	5.18	0.22	0.03	0.85	0.88	0.91	0.03
0.10		0.36		0.22	4.75	4.97	5.19	0.22	0.03	0.82	0.85	0.87	0.03
6000 RPM		Rotation	100 Hz										
0.06		2.09		0.21	2.43	2.64	2.85	0.21	0.07	5.09	5.16	5.24	0.07
0.06		2.01		0.21	2.37	2.58	2.79	0.21	0.07	4.90	4.98	5.05	0.07
0.06		1.95		0.21	2.47	2.68	2.89	0.21	0.07	4.76	4.83	4.90	0.07
0.06		1.92		0.21	2.51	2.72	2.93	0.21	0.07	4.67	4.74	4.80	0.07
0.06		1.88		0.21	2.68	2.89	3.10	0.21	0.07	4.58	4.65	4.72	0.07
0.07		1.74		0.21	2.94	3.15	3.36	0.21	0.06	4.23	4.30	4.36	0.06
0.07		1.64		0.21	3.10	3.31	3.53	0.21	0.06	4.00	4.06	4.12	0.06
0.08		1.53		0.21	3.36	3.58	3.79	0.21	0.06	3.71	3.76	3.82	0.06
0.08		1.46		0.21	3.52	3.74	3.95	0.21	0.06	3.53	3.59	3.64	0.06
0.08		1.34		0.22	3.74	3.95	4.17	0.22	0.05	3.25	3.30	3.36	0.05
0.09		1.22		0.22	4.26	4.48	4.69	0.22	0.05	2.96	3.01	3.06	0.05
0.10		1.17		0.22	4.42	4.64	4.86	0.22	0.05	2.82	2.87	2.92	0.05
0.11		1.08		0.22	4.82	5.04	5.26	0.22	0.05	2.60	2.64	2.69	0.05
0.11		0.98		0.22	5.09	5.31	5.53	0.22	0.04	2.36	2.40	2.45	0.04
0.12		0.89		0.22	5.54	5.76	5.99	0.22	0.04	2.13	2.17	2.21	0.04
0.13		0.82		0.22	5.79	6.01	6.23	0.22	0.04	1.96	2.00	2.04	0.04
0.13		0.76		0.23	6.05	6.27	6.50	0.23	0.04	1.82	1.86	1.90	0.04
0.13		0.64		0.23	6.17	6.39	6.62	0.23	0.04	1.51	1.55	1.58	0.04
0.14		0.58		0.23	6.49	6.72	6.95	0.23	0.03	1.37	1.41	1.44	0.03
0.15		0.48		0.23	6.83	7.06	7.29	0.23	0.03	1.13	1.16	1.19	0.03
0.15		0.41		0.23	7.03	7.26	7.49	0.23	0.03	0.94	0.97	1.00	0.03

0.15		0.31		0.23	7.09	7.32	7.55	0.23	0.03	0.69	0.72	0.75	0.03
0.15		0.27		0.23	7.21	7.44	7.67	0.23	0.03	0.60	0.63	0.65	0.03
7000 RPM		Rotation	116 Hz										
0.07		2.44		0.21	3.16	3.37	3.58	0.21	0.08	5.96	6.04	6.12	0.08
0.07		2.33		0.21	3.08	3.29	3.50	0.21	0.08	5.68	5.76	5.84	0.08
0.07		2.22		0.21	3.17	3.38	3.60	0.21	0.08	5.42	5.50	5.57	0.08
0.08		2.12		0.21	3.49	3.71	3.92	0.21	0.07	5.17	5.24	5.31	0.07
0.08		2.02		0.21	3.64	3.86	4.07	0.21	0.07	4.93	5.01	5.08	0.07
0.09		1.94		0.22	3.81	4.03	4.25	0.22	0.07	4.72	4.79	4.86	0.07
0.09		1.82		0.22	4.11	4.32	4.54	0.22	0.07	4.42	4.49	4.55	0.07
0.10		1.73		0.22	4.44	4.66	4.87	0.22	0.06	4.22	4.28	4.35	0.06
0.11		1.60		0.22	4.86	5.08	5.30	0.22	0.06	3.90	3.96	4.02	0.06
0.12		1.51		0.22	5.28	5.50	5.72	0.22	0.06	3.67	3.73	3.79	0.06
0.12		1.47		0.22	5.49	5.71	5.93	0.22	0.06	3.58	3.63	3.69	0.06
0.12		1.40		0.22	5.77	5.99	6.22	0.22	0.06	3.38	3.44	3.49	0.06
0.13		1.34		0.23	6.03	6.26	6.48	0.23	0.05	3.24	3.30	3.35	0.05
0.13		1.30		0.23	6.22	6.45	6.67	0.23	0.05	3.16	3.21	3.26	0.05
0.14		1.24		0.23	6.49	6.72	6.95	0.23	0.05	3.01	3.06	3.11	0.05
0.15		1.22		0.23	6.84	7.07	7.30	0.23	0.05	2.94	2.99	3.05	0.05
0.15		1.15		0.23	7.04	7.27	7.50	0.23	0.05	2.79	2.84	2.89	0.05
0.15		1.12		0.23	7.26	7.49	7.73	0.23	0.05	2.69	2.74	2.79	0.05
0.16		1.06		0.23	7.44	7.68	7.91	0.23	0.05	2.55	2.60	2.64	0.05
0.16		1.00		0.23	7.61	7.84	8.08	0.23	0.05	2.42	2.46	2.51	0.05
0.17		0.94		0.23	7.94	8.18	8.41	0.23	0.04	2.25	2.30	2.34	0.04
0.17		0.81		0.23	7.87	8.11	8.34	0.23	0.04	1.95	1.99	2.03	0.04
0.17		0.74		0.24	8.18	8.42	8.65	0.24	0.04	1.77	1.81	1.85	0.04
0.18		0.71		0.24	8.47	8.71	8.94	0.24	0.04	1.69	1.72	1.76	0.04
0.18		0.65		0.24	8.63	8.87	9.10	0.24	0.04	1.53	1.57	1.61	0.04
0.19		0.60		0.24	8.80	9.04	9.28	0.24	0.03	1.42	1.46	1.49	0.03
0.19		0.56		0.24	8.94	9.18	9.42	0.24	0.03	1.32	1.35	1.39	0.03
0.19		0.51		0.24	9.13	9.37	9.61	0.24	0.03	1.19	1.23	1.26	0.03
0.20		0.46		0.24	9.44	9.68	9.93	0.24	0.03	1.07	1.10	1.14	0.03
0.20		0.43		0.24	9.43	9.67	9.91	0.24	0.03	1.00	1.03	1.06	0.03

Spreadsheet for hydraulic performance of adult pump with 4 bladed impeller and

Pressure(v)	Flow rate(V)	Press error(-)	Minimum Press	Pressure (mmHg)	Maxim Press	Press error(+)	Flow error(-)	Flow min	Flow rate(LPM)	Flow max	Flow error (+)
4000 RPM											
0.10	2.89	0.22	4.30	4.51	4.73	0.22	0.09	7.07	7.17	7.26	0.09
0.09	2.81	0.22	4.25	4.47	4.69	0.22	0.09	6.88	6.97	7.06	0.09
0.10	2.76	0.22	4.44	4.66	4.88	0.22	0.09	6.75	6.84	6.93	0.09
0.10	2.71	0.22	4.51	4.73	4.95	0.22	0.09	6.64	6.73	6.82	0.09
0.10	2.65	0.22	4.59	4.81	5.03	0.22	0.09	6.48	6.57	6.66	0.09
0.10	2.63	0.22	4.67	4.89	5.11	0.22	0.09	6.42	6.51	6.59	0.09
0.11	2.56	0.22	4.80	5.02	5.24	0.22	0.09	6.25	6.34	6.42	0.09
0.11	2.52	0.22	4.90	5.12	5.34	0.22	0.09	6.15	6.24	6.32	0.09
0.11	2.46	0.22	5.03	5.25	5.47	0.22	0.08	6.02	6.10	6.19	0.08
0.11	2.42	0.22	5.08	5.30	5.52	0.22	0.08	5.91	5.99	6.08	0.08
0.11	2.37	0.22	5.19	5.41	5.63	0.22	0.08	5.79	5.87	5.96	0.08
0.12	2.33	0.22	5.31	5.53	5.75	0.22	0.08	5.68	5.76	5.84	0.08
0.12	2.20	0.22	5.59	5.82	6.04	0.22	0.08	5.36	5.44	5.52	0.08
0.13	2.11	0.22	5.81	6.04	6.26	0.22	0.07	5.13	5.21	5.28	0.07
0.13	2.00	0.23	6.09	6.31	6.54	0.23	0.07	4.87	4.94	5.01	0.07
0.13	1.92	0.23	6.25	6.48	6.70	0.23	0.07	4.66	4.73	4.80	0.07
0.14	1.79	0.23	6.47	6.70	6.92	0.23	0.07	4.35	4.42	4.48	0.07
0.15	1.69	0.23	6.83	7.06	7.29	0.23	0.06	4.11	4.17	4.23	0.06
0.15	1.59	0.23	7.00	7.23	7.46	0.23	0.06	3.87	3.93	3.99	0.06
0.15	1.50	0.23	7.19	7.42	7.65	0.23	0.06	3.65	3.71	3.77	0.06
0.16	1.39	0.23	7.33	7.56	7.79	0.23	0.06	3.36	3.42	3.48	0.06
0.16	1.26	0.23	7.59	7.82	8.06	0.23	0.05	3.05	3.11	3.16	0.05
0.16	1.19	0.23	7.74	7.97	8.20	0.23	0.05	2.88	2.93	2.98	0.05
0.17	1.10	0.23	7.85	8.08	8.32	0.23	0.05	2.65	2.69	2.74	0.05
0.17	0.98	0.23	7.98	8.21	8.45	0.23	0.04	2.36	2.41	2.45	0.04
0.17	0.91	0.24	8.13	8.37	8.60	0.24	0.04	2.18	2.22	2.26	0.04
0.18	0.79	0.24	8.30	8.54	8.77	0.24	0.04	1.90	1.94	1.98	0.04
0.18	0.70	0.24	8.41	8.65	8.89	0.24	0.04	1.66	1.70	1.74	0.04
0.18	0.59	0.24	8.59	8.83	9.07	0.24	0.03	1.39	1.42	1.46	0.03
0.18	0.51	0.24	8.74	8.98	9.22	0.24	0.03	1.21	1.24	1.27	0.03
0.19	0.39	0.24	8.96	9.19	9.43	0.24	0.03	0.90	0.93	0.96	0.03
0.19	0.30	0.24	9.18	9.42	9.66	0.24	0.03	0.67	0.69	0.72	0.03
0.20	0.25	0.24	9.38	9.62	9.86	0.24	0.03	0.57	0.59	0.62	0.03

0.20		0.20		0.24	9.48	9.72	9.96	0.24	0.02	0.43	0.46	0.48	0.02
5000 RPM		Rotation	83.33 Hz										
0.15		3.82		0.23	6.81	7.04	7.27	0.23	0.12	9.38	9.49	9.61	0.12
0.15		3.73		0.23	7.07	7.30	7.53	0.23	0.12	9.14	9.26	9.37	0.12
0.16		3.67		0.23	7.28	7.51	7.74	0.23	0.12	9.00	9.12	9.23	0.12
0.16		3.54		0.23	7.55	7.78	8.01	0.23	0.11	8.68	8.80	8.91	0.11
0.17		3.45		0.23	7.91	8.15	8.38	0.23	0.11	8.45	8.56	8.67	0.11
0.18		3.26		0.24	8.61	8.85	9.09	0.24	0.10	7.99	8.10	8.20	0.10
0.19		3.09		0.24	9.18	9.42	9.66	0.24	0.10	7.55	7.65	7.75	0.10
0.20		2.97		0.24	9.53	9.77	10.02	0.24	0.10	7.27	7.37	7.47	0.10
0.21		2.87		0.24	9.82	10.06	10.31	0.24	0.09	7.03	7.13	7.22	0.09
0.21		2.74		0.24	10.13	10.38	10.62	0.24	0.09	6.69	6.78	6.87	0.09
0.22		2.59		0.25	10.53	10.78	11.02	0.25	0.09	6.34	6.43	6.52	0.09
0.23		2.45		0.25	10.93	11.17	11.42	0.25	0.08	5.97	6.06	6.14	0.08
0.23		2.30		0.25	11.23	11.48	11.73	0.25	0.08	5.62	5.69	5.77	0.08
0.24		2.17		0.25	11.49	11.74	11.99	0.25	0.08	5.30	5.37	5.45	0.08
0.24		2.02		0.25	11.72	11.98	12.23	0.25	0.07	4.93	5.00	5.08	0.07
0.25		1.92		0.25	11.89	12.15	12.40	0.25	0.07	4.69	4.76	4.82	0.07
0.25		1.81		0.25	12.08	12.34	12.59	0.25	0.07	4.41	4.48	4.54	0.07
0.26		1.68		0.25	12.30	12.56	12.81	0.25	0.06	4.08	4.14	4.21	0.06
0.26		1.53		0.25	12.39	12.64	12.89	0.25	0.06	3.71	3.77	3.83	0.06
0.26		1.43		0.26	12.58	12.83	13.09	0.26	0.06	3.46	3.52	3.57	0.06
0.26		1.33		0.26	12.64	12.89	13.15	0.26	0.05	3.22	3.28	3.33	0.05
0.27		1.24		0.26	12.84	13.10	13.35	0.26	0.05	2.99	3.04	3.09	0.05
0.27		0.99		0.26	13.25	13.51	13.77	0.26	0.04	2.38	2.42	2.47	0.04
0.28		0.88		0.26	13.36	13.62	13.88	0.26	0.04	2.10	2.14	2.18	0.04
0.28		0.77		0.26	13.42	13.68	13.94	0.26	0.04	1.85	1.89	1.93	0.04
0.28		0.67		0.26	13.57	13.83	14.09	0.26	0.04	1.59	1.63	1.66	0.04
0.29		0.55		0.26	13.90	14.16	14.42	0.26	0.03	1.29	1.32	1.36	0.03
0.29		0.42		0.26	14.25	14.51	14.78	0.26	0.03	0.98	1.01	1.04	0.03
0.30		0.32		0.26	14.52	14.79	15.05	0.26	0.03	0.73	0.76	0.79	0.03
0.30		0.28		0.26	14.65	14.91	15.18	0.26	0.03	0.63	0.66	0.69	0.03
6000 RPM		Rotation	100 Hz										
0.21		4.74		0.24	9.88	10.12	10.37	0.24	0.14	11.64	11.78	11.92	0.14
0.22		4.60		0.25	10.58	10.83	11.08	0.25	0.14	11.30	11.44	11.58	0.14
0.24		4.45		0.25	11.41	11.66	11.91	0.25	0.14	10.92	11.05	11.19	0.14
0.26		4.21		0.26	12.72	12.97	13.23	0.26	0.13	10.34	10.47	10.60	0.13

0.27		4.06		0.26	13.02	13.27	13.53	0.26	0.13	9.96	10.08	10.21	0.13
0.28		3.95		0.26	13.40	13.66	13.92	0.26	0.12	9.68	9.80	9.92	0.12
0.28		3.81		0.26	13.68	13.94	14.20	0.26	0.12	9.34	9.46	9.58	0.12
0.29		3.68		0.26	14.06	14.32	14.58	0.26	0.12	9.02	9.13	9.25	0.12
0.30		3.55		0.26	14.37	14.63	14.89	0.26	0.11	8.69	8.81	8.92	0.11
0.31		3.46		0.27	14.81	15.07	15.34	0.27	0.11	8.48	8.59	8.70	0.11
0.32		3.24		0.27	15.38	15.65	15.92	0.27	0.10	7.93	8.03	8.14	0.10
0.33		3.07		0.27	16.05	16.32	16.59	0.27	0.10	7.51	7.61	7.71	0.10
0.34		2.91		0.27	16.40	16.67	16.95	0.27	0.10	7.13	7.22	7.32	0.10
0.34		2.78		0.27	16.70	16.98	17.25	0.27	0.09	6.81	6.90	6.99	0.09
0.35		2.66		0.27	16.88	17.15	17.43	0.27	0.09	6.51	6.60	6.69	0.09
0.35		2.56		0.28	17.04	17.31	17.59	0.28	0.09	6.24	6.33	6.42	0.09
0.36		2.41		0.28	17.33	17.61	17.89	0.28	0.08	5.90	5.98	6.06	0.08
0.36		2.25		0.28	17.60	17.88	18.16	0.28	0.08	5.49	5.57	5.64	0.08
0.36		2.16		0.28	17.74	18.02	18.30	0.28	0.08	5.27	5.34	5.42	0.08
0.37		2.00		0.28	18.27	18.55	18.83	0.28	0.07	4.88	4.95	5.02	0.07
0.38		1.85		0.28	18.61	18.89	19.17	0.28	0.07	4.50	4.57	4.64	0.07
0.39		1.70		0.28	18.82	19.10	19.38	0.28	0.06	4.13	4.19	4.25	0.06
0.39		1.54		0.28	19.07	19.35	19.64	0.28	0.06	3.74	3.80	3.86	0.06
0.39		1.41		0.29	19.21	19.49	19.78	0.29	0.06	3.43	3.48	3.54	0.06
0.40		1.26		0.29	19.39	19.68	19.96	0.29	0.05	3.05	3.10	3.15	0.05
0.39		1.09		0.28	19.10	19.39	19.67	0.28	0.05	2.62	2.67	2.72	0.05
0.40		0.98		0.29	19.41	19.70	19.98	0.29	0.04	2.35	2.39	2.44	0.04
0.40		0.85		0.29	19.65	19.94	20.23	0.29	0.04	2.03	2.07	2.12	0.04
0.41		0.68		0.29	20.12	20.40	20.69	0.29	0.04	1.63	1.66	1.70	0.04
0.42		0.55		0.29	20.54	20.83	21.12	0.29	0.03	1.30	1.33	1.36	0.03
0.43		0.39		0.29	21.19	21.48	21.78	0.29	0.03	0.91	0.94	0.97	0.03
0.44		0.27		0.30	21.61	21.90	22.20	0.30	0.03	0.60	0.63	0.65	0.03
7000 RPM		Rotation	116 Hz										
0.32		5.18		0.27	15.57	15.84	16.11	0.27	0.15	12.73	12.88	13.04	0.15
0.33		5.12		0.27	15.79	16.06	16.33	0.27	0.15	12.58	12.74	12.89	0.15
0.34		4.99		0.27	16.60	16.87	17.15	0.27	0.15	12.25	12.40	12.55	0.15
0.35		4.88		0.28	17.10	17.38	17.66	0.28	0.15	12.00	12.14	12.29	0.15
0.36		4.75		0.28	17.49	17.77	18.05	0.28	0.14	11.68	11.82	11.96	0.14
0.37		4.63		0.28	18.18	18.46	18.74	0.28	0.14	11.37	11.51	11.65	0.14
0.38		4.50		0.28	18.66	18.94	19.22	0.28	0.14	11.05	11.19	11.32	0.14
0.40		4.39		0.29	19.44	19.72	20.01	0.29	0.13	10.77	10.90	11.04	0.13

0.41		4.28		0.29	19.96	20.25	20.54	0.29	0.13	10.51	10.64	10.77	0.13
0.41		4.20		0.29	20.15	20.44	20.73	0.29	0.13	10.29	10.42	10.55	0.13
0.42		4.09		0.29	20.60	20.89	21.18	0.29	0.13	10.04	10.17	10.29	0.13
0.42		4.04		0.29	20.70	20.99	21.29	0.29	0.12	9.91	10.04	10.16	0.12
0.43		3.94		0.29	21.05	21.35	21.64	0.29	0.12	9.67	9.79	9.91	0.12
0.44		3.80		0.30	21.44	21.73	22.03	0.30	0.12	9.31	9.43	9.55	0.12
0.44		3.67		0.30	21.78	22.08	22.38	0.30	0.12	8.99	9.11	9.22	0.12
0.45		3.59		0.30	22.06	22.36	22.66	0.30	0.11	8.80	8.91	9.03	0.11
0.46		3.49		0.30	22.35	22.65	22.95	0.30	0.11	8.56	8.67	8.78	0.11
0.46		3.40		0.30	22.52	22.82	23.12	0.30	0.11	8.33	8.44	8.55	0.11
0.46		3.30		0.30	22.66	22.96	23.27	0.30	0.11	8.09	8.19	8.30	0.11
0.47		3.16		0.30	23.00	23.31	23.61	0.30	0.10	7.74	7.84	7.94	0.10
0.48		2.97		0.30	23.41	23.72	24.02	0.30	0.10	7.26	7.36	7.46	0.10
0.48		2.84		0.31	23.60	23.90	24.21	0.31	0.09	6.96	7.05	7.15	0.09
0.49		2.77		0.31	23.92	24.22	24.53	0.31	0.09	6.77	6.86	6.95	0.09
0.49		2.67		0.31	24.03	24.34	24.65	0.31	0.09	6.53	6.62	6.71	0.09
0.49		2.55		0.31	24.25	24.56	24.87	0.31	0.09	6.24	6.33	6.41	0.09
0.50		2.42		0.31	24.37	24.68	24.98	0.31	0.08	5.91	5.99	6.07	0.08
0.50		2.26		0.31	24.60	24.91	25.22	0.31	0.08	5.52	5.60	5.68	0.08
0.50		2.17		0.31	24.69	25.00	25.31	0.31	0.08	5.30	5.37	5.45	0.08
0.50		2.09		0.31	24.76	25.07	25.38	0.31	0.07	5.10	5.17	5.24	0.07
0.51		1.97		0.31	24.99	25.30	25.61	0.31	0.07	4.79	4.86	4.93	0.07
0.52		1.82		0.31	25.37	25.69	26.00	0.31	0.07	4.42	4.49	4.55	0.07
0.52		1.71		0.31	25.54	25.86	26.17	0.31	0.06	4.16	4.22	4.28	0.06
0.52		1.60		0.32	25.75	26.06	26.38	0.32	0.06	3.88	3.94	4.00	0.06
0.52		1.41		0.32	25.79	26.11	26.43	0.32	0.06	3.43	3.48	3.54	0.06
0.52		1.16		0.32	25.75	26.06	26.38	0.32	0.05	2.81	2.86	2.91	0.05
0.53		1.01		0.32	26.10	26.42	26.74	0.32	0.05	2.44	2.48	2.53	0.05
0.54		0.89		0.32	26.47	26.78	27.10	0.32	0.04	2.13	2.17	2.22	0.04
0.55		0.76		0.32	26.99	27.31	27.63	0.32	0.04	1.80	1.84	1.88	0.04
0.56		0.63		0.32	27.35	27.67	27.99	0.32	0.04	1.49	1.52	1.56	0.04
0.57		0.46		0.32	27.89	28.21	28.54	0.32	0.03	1.08	1.11	1.14	0.03
0.58		0.32		0.33	28.35	28.67	29.00	0.33	0.03	0.72	0.75	0.78	0.03

Vita

Jugal Yatinkumar Kapadia was born on November 1, 1984, in Gujarat, India and is an Indian citizen. He graduated from Baroda High School, Baroda, Gujarat in 2003. He received his Bachelor of Science in Biomedical and Instrumentation Engineering from U.V. Patel College of Engineering, Gujarat in 2007 and subsequently worked as an intern at Apollo Hospital and Electronic Engineering Corporation for 6 months. As an intern he designed Electro Stethoscope and Digital Algometer as well as was responsible for PCB troubleshooting and maintaining Biomedical instruments of the Hospital.

To pursue a Masters degree in Mechanical Engineering, he joined Virginia Commonwealth University, Richmond,VA. He worked as a Research Assistant in the Bio-Circ Laboratory at VCU, Richmond,VA. He is an active member of ASAIO (American Society of Artificial Internal Organs). He got an honorable mention at the 55th Annual Conference of ASAIO for top ASAIO-*fyi*.